FOI

The Impact of System Characteristics on Noble Gas Network Verification Capability for CTBT

ANDERS AXELSSON, ANDERS RINGBOM,
MATTIAS ALDENER, TOMAS FRITIOFF, ANDERS MÖRTSELL

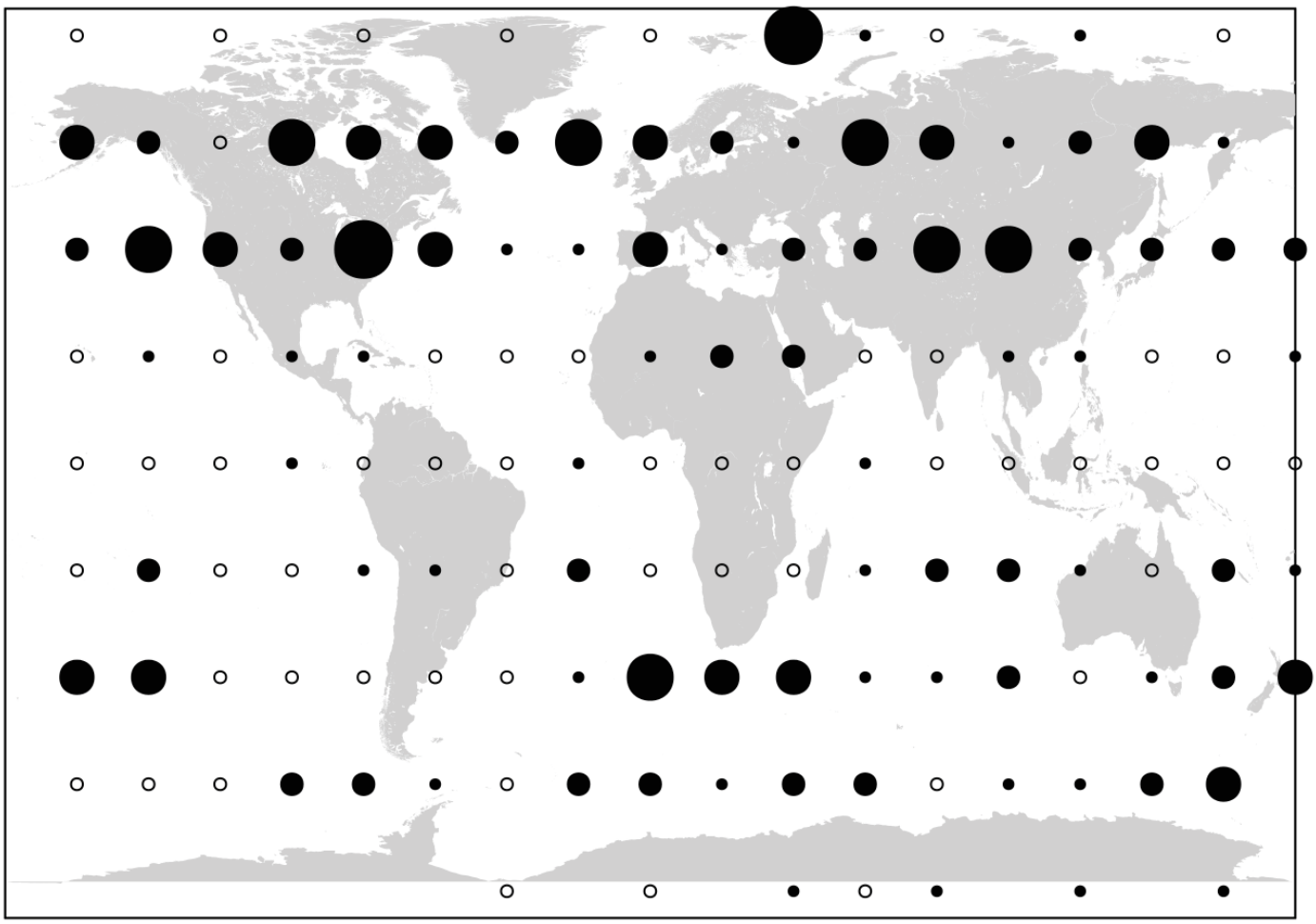

FOI-R--3856--SE
ISSN 1650-1942 March 2014

Anders Axelsson, Anders Ringbom,
Mattias Aldener,Tomas Fritioff,
Anders Mörtsell

The Impact of System Characteristics on Noble Gas Network Verification Capability for CTBT

Titel	Inverkan av systemkaraktäristika på verifikationsförmågan för CTBT hos ädelgasnätverk
Title	The Impact of System Characteristics on Noble Gas Network Verification Capability for CTBT
Report no	FOI-R--3856--SE
Month	March
Year	2014
Pages	120
ISSN	ISSN-1650-1942
Customer	Pacific Northwest National Laboratory (PNNL), USA
Project no	E28284
Approved by	Torgny Carlsson
Division	Defence & Security, Systems and Technology

FOI Swedish Defence Research Agency

Abstract

This document constitutes the final report of Task 1 of the project *Xenon International Paper Study*, performed under a Pacific Northwest National Laboratory (PNNL) contract. In this report we present the outcome of studies performed to increase the understanding on how the network of radioxenon measurement stations, being a part of the the international monitoring system (IMS) for verification of the Comprehensive Nuclear-Test-Ban Treaty, is affected by network and measurement station parameters. The study was performed by analyzing the network response to a synthetic data set of concentration profiles from a large number of sources of radioxenon releases with compositions characteristic of nuclear explosions. The response was studied for different model radioxenon systems populating the network. In addition, the dependence of system level performance indicators on actual system parameters was modelled.

Keywords

Noble Gas, Xenon, SAUNA, System Performance, Verification Capability, CTBT

Sammanfattning

Denna rapport utgör slutleverans för del 1 av projektet *Xenon International Paper Study*, utfört på uppdrag av Pacific Northwest National Laboratory (PNNL). I rapporten presenteras resultaten av de studier som utförts för att öka förståelsen av hur nätverket med mätstationer för ädelgaser, som är en del av det internationella övervakningssystemet (IMS) för verifikation av det fullständinga provstoppsavtalet, påverkas av nätverks- och mätstationsparametrar. Analysen genomfördes genom att analysera nätverksresponsen på ett syntetiskt dataset med koncentrationsprofiler genererat av ett stort antal hypotetiska radioxenonutsläpp med en sammansättning karaktärisktiskt för en kärnvapenexplosion. En uppskattning av hur olika tekniska parametrar för mätsystem för radioxenon påverkar nätverkets prestanda genomfördes. Dessutom studerades kopplingen mellan den högnivåparametrisering av mätstationskarakteristik som använts i studien till tekniska parametrar av verkliga system.

Nyckelord

Ädelgas, Xenon, SAUNA, Systemprestanda, Verifikationsförmåga, CTBT

Contents

1 Introduction and Summary

1.1 Introduction

The importance of radioxenon measurements in detecting and identifying possible clandestine nuclear explosions has become increasingly apparent in recent years. Within the international monitoring system (IMS) for verification of the CTBT, seismoacoustic measurements provide very low detection thresholds for explosions and are also able to provide good location and timing information. However, the specificity of seismoacoustic measurements for nuclear explosions is low, with the IMS network producing a very high rate of events that cannot be screened out as non-CTBT relevant. The mission of atmospheric radionuclide measurements, and radioxenon measurements in particular, in CTBT verification is therefore to provide corroborating evidence that a source of radionuclides consistent with a nuclear explosion is located in an area and within a time window that contain a relevant seismoacoustic event.

The performance of a radioxenon measurement system is often expressed by the Minimum Detectable Concentration, MDC. However, even for a single measurement system, the MDC is not the only performance parameter of interest, and there is a need in technical development to consider trade-offs between the utility of a lower MDC and e.g. the time resolution of the measurements (sampling interval). Furthermore, radioxenon measurement systems are currently deployed in a global network that comprises 40 planned radionuclide monitoring stations. It is the response of the entire network of monitoring systems that determines the success of the overall verification mission.

Clearly therefore, technical development in the field of atmospheric radioxenon measurements needs to be guided by systematic studies of the impact of different radioxenon measurement parameters on measurement system characteristics of the capability of a global network of such systems to locate, identify and characterize possible nuclear explosions. This report presents the results of such a study. To the authors' knowledge, this is the first study that attempts to model in detail location and characterization on a network level in order to obtain a more complete picture of verification capability. Furthermore, the study investigates the impact of increasing the IMS network density from 40 to 80 stations.

The approach to studying the interaction of station properties with network properties is to use metrics to evaluate and optimize these properties. These metrics are being introduced in some cases for the first time. For this reason, this paper is intended to stimulate discussion to find the most effective and acceptable metrics.

1.2 Summary

By simulation of 144 globally distributed radioxenon releases from hypothetical nuclear explosions, the IMS network response was studied with respect to verification capability. A small set of global network quality indicators or Figures of Merit (FoMs) that we believe capture the essential aspects of the verification mission of a radionuclide network for CTBT verification were defined: Detection of effluents, location of the release and characterization of the source, which incorporates both event timing and the ability to discriminate between different types of sources.

The concept was studied with respect to different noble gas technology im-

provements (model systems) and technology applications (network densities). Network density was studied by comparing the currently planned International Monitoring System (IMS) noble gas component comprising 39 measuring stations to a network with noble gas capability installed at all 79 currently planned radionuclide stations of the IMS. Each network configuration (network density and equipment in terms of model system) was modeled for different assumptions on sample collection time (varying from 3 to 24 hours). The response was studied for two different release scenarios, with a ^{133}Xe release of $5.1 \cdot 10^{14}$, and $1.1 \cdot 10^{16}$ Bq, respectively. Many of the results can be scaled to any release activity, corresponding to different release fractions and/or nuclear yield. The main conclusions from the study are:

Using current systems, the detection capability is already close to optimal for the two release scenarios, and it is not very sensitive to the sample collection time. Significant improvement of the detection capability is possible but would require a denser network.

The maximum achievable value of the fraction of detected explosions, which is approached even with current measurement technology, is considerably less than 100 % due to global atmospheric conditions: Weather patterns can prevent detection within a given time span of some releases no matter how large (or equivalently, no matter the measurement sensitivity of network monitoring equipment). The time span used in this study is one week; a longer time would have raised the maximum achievable detection capability, but the additional detections would be increasingly unlikely to yield data useful for verification. The problem is particularly severe in the equatorial region. It can be mitigated but not solved by increasing the number of monitoring stations from 39 to 79.

The ability to locate the releases is not very sensitive to system collection time, nor to detection technology improvements. The improvement when using a denser network is also quite limited. The ability to locate a release is determined not only by network configuration, measurement sensitivity and data quality but also by Atmospheric Transport Modeling (ATM) capability.

Characterization of the release is relatively insensitive to changes in collection time but can be significantly improved by higher network density and detection technology improvements.

The overall verification capability is almost insensitive to changes in collection time but can be improved both by higher network density and detection technology improvements.

The study has not explicitly addressed the issue of radioxenon background. For successful use of verification data, the background problem must be handled by several methods, including characterization and identification of prominent individual sources of background and exclusion or subtraction of such sources. We believe that the measurement system and network properties ultimately measured by each of the FoMs all contribute to the capability of analysts to accomplish this.

Since this is the first study to address the complete verification capability of a radionuclide network, it includes several new suggested concepts that needs to be further scrutinized. We also believe that further studies are needed, using e.g. a larger number of hypothetical explosions distributed over several years

and seasons. Furthermore, a deeper analysis of the reasons behind some of the results obtained is necessary.

2 Methodology

One major objective of the study has been to quantify the quality of data obtained from the IMS radioxenon network by a small set of Figures of Merit (FoMs) that rate three basic functions of the network:

> The *detection* of a radioxenon release from a nuclear explosion.
>
> The *location* of a source of radionuclides by Atmospheric Transport Modeling (ATM) in backtracking mode from detecting monitoring stations.
>
> The *characterization* of the source based on measurement results, including first and foremost the discrimination of nuclear explosion sources from other sources of radionuclides.

The network-level FoMs, defined in Sect. 2.1, are expressed as functions of aggregate measurement system parameters – parameters that avoid the full complexity of the set of technical parameters that govern the performance of a real radioxenon measurement systems while preserving the essential features of the measurement and analysis process. These FoMs express the response of the IMS network to synthetic atmospheric radioactivity concentration distributions in time and space generated by forward-mode ATM from a set of globally distributed notional explosion sources. The FoMs are obtained using algorithms similar to methods typically used by the CTBTO International Data Center (IDC) as well as many National Data Centers (NDCs), and are meant to quantify the outcome of a typical verification process involving radioxenon data. The algorithms assumes that the explosion time is known from seismic information.

The connection between the aggregate measurement system parameters used for the network analysis and the "real" technical parameters that are the subject of system design must also be provided, so that a high-level data quality specification for the network can be traced down to actual system design parameters and vice versa. The impact on single-system measurement sensitivity from varying different technical system parameters was also an objective in itself.

In order to accomplish the above, the study has incorporated five distinct elements (see also Fig. 2.1):

> The generation of a synthetic nuclear explosion data set by forward-mode ATM from a number of globally distributed radioxenon sources, each producing the same release, with a composition characteristic of a nuclear explosion. For each notional explosion, radioxenon concentration time profiles at each monitoring location in the network were generated.
>
> The activity collected by the sampling of each concentration profile during consecutive intervals of time of varying length (3 h, 6 h, 9 h and 12 h) was computed and resulted in a set of *station-measured concentrations* for each notional explosion (a different set for each sample collection time). This was repeated for two different released activities and for two IMS station densities (39 and 79 stations)[1].

[1] IMS is planned to consist of 80 radionuclide stations, of which 40 are initially planned to include radioxenon systems. For political reasons, only 79 station locations are specified in the Treaty. The single unassigned station is reserved for a state not yet party to the Treaty.

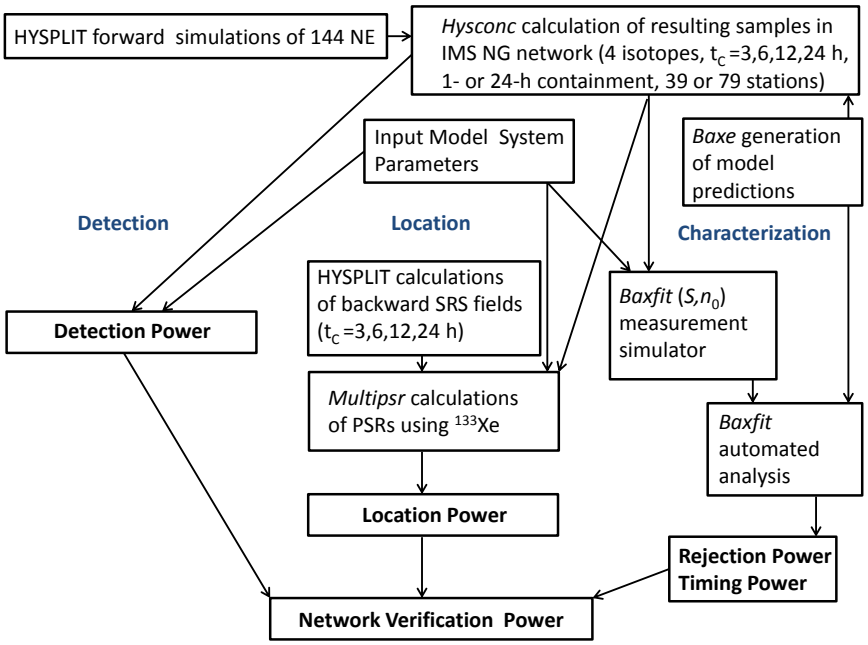

Figure 2.1: Schematic illustration of the workflow applied in the study presented in this report.

The station-measured concentration sets were each used to extract information on which and how many explosions were detected when applying various assumptions, such as MDC and sampling time.

The station-measured concentration sets were each used as input to ATM backtracking calculations aimed at producing so called Possible Source Regions (PSR) – maps of the correlation between measured data and ATM source-receptor sensitivity (SRS) values. Such correlation maps are routinely generated by the Provisional Technical Secretariat of the CTBTO Preparatory Commission (PTS). The PSRs were used to quantify the capability to locate the explosions, as well as the capability to estimate the released activity.

The station-measured concentration sets were also used as input to a radioxenon measurement simulator that generated synthetic measurement results based on specified high-level measurement system characteristics. The quality of measurement results obtained for each notional explosion were tested in various ways, including the power to reject a false source hypothesis and the precision of source timing based on the results.

The impact of varying technical parameters of radioxenon measurement systems on various performance indicators was studied. The performance indicators included the usual sensitivity indicator, the Minimum Detectable Concentration (MDC). This study was also necessary in order to connect other high-level parameters used in the network-level analysis of source characterization to actual system parameters.

The study was limited to one week transport time backward and forward, and contributions from other radioxenon sources such as isotope production

facilities and nuclear power plants were not included. To include this background would have been more representative of a real detection, but since the focus of this study was to investigate relative capability differences between various network configurations, and since the results would be more difficult to interpret if the background was included, this component was left out.

2.1 Definitions of Global Network Figures of Merit

The network response was, as mentioned in the previous section, modeled using a small set of FoMs, capturing the possibility to *detect, locate,* and *characterize* the release. The FoMs were defined as follows:

Data sets C_i of measured data are obtained by a given network configuration C for a set of N explosions $i = 1, 2, .., N$.

Detection Power (D): The fraction of explosions for which C_i results in at least one sample exposed to a mean activity concentration exceeding the MDC for any of the four CTBT relevant xenon isotopes.

Location Power (L): The fraction of explosions for which C_i results in a location error less than 25 %.

Rejection Power (R): The fraction of explosions for which C_i allows a given false scenario to be rejected based on isotopic ratios.

Timing Power (T): The fraction of explosions for which C_i allows a fission time estimate, based on $^{135}\mathrm{Xe}/^{133}\mathrm{Xe}$ ratios and correct scenario, better than 6 hours.

Network Verification Power (V): The average of D, L, R, and T:

$$V = \frac{D + L + R + T}{4} \tag{2.1}$$

In the interest of clarity, and the absence of any obvious *a priori* reason to do otherwise, we have chosen to weight each of the FoMs D, L, R and T equally in the Network Verification Power V. Perhaps needless to say, it is possible to place greater emphasis on some of the component FoMs than on others by introducing different weighting factors. For example, a network designer that values the capability to assess whether a set of radioxenon detections are consistent with a source co-located with a seismic event over the capability to detect radioxenon *per se* and/or the capability to discriminate different kinds of sources may choose to bias V in favor of L and T.

2.2 Model Measurement Systems

In order to evaluate the effect on network-level measurement and analysis for different characteristics of measurement systems, six model systems were defined. Their characteristics were expressed in terms of MDCs and in terms of a generic model for noble gas measurement and analysis based on two parameters: S, analysis power (in counts per concentration unit) and n_0, a generic background (in counts), described in greater detail in Sect. 6.3. These parameters need to be specified as a function of sample collection time, t_c, for each of the six model systems.

The parameters (S,n_0) are designed so that S can easily be computed from a known set of technical system parameters (air flow Φ, beta-gamma counting efficiency $\varepsilon_{\beta\gamma}$, sample collection time t_c, sample processing time t_p and sample

counting time t_a), and the MDC can be computed from S and n_0. Therefore, once a set of parameters (Φ,$\varepsilon_{\beta\gamma}$,$t_p$,$t_a$)$_i$ has been fixed for a given model system i, the MDC$_i$ and (S,n_0)$_i$ can be computed for that system as a function of t_c.

The specific six model systems used in the study were designed by varying selected technical parameters relative to values typical for a present SAUNA system. The baseline values were derived by selecting nuclide MDCs deemed typical for SAUNA systems installed in the IMS and typical values for corresponding beta-gamma counting efficiencies $\varepsilon_{\beta\gamma}$. The value of the generic background parameter n_0 was set for each isotope so that together with known IMS SAUNA sampling rate Φ and sample collection, processing and counting times, the "typical" MDC would be reproduced. The resulting baseline values are shown in Tab. 2.1, together with values consistent with an optimistic projection of the characteristics of the Xenon International (XI) system that has been proposed by the Pacific Northwest National Laboratory [1].

Parameter	Value	
	SAUNA	XI
Sampling rate Φ (m^3/h)	1.2	6
Sample processing time t_p (h)	6	6
Sample counting time t_a (h)	11	12
Counting efficiency $\varepsilon_{\beta\gamma}$		
^{131m}Xe	0.350	0.350
^{133}Xe	0.465	0.465
^{133m}Xe	0.352	0.352
^{135}Xe	0.470	0.470
Generic background n_0 (counts)		
^{131m}Xe	38	21
^{133}Xe	280	153
^{133m}Xe	25	14
^{135}Xe	309	169
^{133}Xe MDC @ t_c=12 h (mBq/m^3)	0.240	0.033
^{133}Xe S @ t_c=12 h (cts/mBq/m^3)	241	1309

Table 2.1: Baseline technical parameters; representative of present SAUNA system (second column) and projected values for XI system (third column)

Relative to the baseline system, System A (present-day SAUNA), shown in column two of Tab. 2.1, the six model systems were defined by the variations described in Tab. 2.2.

The MDCs for the six model systems, for each of the relevant nuclides, are given in Tab. 2.3 for each of the sample collection times, t_c = 3 h, 6 h, 12 h and 24 h, studied. The two parameters, S and n_0, for the six model systems are given in Tab. 6.1.

Designation	Basis for specification	Detailed assumptions
System A	Present-day SAUNA	S from typical SAUNA values of Φ,$\varepsilon_{\beta\gamma}$,$t_c$,$t_p$,$t_a$. Given S, n_0 is selected to produce SAUNA typical MDCs
System B	System A with super detector	$\varepsilon_{\beta\gamma}$=100%, $n_0 = 0.1 \cdot n_{0,A}$
System C	System A with super collection	$\Phi = 10 \cdot \Phi_A$
System D	System A with super detector and collection	$\varepsilon_{\beta\gamma}$=100%, $n_0 = 0.1 \cdot n_{0,A}$, $\Phi = 10 \cdot \Phi_A$
System E	System A with cheap detector	$\varepsilon_{\beta\gamma} = 0.5 \cdot \varepsilon_{\beta\gamma,A}$, $n_0 = 10 \cdot n_{0,A}$
System F	XI optimistic projection	n_0 assuming half SAUNA ROI background rate (taken as n_0/t_a) and t_a=12 h (SAUNA 11 h). S assuming SAUNA parameters except Φ = 6m^3/h (SAUNA 1.2m^3/h), t_a=12 h (SAUNA 11 h).

Table 2.2: Basis and details of specifications for the six model systems used in the study. The subscript A refers to the reference values (system A) shown in column two of Tab. 2.1.

System	Collection time	MDC (mBq/m^3) ^{131m}Xe	^{133}Xe	^{133m}Xe	^{135}Xe
System A	3 h	0.48	0.94	0.45	2.4
	6 h	0.24	0.47	0.23	1.3
	12 h	0.12	0.24	0.12	0.80
	24 h	0.061	0.12	0.065	0.57
System B	3 h	0.12	0.18	0.12	0.43
	6 h	0.059	0.089	0.061	0.24
	12 h	0.030	0.045	0.032	0.15
	24 h	0.015	0.023	0.017	0.10
System C	3 h	0.048	0.094	0.045	0.24
	6 h	0.024	0.047	0.023	0.13
	12 h	0.012	0.024	0.012	0.080
	24 h	0.0061	0.012	0.0065	0.057
System D	3 h	0.012	0.018	0.012	0.043
	6 h	0.0059	0.0089	0.0061	0.024
	12 h	0.0030	0.0045	0.0032	0.015
	24 h	0.0015	0.0023	0.0017	0.010
System E	3 h	2.8	5.7	2.6	14
	6 h	1.4	2.9	1.3	8.0
	12 h	0.70	1.5	0.69	4.9
	24 h	0.36	0.76	0.37	3.5
System F	3 h	0.067	0.13	0.065	0.33
	6 h	0.034	0.065	0.033	0.19
	12 h	0.017	0.033	0.017	0.11
	24 h	0.0086	0.017	0.0092	0.081

Table 2.3: MDCs for all four relevant nuclides for the six model systems, for four different sample collection times.

3 The Synthetic Explosion Data Set

3.1 Forward Calculation of Hypothetical Nuclear Explosions

The study described in this report is based on forward Lagrangian particle dispersion modeling of xenon releases from 144 hypothetical nuclear explosions. Activities of radioxenon isotopes created in the explosions were calculated using the in-house developed *Baxe* code, assuming 1 h or 24 h containment of fission products created in a 1 kt nuclear explosion with ^{239}Pu as fissile fuel. Before release, all fission products are assumed to be fully contained, and after separation, only xenon is assumed to be released. This means that no iodine contributes to the decay after release. In order to be able to easily scale the results to other yields and/or system sensitivities, we assume that the full xenon inventory was emitted into the atmosphere. The resulting released activities are given in Tab. 3.1.

Containment time (h)	^{133}Xe Activity(Bq)	^{131m}Xe Activity (Bq)	^{133m}Xe Activity (Bq)	^{135}Xe Activity (Bq)
1	$5.1 \cdot 10^{14}$	$6.2 \cdot 10^{10}$	$2.8 \cdot 10^{14}$	$5.8 \cdot 10^{16}$
24	$1.1 \cdot 10^{16}$	$2.9 \cdot 10^{12}$	$8.8 \cdot 10^{14}$	$6.2 \cdot 10^{16}$

Table 3.1: Released activities used in this study, calculated assuming a 1 kt ^{239}Pu nuclear explosion.

The hypothetical releases were distributed on a $20^\circ \times 20^\circ$ grid except along latitudes -80° and 80°, where the spacing was a less dense (see Fig. 3.1). We realize that this distribution will cause a slight over representation of the polar regions compared to the equatorial, but the approach was chosen for simplicity reasons.

The releases were assumed to have occurred in the period 7-14 October 2012, and following each latitude clockwise each release occurred one day later than the previous, using the 7-day cycle. Each release had a duration of one hour. The dispersion modeling was performed using the NOAA HYSPLIT software [2]. The model used GDAS weather data with a $1^\circ \times 1^\circ$ spatial resolution and a time resolution of three hours. Since one of the tasks in the study was to investigate network configurations with radioxenon systems having much better sensitivity compared to the ones installed today, it was important to reasonably well predict very small activity concentrations. The model measurement systems have MDCs down to about 0.001 mBq/m^3 (see Tab. 2.3), i.e. more than 100 times lower than today's systems. The required statistics (i.e. number of particles) required to model this can be estimated as follows:

The HYSPLIT output consists of a set of dilution factors for all geo-spatial grid points. Neglecting in-growth from other isotopes, the resulting activity concentration C at a given grid location and time is given by

$$C = A_0 D e^{-\lambda t}, \tag{3.1}$$

where A_0 is the source release activity and D is the dilution factor. According to Tab. 3.1, the released ^{133}Xe activity after 1 h from 1 kt was $5.1 \cdot 10^{14}$ Bq. This means that in order to reach a concentration of 0.001 mBq/m^3 after

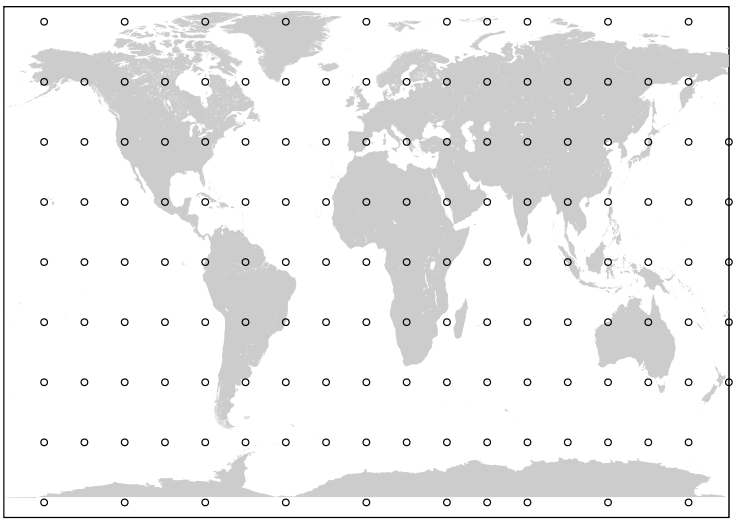

Figure 3.1: The distribution of the hypothetical nuclear explosions used in this study.

one week, a dilution factor of $6.3 \cdot 10^{-21}$ m^{-3} is required, i.e. the HYSPLIT dispersion calculation has to be able to reproduce dilution factors of the order of 10^{-21} m^{-3}.

What is the number of particles required to model this? In pure 3D particle mode, the concentration contribution, Δc, from a single particle is calculated [3] according to

$$\Delta c = \frac{m}{\Delta x \Delta y \Delta z}, \tag{3.2}$$

where m is the mass of the particle, and $\Delta x, \Delta y, \Delta z$ are the grid dimensions. If the total mass is set to 1, the mass of each particle is $1/N$, where N is the number of particles used. The average concentration for each concentration averaging period is calculated by adding all particles passing through the grid cell for each integration time step and dividing by the number of time steps. The time steps will in default mode vary between 1 and 60 minutes according to stability criteria taking into account the wind speed, in order to prevent particles from skipping cells from one time step to the next. From this it is possible to estimate the minimum dilution factor for a specific HYSPLIT run. For a $1^\circ \times 1^\circ$ concentration grid with 100 m height, the maximum volume (at the equator) is approximately 10^{12} m^3. For a 10^5 particle run with 3 h averaging period, the minimum dilution factor becomes $5.5 \cdot 10^{-20}$, using an extreme value of 180 time steps. Generally, the minimum value will an order of magnitude higher since the grid cells becomes smaller towards the poles, and the number of time steps normally is much smaller than the maximum value. Hence, in order to simulate the required dilution factors with reasonable statistics, at least 10^7 particles are needed. Due to limited computer resources, we had no possibility to use the number of particles required using a full 3D model, and an alternative method was used.

One way to increase the dynamic range of the calculation with limited CPU resources is to use a puff model in combination with a pure particle model. HYSPLIT offers several types of such running options. Two types of puff models can be used, Gaussian or Top-Hat. The difference between a full 3D particle model and one type of hybrid particle-puff model (pure particle model until 48 hours, then converted to Top-Hat horizontal puff and vertical particle distribution; option 104 in HYSPLIT) is presented in Fig. 3.2. As can be seen, the particle-puff model results in a less scattered concentration distribution. The resulting accumulated dilution factors for all grid cells and time steps for the two cases are also shown in Fig. 3.2. The Top-Hat run with 10^5 particles corresponds, at least with respect to dynamic range, to a pure particle run with 10^8 particles. In this work, we chose to use the hybrid Top-Hat-particle mode for the forward calculations. Each explosion was simulated using 10^5 particles/puffs, and was tracked one week forward in time.

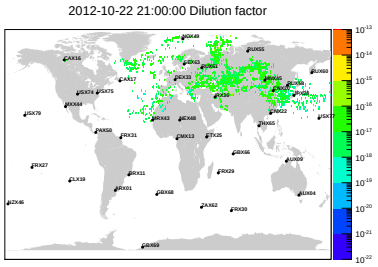

(a) Resulting ^{133}Xe concentration distribution after 14 days using a full 3D particle model with 100k particles.

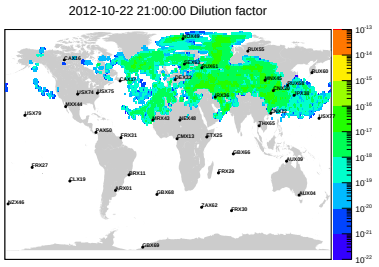

(b) Resulting ^{133}Xe concentration distribution after 14 days using a particle-puff model with 100k particles.

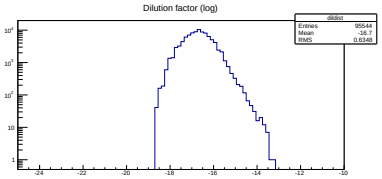

(c) Distribution of dilution factors for all grid cells and time steps for a full 3D particle model with 100k particles.

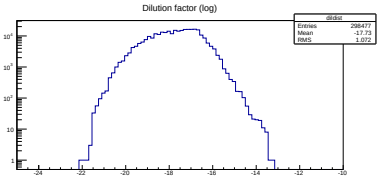

(d) Distribution of dilution factors for all grid cells and time steps for a particle-puff model with 100k particles.

Figure 3.2: Resulting concentration distributions and dilution factor distributions with full 3D particle and particle-puff models.

3.2 Modeling the Station-Measured Activity Concentrations

A C++ script named *Hysconc*, utilizing the ROOT data analysis framework [4], was developed to extract xenon activity concentrations for all four CTBT relevant xenon isotopes for given station locations, using the results from the HYSPLIT forward calculations described in previous section. *Hysconc* is able to calculate activity concentrations measured using varying sampling time and sampling start time, provided in an input file together with each station location. The source terms for the xenon isotopes ^{133}Xe,^{131m}Xe,^{133m}Xe,^{135}Xe, and ^{135m}Xe are provided in a second input file.

The activities are corrected for decay, also taking the in-growth from ^{133m}Xe and ^{135m}Xe into account. *Hysconc* produces activity concentration series for

^{133}Xe,^{131m}Xe,^{133m}Xe, and ^{135}Xe, with sampling times set individually for each station. The sample activity concentration is obtained by calculating the average of all 3 h time bins within a sample, after decay correcting the individual bins to the sample start time. A minimum activity concentration cut-off value of 0.1 nBq/m^3 was used.

The *Hysconc* output file stores all input information (network configuration, collection start times, collection times for individual stations, and source terms) as well as sample information (station, time after fission, collection start, collection stop, dilution factor, and activity concentration for ^{133}Xe,^{131m}Xe,^{133m}Xe, and ^{135}Xe). Data were calculated for 1 h and 24 h containment, and 3 h, 6 h, 12 h and 24 h collection time. This was done both for a 39 and 79 IMS station configuration, in total resulting in 16 different data sets described in the next section.

3.3 Initial Observations for the Synthetic Data Set

Some basic statistics for the 16 calculated data sets are shown in Tab. 3.2. The number of samples varies between 357 and 3356, depending on collection time and network configuration (including all samples exceeding the cut-off value of 0.1 nBq/m^3). The activity concentrations are given in mBq/m^3/kt, since they scale linearly with yield (as well as release fraction). In this way, data for any yield or leakage fraction can be obtained by multiplying with appropriate factor.

Number of stations	Cont. time h	Coll. time h	Number of samples	^{133}Xe	^{131m}Xe	^{133m}Xe	^{135}Xe
				Median activity concentration mBq/m^3/kt			
39	1	3	1832	1.59	0.0002	0.230	0.0068
		6	995	1.32	0.0002	0.200	0.0071
		12	578	1.27	0.0002	0.196	0.0084
		24	357	1.00	0.0001	0.176	0.0122
	24	3	1832	28.8	0.0109	0.739	0.0069
		6	995	23.8	0.0088	0.640	0.0072
		12	578	23.1	0.0084	0.622	0.0085
		24	357	18.8	0.0066	0.558	0.0123
79	1	3	3356	1.84	0.0003	0.276	0.0089
		6	1835	1.54	0.0002	0.232	0.0091
		12	1064	1.36	0.0002	0.234	0.0105
		24	662	1.07	0.0002	0.184	0.0146
	24	3	3356	33.5	0.0126	0.876	0.0090
		6	1835	27.9	0.0105	0.736	0.0092
		12	1064	25.3	0.0092	0.742	0.0107
		24	662	19.5	0.0070	0.585	0.148

Table 3.2: Basic statistics for the 16 generated data sets. All samples with activity concentrations larger that the cut-off value of 0.1 nBq/m^3 are included.

As an example of resulting distributions of radioxenon activity concentrations, the case with 1 h containment, 40 stations, and 6 h sampling time is shown in Fig. 3.3. The ^{133}Xe and ^{133m}Xe measurements cover 9 orders of magnitude, with the highest activity concentrations around 10^4 mBq/m^3/kt and the weakest samples in the range 10^{-5} mBq/m^3/kt. The ^{135}Xe measurements cover an even wider interval, due to larger initial activity and its shorter half-life

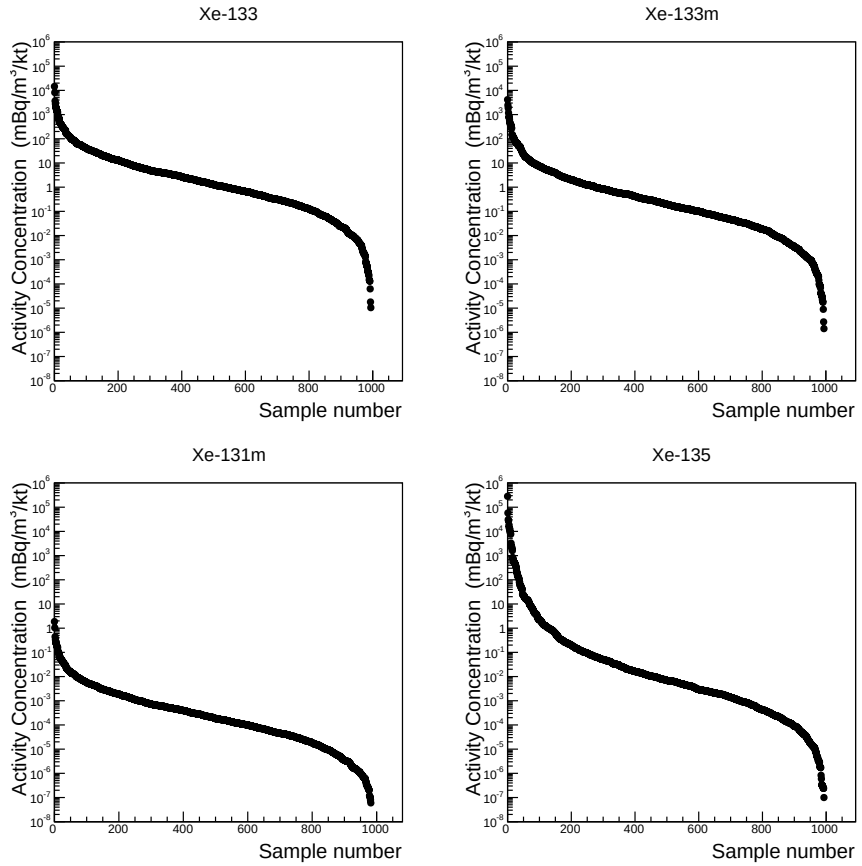

Figure 3.3: Calculated activity concentrations for the 39 IMS station case, assuming 1 h containment and 6 h sampling time.The diameter of the black circles are proportional to the number of sites exposed to an activity concentrations larger than 0.1 mBq/m^3. Open circles indicate explosions not detected within one week.

compared to ^{133}Xe. As expected, ^{131m}Xe displays the lowest concentrations, ranging from 1 to 10^{-7} mBq/m^3/kt. The small minimum values of the modeled activity concentrations gives us confidence that very sensitive systems can be reasonably well modeled for this study.

The number of stations hit by releases from individual explosions (using 1 h containment and 6 h sampling time) is illustrated in Fig. 3.4 for both the 39 and 79 IMS station cases. Generally, one can note the already well known result that many explosions in the equatorial region will go undetected, even with 79 stations. With 39 stations, 38 % of the explosions will not be detected within one week and the corresponding number for 79 stations is 23.4 %. At higher or lower altitudes, more explosions are detected due to increased air mobility in the atmosphere. The consequences of this for the network Detection Power is discussed in Chap. 4.

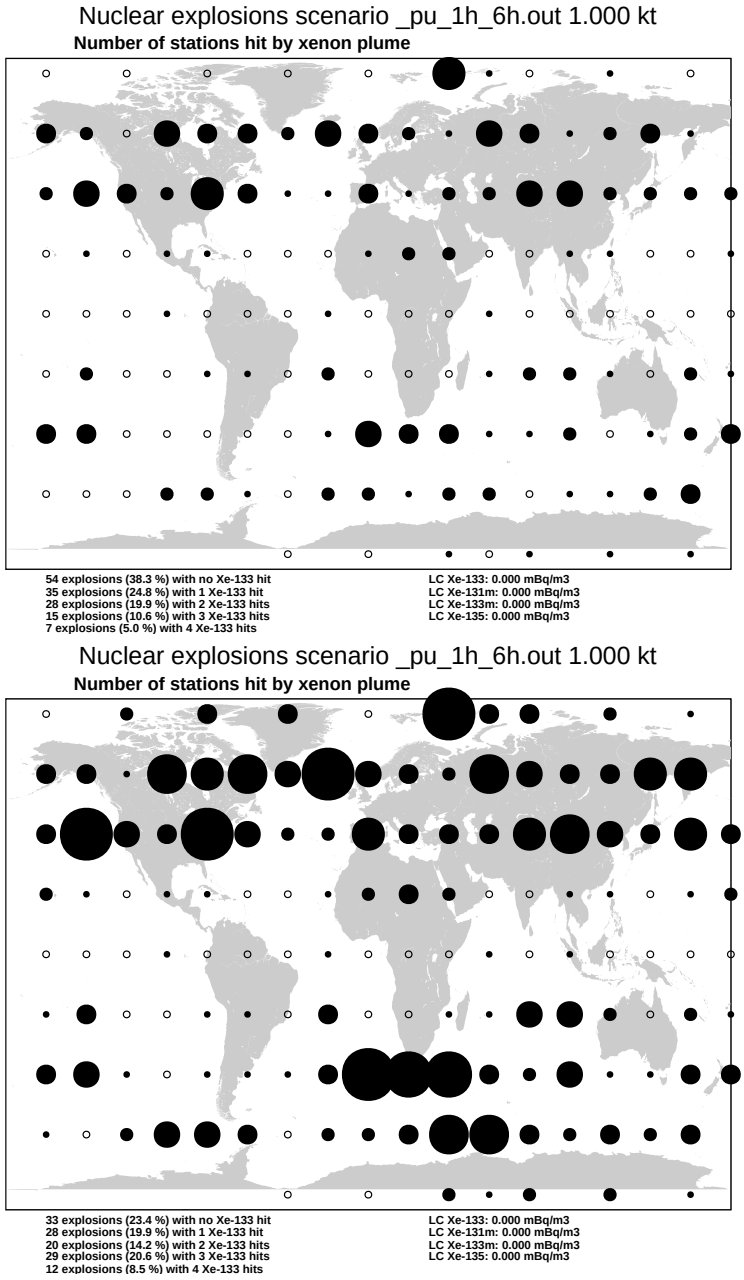

Figure 3.4: Number of stations hit for each explosion for the 40 (upper panel) and 80 (lower panel) IMS station cases, assuming 1 h containment and 6 h sampling time.

4 Network Source Detection

4.1 Detection Power as a Function of MDC

The Detection Power, defined in Chap. 2, was calculated as a function of MDC/yield for all cases in Tab. 3.2 as well as for all isotopes. Two examples from the results are shown in Fig. 4.1 and 4.2. A complete set of figures of D as a function of MDC/yield for the cases with 1 h containment time can be found in Appendix A. The corresponding graphs for the cases with 24 h containment time (not shown) are very similar.

The graphs can be used to obtain the D for systems with different MDCs as well as for different yields or release fractions. More accurate activity concentration measurements or larger activities released will move you to the left in the graph, and less accurate measurements or smaller releases will move you to the right.

Three different curves are displayed in each figure, showing the result when requiring at least one, two, or three samples detected. Detecting more than one sample per explosion is of course valuable for verification purposes. In particular, three samples are required to make a Possible Source Region used for source location (see Chap. 5).

Several interesting facts can be noted from the graphs in Appendix A:

The Detection Power will almost exclusively be determined by the capability to detect ^{133}Xe. For all other radioxenon isotopes, D will be smaller for a given MDC/yield for almost all cases. A detailed study of individual explosions showed one case where only ^{135}Xe was detected. This can occur if a station is close to the source, and the activity concentration is just exceeding the MDC for ^{135}Xe, but not for ^{133}Xe. In the first few hours following an explosion, the ^{135}Xe activity concentration will be larger than the ^{133}Xe activity concentration.

Since a relatively large part of the explosions, mostly located in the equatorial regions, are not at all detected the first week, D reaches a maximum value less than 100 %, no matter how sensitive the systems are. If only one sample is required, the maximum D is 61.8 % and 77.1 % for the 39 and 79 station cases, respectively. For ^{133}Xe, D stays relatively constant around this value for several orders of magnitudes of the MDC/yield, and starts to drop at 0.1 – 1 mBq/m^3/kt. Assuming a yield of 1 kt, this number is close to the measurement capability of current systems installed in the network. According to Tab. 3.1, an MDC/yield of 1 mBq/m^3/kt corresponds to a ^{133}Xe release of $5 \cdot 10^{14}$ Bq for a 1 kt explosion. Apparently, the capabilities of today's noble gas systems are enough to reach close to maximum detection power for such a release.

The Detection Power increases considerably when the IMS network density is increased from 39 to 79 stations. In particular one can note that for a 79 station network, it is possible to achieve same D for a 1 kt explosion as is obtained with current systems by employing equipment with about 30 times higher MDC. An MDC/yield of 0.3 mBq/m^3/kt for current systems results in a ^{133}Xe Detection Power of 55 % for 39 stations and at least one sample detected. The same D corresponds to about 10 mBq/m^3/kt in the graph for 79 stations.

The isotopic specific Detection Power for ^{135}Xe is very low for a 39 station network. To reach a D of 50 %, an MDC/yield of about 0.005 mBq/m^3/kt is required. The corresponding MDC for 79 stations is about 0.1 mBq/m^3/kt, i.e. 20 times higher.

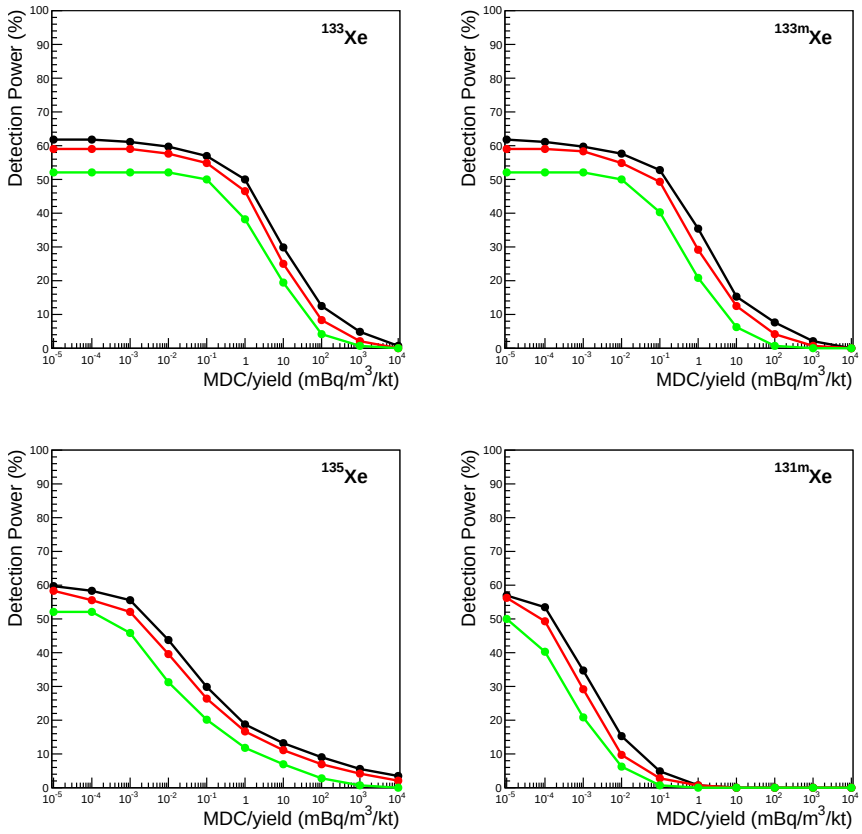

Figure 4.1: Detection Power as a function of MDC/yield for the case 1 h containment, 6 h sampling time and 39 IMS stations. The three different curves correspond to at least one (black), two (red), and three (green) samples detected.

The main difference in Detection Power as function of MDC/yield when increasing the sampling time is the number of detected samples. Requiring only one sample will give almost identical results irrespective of sampling time. However, when two or three samples are required, the advantage of decreasing the sampling time becomes obvious. For a 3 h sampling time, the difference in maximum D is only a few percent for one sample compared to three. For a 24 h sampling time, the difference is more than 20 %. The difference in D for different samples required is smaller for a network with 79 stations compared to a network with 39 stations.

4.2 Detection Power for the Model Measurement Systems

Detection Powers for different sampling times (3 h, 6 h,12 h, and 24 h) were calculated for the six model systems given in Tab. 2.2. The results for the 39 and 79 station configurations, and 1 h and 24 h containment times, are presented in Fig. 4.3.

As can be seen in these figures, the Detection Power generally is a very weak function of collection time for the different systems. For a given plume passing a measurement station, shorter sampling times will report a higher

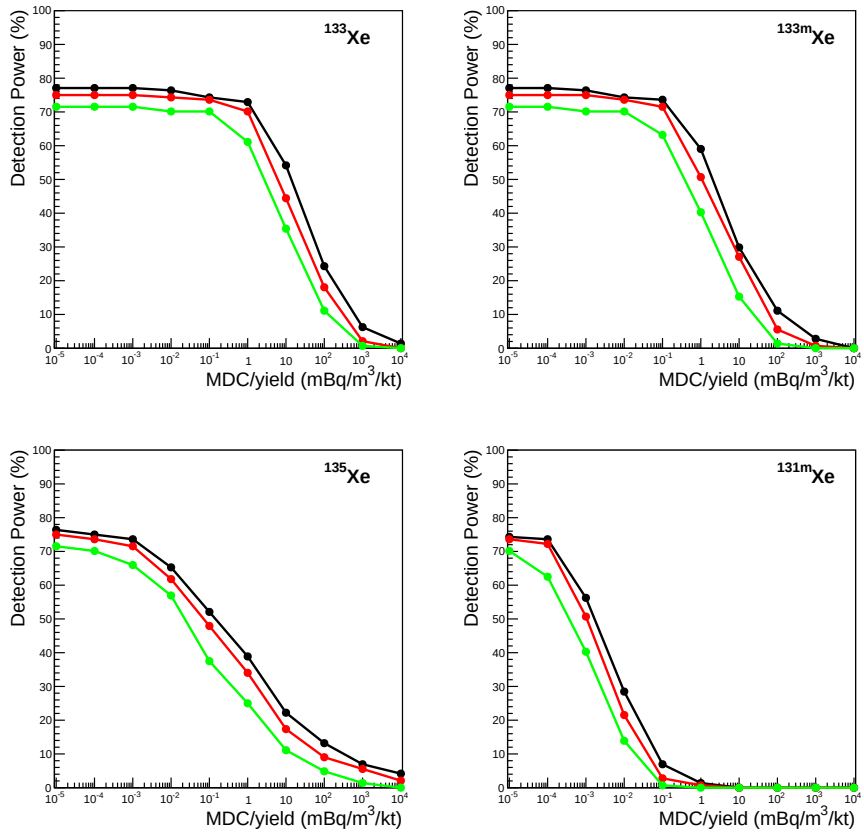

Figure 4.2: Detection Power as a function of MDC/yield for the case 1 h containment, 6 h sampling time and 79 IMS stations. The three different curves correspond to at least one (black), two (red), and three (green) samples detected.

peak activity concentration compared to a system with longer sampling time. On the other hand, the longer the sampling time, the smaller the MDC for a given system configuration, see Tab. 2.3. These two effects will generally cancel, and result in the flat distributions seen in Fig. 4.3. Only for the two least accurate of the model systems (A and E), the Detection Power shows some dependence on sampling time, increasing with longer sampling times due to the improved MDC. One should note that for ^{135}Xe, with a 9 h half life, this is less true. However, this will have no effect on D, since it is determined by the capability to detect ^{133}Xe.

It can also be observed that the difference in Detection Power is relatively small for different model systems. In the case with 39 stations and 1 h containment time the difference is less than 10 % except for system E, and in the 80 station case even smaller.

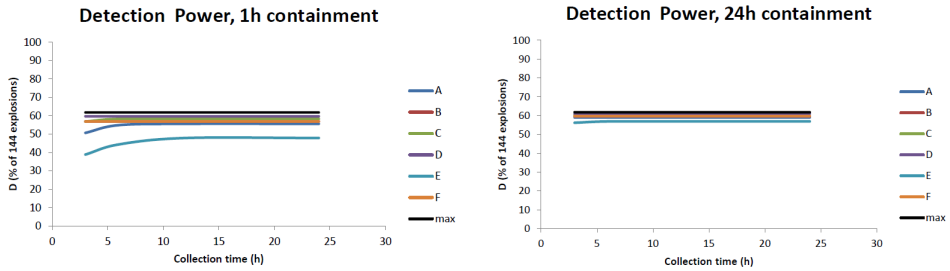

(a) Detection Power for a 39 station IMS network as a function of sampling time.

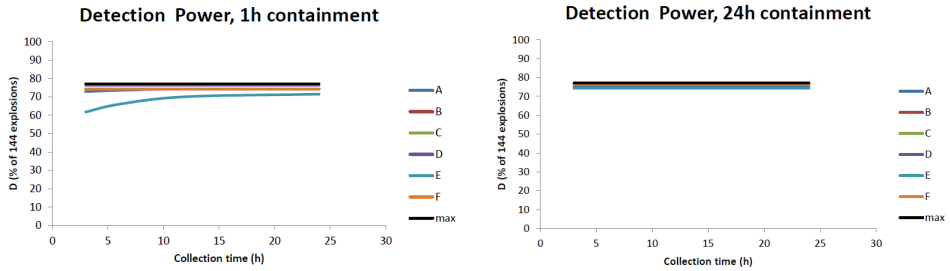

(b) Detection Power for a 79 station IMS network as a function of sampling time.

Figure 4.3: Detection Power for 39 and 79 station IMS networks as a function of sampling time using the six model systems in Tab. 6.1. The black line shows the maximum achievable Detection Power according to the simulations.

5 Network Source Location

5.1 Calculation of PSR Fields

The source location analysis was performed by calculating Possible Source Regions (PSRs) according to reference [5]. This method is based on Source-Receptor Sensitivity (SRS) fields which are backward dispersion calculations using constant particle release during the station collection time for a particular sample. The SRS fields describe the sensitivity for a particular measurement to a set of geotemporal grid points at earlier times. The PSR is a map of correlations of the SRS field and a set of measured activity concentrations at a certain time step, showing areas where the release causing the detections might be located. Grid cells with high correlations are more likely to contain the source compared to areas with low correlation. The released activity is calculated by a linear fit of the SRS field to the measured concentrations.

SRS fields were calculated using the HYSPLIT model with one degree spatial and three hour temporal resolution GDAS weather data for all the 39 or 79 noble gas stations in the IMS network. 10^5 particles were released at a height of 100 m during three hours and modeled one week backward in time from the release. This was done for a two-week period (October 7 to 21, 2012) to cover all simulated nuclear explosions. To get the SRS fields for the longer release times, i.e. 6 h, 12 h and 24 h, the 3 h releases were added.

The Swedish NDC at FOI uses the in-house developed ROOT-script *Multipsr* to calculate PSRs. To assemble the PSR fields required for this study, a script was written that produces input files to *Multipsr* for each hypothetical explosion using the *Hysconc* (see Sect. 3.2) output. The PSRs were calculated using all detected ^{133}Xe activity concentrations. The PSR for each detected explosion was calculated at explosion time, which was assumed to be known from seismic information. PSRs were calculated for all explosions, network configurations, containment times, sampling, and model systems. In total, 13824 PSRs were calculated.

5.2 Analysis of PSR Fields

5.2.1 General Results

Since time and place of the explosion is known, it is possible to analyze the usefulness of the PSR fields in many different ways. For each explosion and detection scenario, several distributions were created, such as distributions of estimated source terms, correlation at explosion location, total area of PSR, and distance and time to first station hit. Examples of such distributions are found in Fig. 5.1. The examples are from using model system F (Xenon International) with 3 h sampling time, 39 IMS stations, and 1 h containment time.

As can be seen in the figure the statistics are not very good. As seen in Tab. 2.3 the MDC for ^{133}Xe for system F with 3 h sampling time is 0.13 mBq/m^3. Fig. A.1 in Appendix A show that 55 % (79 out of 144) of the explosions will result in at least three samples detected using this MDC (at least three samples are required to make a PSR). For cases with longer sampling times (resulting in fewer samples), the statistics will be even lower. As can be seen in Fig. A.4, only 25 % of the explosions can be located using the PSR technique if the collection time is 24 h and all other parameters stay the same.

Nevertheless, several conclusions, which are similar for all cases studied,

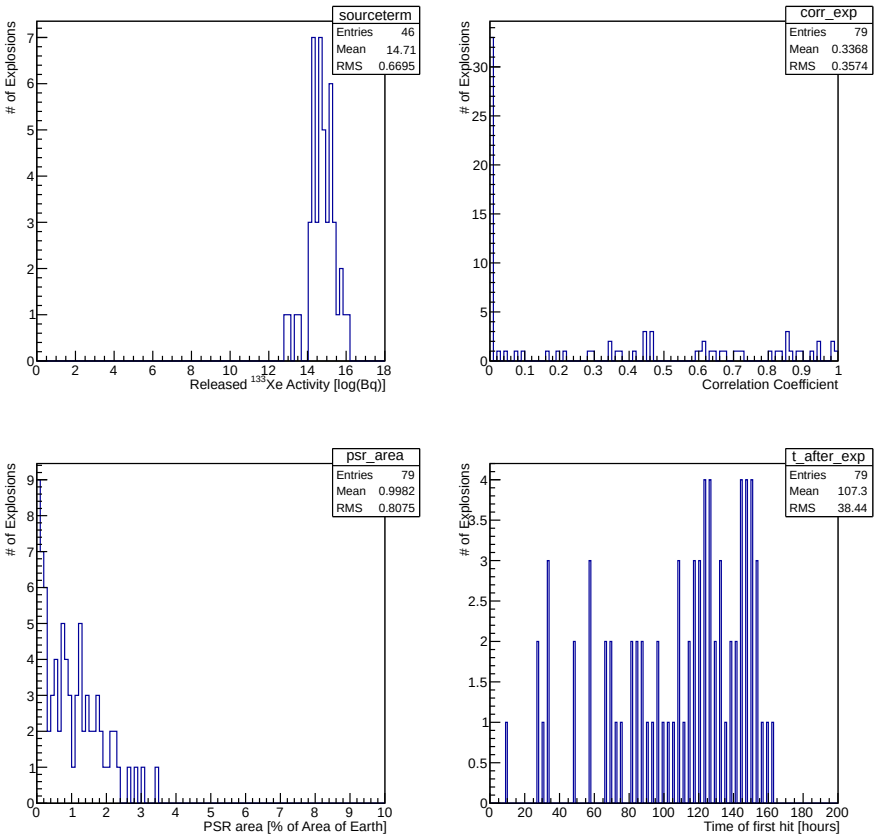

Figure 5.1: Examples of results from the PSR analysis. Results are shown for the following case: Model system F, 3 h sampling time, 39 IMS stations, and 1 h containment time. The analyzed PSRs are calculated at explosion time. Upper left panel: Calculated released ^{133}Xe activity for the explosion location. Upper right: Correlation coefficient at explosion location. Lower left: Area of the PSR as fraction of Earths area. Lower right: Time between explosion and first sample measurement in the station network.

can be drawn using Fig. 5.1:

The correlation coefficient at the grid point containing the explosion location and time is zero in about 40 % of the cases. This is attributed to the uncertainties in the SRS field, partly caused by the limited number of particles used in the simulation, but also due to other model uncertainties.

The estimation of released activity at the explosion location, only possible when the correlation coefficient was larger than zero at that grid point, agrees well with the assumed release. In the case shown in Fig. 5.1, the released ^{133}Xe activity was $5.1 \cdot 10^{14}$ Bq, see Tab. 3.1. The distribution of calculated activities had a mean of $6.2 \cdot 10^{14}$ Bq, with a one standard deviation range between $1.6 \cdot 10^{14}$ and $2.3 \cdot 10^{15}$ Bq.

The mean PSR area was in this case 1.00 % of the area of Earth, corresponding to $5.1 \cdot 10^{6}$ km^2. The PSR area was defined as all grid points with correlation coefficient larger than zero.

The mean time between explosion and first detection was 107 hours, or 4.5 days. The shortest detection time was 10 hours. Selected results from the

Number of stations	System	Coll. time (h)	Number of explosions detected	Number of explosions located	PSR Source Activity Bq	Mean PSR area (% of Earth)
39	A	3	71	41	$6.2 \cdot 10^{14}$	0.91
		6	59	36	$6.3 \cdot 10^{14}$	1.06
		12	52	33	$9.3 \cdot 10^{14}$	1.24
		24	40	28	$1.6 \cdot 10^{15}$	1.64
79		3	100	58	$3.1 \cdot 10^{14}$	0.81
		6	91	56	$6.3 \cdot 10^{14}$	0.95
		12	81	54	$7.4 \cdot 10^{14}$	1.13
		24	71	53	$1.2 \cdot 10^{15}$	1.34
39	F	3	79	46	$5.1 \cdot 10^{14}$	1.00
		6	72	39	$6.6 \cdot 10^{14}$	1.27
		12	62	42	$7.6 \cdot 10^{14}$	1.45
		24	47	33	$1.6 \cdot 10^{15}$	1.67
79		3	103	61	$5.0 \cdot 10^{14}$	0.88
		6	99	59	$6.2 \cdot 10^{14}$	1.09
		12	85	58	$6.5 \cdot 10^{14}$	1.23
		24	78	58	$1.0 \cdot 10^{15}$	1.45

Table 5.1: Selected results from analysis of PSRs for model systems A (present SAUNA) and F (Xenon International). In total 144 explosions were analyzed. The PSR source activity is calculated at the correct time and position of the explosion. The released activity was $5.1 \cdot 10^{14}$ Bq.

PSR analysis for the present SAUNA and XI are shown in Table 5.1. As can be seen, both the estimated release source term and the PSR area increase with sampling time. The release source term agrees best with the correct value ($5.1 \cdot 10^{14}$ Bq) for 3 h collection time. For 24 h collection time, the released activity is overestimated a factor 2 to 3.

5.2.2 Location Error

The capability of the IMS network to locate a release source was in this study estimated using the FoM Location Power, defined in Sect. 2.1. The definition of Location Power requires the location error to be estimated. In a real situation, possible locations of a release source would be identified by calculating the PSR and manually identify areas with high correlations. This information would then be combined with other information, such as seismic events, known nuclear sites and geographic information. The area with highest correlation does not necessarily indicate the position of actual release source. Such a process is not easily automated, as is required in this study. Instead, we apply a simplified algorithm. We assume that the analyst concludes that the source is located at the grid point with highest correlation coefficient in the PSR calculated at the time of the explosion, given by a seismic signal. The location error is then given by the distance between this point and the real explosion location. A similar approach has been used in the past [5].

An example is given in Fig. 5.2, were we show the resulting location error for one of the notional explosions, using the XI system with different sampling times. In this case, the location error stay approximately the same for different collection times.

The location error shows large variations for the different explosions, as

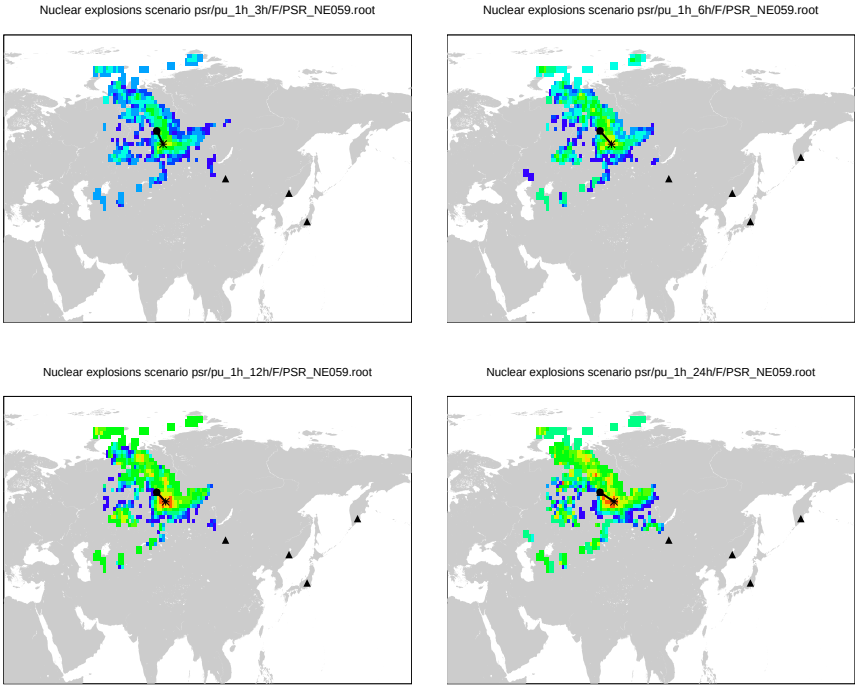

Figure 5.2: Examples of resulting location errors for one of the notional releases, using model System F (XI), assuming 1 h containment time and a 39 station IMS network. The location error is indicated with the solid line between the actual release point (circles) and maximum correlation (stars). The stations detecting the release, used to calculate the PSR, are marked with black triangles.

can be seen in the left panel of Fig. 5.3, showing resulting location errors for all detected explosions using model system F (Xenon International), with 6 h sampling time, 1 h containment time and 39 IMS stations. The majority of location errors are below 1000 km, with a small tail ranging up to much larger errors.

An alternative way to obtain the location error was also investigated. Instead of using the absolute maximum correlation in the PSR, the closest grid cell with a local maximum larger that 0.7 was used. This generally resulted in smaller location errors, as can be seen in the right panel in Fig. 5.3.

The median location error, using both error methods, is plotted as a function of system sampling time in Fig. 5.4, again using model system F as an example. Only explosions that were detected for all sampling times were included in the calculation of the median location error. As can be seen, the location error using the absolute maximum correlation, quite counterintuitive, generally improves with sampling time. With the other definition of location error, the error stays constant with sampling time. One reason for this behavior could be that the plume width at the stations many times is larger than the maximum collection time of 24 hours, and thus one gains little by decreasing the sampling time. A preliminary study of the plume widths indicated that this could be the case.

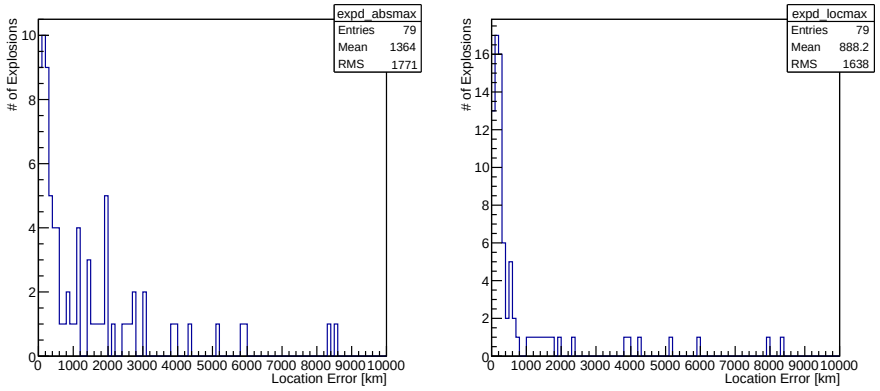

Figure 5.3: Location error distributions for model system F (Xenon International), using 6 h sampling time, 1 h containment time and 39 IMS stations. Left panel: location error defined as distance between actual release and maximum correlation in PSR. Right panel: location error defined as distance between actual release and closest local correlation maximum larger than 0.7.

5.3 Results for Location Power

Like all network FoMs used in this study, Location Power is given by a binary decision performed for each explosion, in this case whether or not the location error exceeds a certain threshold value. The simplest option would have been to choose a specific distance as threshold. But since we wanted to allow for a location error increasing with transport time, a relative error was used, based on transport time to first detection in the network. The maximum allowed location error was therefore set to 1500 km after a transport time to first detecting station of one week. Using a mean air transport velocity of 10 m/s, this corresponds to a location error of 25 %. The explosions fulfilling this condition were considered "located" according to the Location Power definition. The method is illustrated in Fig. 5.5, using the same location errors as in Fig. 5.3.

The resulting Location Powers for all model systems, containment times and network configurations are shown in Fig. 5.6. All reported Location Power results are obtained by taking the error as the distance between true release position and the absolute maximum correlation in PSR.

As a consequence of the behavior of the location error, the Location Power also stays approximately constant with sampling time. The difference between the present SAUNA and e.g. model system F is 5 – 10 % for 39 stations and 1 h containment time. For a 79 station network, as well as for 24 h containment, the difference is slightly smaller. The Location Power for short sampling times increases from about 30 % to about 40 % when the number of stations is doubled.

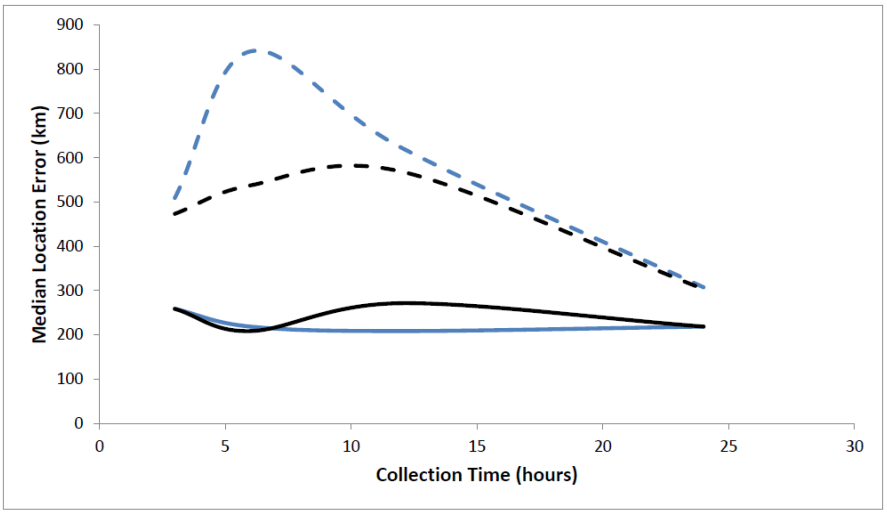

Figure 5.4: Median location error for model system F (Xenon International) versus system sampling time, assuming 1 h containment time and 39 (blue) and 79 (black) station network configurations. Dashed lines show the results when assuming the location error to be the distance between the absolute maximum correlation in the PSR and the real release location. Solid lines are obtained using the closest local maximum correlation larger than 0.7.

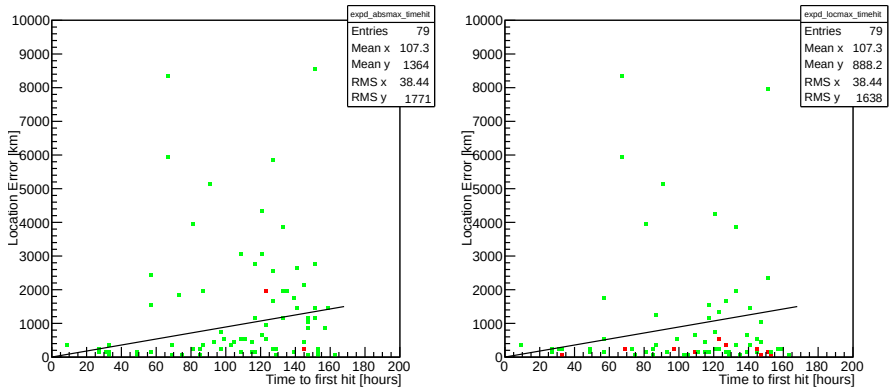

Figure 5.5: Illustration of the method used to calculate Location Power. The graphs show time between explosion and first station hit versus location error, using the same case as in Fig. 5.3. Explosions with location errors fulfilling the criterion corresponding to 1500 km after one week will fall below the solid black line, and count at "located". The left panel shows location errors calculated using the absolute maximum correlation, and in the right panel, the location error is obtained by using closest local correlation maximum larger that 0.7.

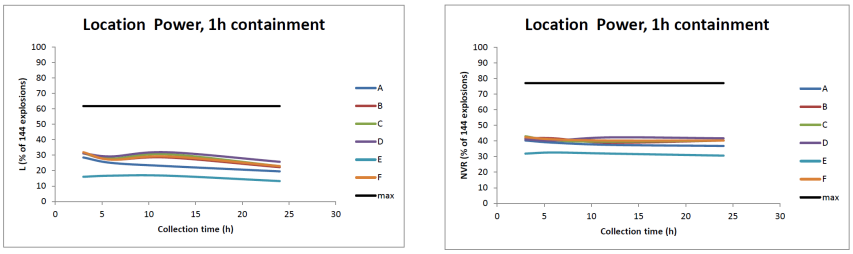

(a) The Location Power as a function of sampling time for the 39 (left) and 79 (right) station network configurations and 1 h containment time.

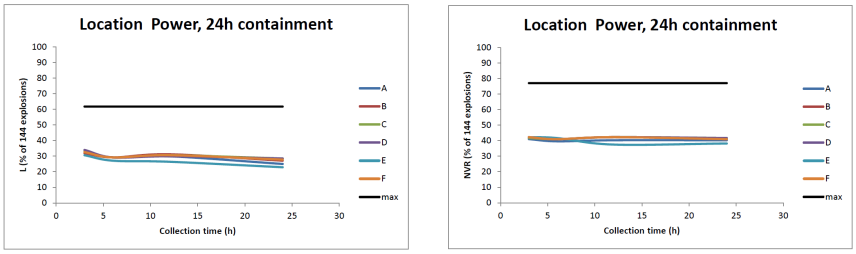

(b) The Location Power as a function sampling time for the 39 (left) and 79 (right) station network configurations and a 24 h containment time.

Figure 5.6: The Location Power as a function of model systems A-F sampling time for the 39 and 79 station network configurations and 1 h and 24 h containment time. The black line corresponds to maximum possible Location Power according to the calculations.

6 Network Source Discrimination and Timing

In addition to source location, the data obtained from measurements of noble gas produced by a nuclear explosion would be used to draw conclusions on the source itself. The objectives of such analysis would include evaluating the likelihood of various hypotheses concerning the process that produced the effluents detected, e.g. whether it was a nuclear explosion or a reactor emission, and determining the *event timing* based on each hypothesis found to be competitive.

The type of analysis required to produce this sort of information is based on nuclear properties: the formation and decay of nuclides in quantities and rates that can be predicted for any given scenario, if by scenario we understand the release into atmosphere at specified time and rate of a specified fraction of each nuclide produced in a specified nuclear process. Consequently, we use the term *nuclear analysis* for this type of source characterization.

6.1 Network Data Quality Indicators for Source Characterization

The Rejection Power (R) and Timing Power (T) Figures of Merit defined in Sect. 2.1 were developed to capture the essential elements of the nuclear analysis for source characterization. Additional indicators of interest include

> *Timing Error*, defined as the average (over the timed fraction T of explosions) *error* in the source event timing;
>
> *Timing Uncertainty*, defined as the average (over the timed fraction T of explosions) *uncertainty* in the source event timing;

The single-data set timing uncertainty (the same quantity that is averaged over all explosion data sets to produce the *Timing Uncertainty*) was used as a quality filter for the Timing Power (T) statistic: only explosions resulting in network data sets allowing timing to better than 6 h precision were allowed to contribute to the scoring of T.

6.2 Generating Source Characterization Figures of Merit from Synthetic Concentrations

Implementing the FoMs defined in Sect. 2.1 and 6.1 requires the choice of a *correct scenario* and a *false scenario* and a method of generating the network response to a release of radioxenon (consistent with the correct scenario) in the form of a set of measured values, $c_{i=1-4}$, for all four xenon isotope concentrations, including measurement uncertainties, σ_{c_i}, critical levels, L_{c_i}, and detection limits, MDC_i. L_{c_i} and MDC_i can be part of hypothetical system specification, while c_i and σ_{c_i} must be internally consistent, i.e. the measurement-to-measurement variation in c_i must be consistent with σ_{c_i}, and with the specified L_{c_i} and MDC_i.

6.2.1 Synthetic Data Sets

The generation of synthetic data sets of *measurements* including *associated uncertainties* consistent with given L_{c_i} and MDC_i was done by a numeri-

cal simulation based on the ATM forward-modeling results, see Chap. 3, and on a simplified two-parameter measurement and analysis model described in Sect. 6.3. In the following, we will use the term *data set* for a set of synthetic measurement results (isotopic concentrations with uncertainties) generated by a given network in response to a given xenon release, i.e. notional explosion. The full set of 144 notional explosions would generate 144 data sets (some consisting of no measurements at all) for each network, where a network is defined by a number of sampling locations (39 or 79) and the two parameters of the measurement and analysis model for the systems installed in the network; the analysis power S , and the expectation value of background counts, n_0, for the measurement system.

The sample collection time is not explicitly a network parameter in this sense since it is embedded in the parameter S, see Eqn. 6.3. However, the data sets generated by each notional explosion are of course also influenced by the sample collection times used in the network, because with constant measurement system parameters (S,n_0) and more samples collected, potentially more non-zero data would be generated and this would affect the characterization FoMs. In order to evaluate the effect of changing the sample collection time (but nothing else), a set of measurement systems was used, each defined by its two parameters (S,n_0) at a given sample collection time; then with each different sample collection time, a new system parameter S (and equivalently, new L_c and MDC) consistent with the new sample collection time was computed assuming the change in sample collection time but no change in any other technical system parameters.

In summary, as with the localization part of the study presented in Sect. 5, networks of 39 and 79 noble gas model systems of type A – F, defined in Tab. 2.2, were evaluated based on sample collection times of 3, 6, 12 and 24 hours. The (S,n_0) parameters of the model systems for each of the four relevant xenon isotopes and for each sample collection time are given in Tab. 6.1.

6.2.2 Source Scenarios

The scenarios defined for the hypothesis testing were generated using the *Baxe* code, with the correct scenarios being based on radioxenon release from nuclear explosions and also supplying the source terms for the generation of the synthetic concentrations (see Chap. 3). The network response to two different correct scenarios was studied, both based on fast-neutron fission of ^{239}Pu, see upper part of Tab. 6.2. The *Rejection Power* was defined using two very different false scenarios, both based on irradiation of uranium in thermal reactors, see lower part of Tab. 6.2.

The isotopic ratio trajectories expected from the four scenarios in Tab. 6.2 are shown in the multi-isotope ratio correlation (MIRC) plots [8] in Fig. 6.1. These five sets of relationships were used in an automatic analysis of each synthetic data set.

6.2.3 Automated Nuclear Analysis of Synthetic Data Sets

The automated analysis of the synthetic data is performed by the *Baxfit* code according to a set of prescriptions designed to emulate, to some degree, a real-life analysis of verification data.

6.2.3.1 Method and Definitions

To facilitate presentation and discussion of the process and results, some terms need to be defined:

System	Coll. time	^{131m}Xe		^{133}Xe		^{133m}Xe		^{135}Xe	
	h	S $\frac{\text{cts}}{\text{mBq/m}^3}$	n_0 cts	S $\frac{\text{cts}}{\text{mBq/m}^3}$	n_0 cts	S $\frac{\text{cts}}{\text{mBq/m}^3}$	n_0 cts	S $\frac{\text{cts}}{\text{mBq/m}^3}$	n_0 cts
A	3 h	48	38	62	280	42	25	26	309
	6 h	96	38	122	280	83	25	46	309
	12 h	191	38	241	280	160	25	76	309
	24 h	377	38	466	280	296	25	106	309
B	3 h	77	3.8	114	28	66	2.5	49	30.9
	6 h	154	3.8	226	28	129	2.5	88	30.9
	12 h	305	3.8	445	28	248	2.5	144	30.9
	24 h	602	3.8	862	28	461	2.5	202	30.9
C	3 h	483	38	617	280	423	25	258	309
	6 h	963	38	1223	280	831	25	463	309
	12 h	1912	38	2407	280	1598	25	757	309
	24 h	3769	38	4658	280	2964	25	1062	309
D	3 h	772	3.8	1141	28	658	2.5	492	30.9
	6 h	1538	3.8	2263	28	1291	2.5	883	30.9
	12 h	3054	3.8	4451	28	2484	2.5	1443	30.9
	24 h	6020	3.8	8616	28	4605	2.5	2024	30.9
E	3 h	24	380	31	2800	21	250	13	3090
	6 h	48	380	61	2800	42	250	23	3090
	12 h	96	380	121	2800	80	250	38	3090
	24 h	188	380	233	2800	148	250	53	3090
F	3 h	263	21	336	153	230	14	136	169
	6 h	525	21	666	153	450	14	245	169
	12 h	1042	21	1309	153	866	14	400	169
	24 h	2053	21	2534	153	1606	14	561	169

Table 6.1: Measurement and analysis parameters (S,n_0) used in the nuclear analysis evaluation for the model systems A–F, for different sample collection times.

A *concentration* is an "actual value" for radioxenon isotope activity concentration that a sample is exposed to (as given by the *Hysconc* ATM post-processing code, see Sect. 3.2). *Hysconc* computes the *concentration* from the released source term, the appropriate HYSPLIT atmospheric transport calculation result and the sampling period (sampling start time and duration of sampling).

A *measurement* is an analysis result, with an uncertainty, for one isotopic activity concentration in one sample. This is a stochastic value determined in each instance by the *concentration* (used as an expectation value) and the appropriate (S,n_0) measurement and analysis parameters (see Sect. 6.3).

A *detection* is a *measurement* that is above the critical level (L_c) for the isotope concerned.

A *data set* is the set of network *measurements* within one week (168 hours) after the release of radioxenon from a notional explosion.

Data points are relationships among *detections* in the same sample, e.g. the isotopic ratios used in *MIRC plots* (see below).

Nuclear explosion scenario	Prompt fission nuclide		Containment time
baxe_pu239_1	^{239}Pu		1 h
baxe_pu239_24	^{239}Pu		24 h
Fission yields and decay data from ENDF/B-VII.1 [6]			
Reactor irradiation scenario	Reactor fuel	Irradiation time	Containment time
baxe_pwr_300d	PWR (UO_2) 5 %	300 d	1 h
baxe_nrx93prc_30min	HEU metal 93 %	30 min	15 min
Fuel depletion using SCALE [7] models; decay data for post-release period from ENDF/B-VII.1 [6]			

Table 6.2: Details of *Baxe* code scenarios used for source term generation and timing analysis (upper part) and for rejection power estimates, i.e. false scenarios (lower part).

Multi-isotope ratio correlation (MIRC) plots are five specific isotopic ratio relationships used in the analysis of *data sets*. The definitions of these plots are based on the detailed analysis by Kalinowski et al. [8] on the utility of xenon isotopic ratio relationships in source discrimination and they are most easily explained graphically (see Fig. 6.1):
Plot 0 has the ratio ^{135}Xe/^{133}Xe on the vertical axis and ^{133m}Xe/^{131m}Xe on the horizontal,
Plot 1 has ^{133m}Xe/^{133}Xe on the vertical axis and ^{133m}Xe/^{131m}Xe on the horizontal,
Plot 2 has ^{135}Xe/^{131m}Xe on the vertical axis and ^{135}Xe/^{131m}Xe on the horizontal,
Plot 3 has ^{135}Xe/^{133m}Xe on the vertical axis and ^{135}Xe/^{131m}Xe on the horizontal,
Plot 4 has ^{135}Xe/^{133}Xe on the vertical axis and ^{133m}Xe/^{133}Xe on the horizontal.

Rejection of the *false scenario* is a possible outcome of the analysis of a *data set*, or equivalently of the network response to radioxenon emission from a given notional explosion. It means that the *data set* contains enough information to support the conclusion that the source of detected radioxenon *was not* the *false scenario* (which typically would be a non-CTBT relevant source such as a reactor emission). The rules for registering a *rejection* on the basis of a *data set* are given in Sect. 6.2.3.2.

Note that only *detections* were used in the nuclear analysis; i.e. in order to be used either to test the "false scenario" hypothesis (R score) or explosion timing (T score), measurement and "analysis" of an isotope in a sample had to yield a value greater than the 95 % critical level L_c. This is not self-evidently the best way to utilize verification data in every conceivable case. Nevertheless, for use in an automated algorithm it was deemed the most feasible and transparent method. The only exception to this rule was to allow use of the MDC for ^{133m}Xe or ^{135}Xe to set an upper limit on the ratio of either of these isotopes to ^{133}Xe for use in certain cases in connection with *Plot 4* (see below).

Another non-trivial choice of method for the analysis simulation underlying the nuclear analysis part of the study was whether to allow zero or very low-level

concentrations to influence the results. To re-capitulate, 5 % of measurements on a zero concentration will yield a detection if the detection criterion (L_c) is set at this false alarm rate, as it conventionally is. Measurements on progressively higher concentrations will yield progressively higher likelihood of returning a detection, until when the concentration reaches the MDC, the probability that measurement will result in a detection is 95 %. If one wishes to avoid the effect of false alarms in the data sets, some sort of threshold may be set on the *concentrations* allowed in the analysis, such as restricting them to be non-zero or only allowing concentrations above the MDC to result in detections.

The effect of false alarms may be seen by comparing overlaid sets of data points from all 144 explosions in Fig. 6.2 (where no conditions have been set on the concentrations) with Fig. 6.3 (where only concentrations greater than MDC have been allowed). The effect on Rejection Power appears from this comparison to be marginal. It is also difficult to predict for a general case, since the distribution of data points from false alarms will not be uniform in the MIRC, but will depend on details in the relative error structure of the measurements for the isotopes involved. In any case, the appearance of false alarms in data sets is a realistic effect in the sense that it would also be present in a real analysis of real verification data. Consequently, it was decided not to employ any filter for the concentrations to be analyzed, and Fig. 6.2 rather than Fig. 6.3 is representative of the sets of data points used in the study.

6.2.3.2 Determination of Rejection Power

To register a rejection on the basis of a data set, the data points formed from the data set for any one of the five MIRC plots must deviate sufficiently from the model trajectory of the false scenario in that MIRC plot. The degree of deviation of a data set with N data points from the false scenario trajectory is expressed by the parameter Δ:

$$\Delta = \frac{1}{N}\sum_{i=0}^{N-1}\frac{d_i^2}{\sigma_i^2} \tag{6.1}$$

where d_i is the distance of closest approach of the false scenario trajectory to data point i, and σ_i is the distance from the data point to its uncertainty ellipse in the direction of closest approach (see Fig. 6.4), so that d/σ is a measure of the significance of the deviation of the data point from the scenario trajectory.

A rejection is generated if $\Delta > a$, where a is chosen based on the quantiles of the χ^2 distribution with N degrees of freedom so that $P(\chi^2_\nu/\nu > a) = 0.01$ if $\nu = N$.

In case ^{133}Xe and ^{133m}Xe, but not ^{135}Xe, are among the detections for a sample, the MDC for ^{135}Xe is used with ^{133}Xe and ^{133m}Xe to test for rejection based on the relationship expressed by *Plot 4* (^{135}Xe/^{133}Xe versus ^{133m}Xe/^{133}Xe). Explicitly, for such cases rejection is triggered *unless* all of the following three conditions are fulfilled for any time t at which the false scenario is defined:

$$\begin{aligned}
\frac{\mathrm{MDC}_{135}}{c_{133}-\sigma_{133}} &\geq \left[\frac{c_{135}(t)}{c_{133}(t)}\right]_{\text{false scenario}} \\
\left[\frac{c_{133m}}{c_{133}}\right]_{\text{upper limit}} &\geq \left[\frac{c_{133m}(t)}{c_{133}(t)}\right]_{\text{false scenario}} \\
\left[\frac{c_{133m}}{c_{133}}\right]_{\text{lower limit}} &\leq \left[\frac{c_{133m}(t)}{c_{133}(t)}\right]_{\text{false scenario}}
\end{aligned} \tag{6.2}$$

where MDC_{135} is the MDC for ^{135}Xe, c_{133} and c_{133m} are the activity concentrations of ^{133}Xe and ^{133m}Xe, respectively, σ_{133} is the uncertainty in c_{133} and the upper and lower limits on the ratios are determined using Fieller's theorem [9]. Fig. 6.5 illustrates schematically rejection or non-rejection of a scenario based on conditions of the kind specified in Eqn. 6.2.

In case ^{133}Xe and ^{135}Xe, but not ^{133m}Xe, are among the detections for a sample, the MDC for ^{133m}Xe is used in the corresponding way with ^{133}Xe and ^{135}Xe to test for rejection.

As defined in Sect. 2.1, the Rejection Power (R) for a given network is the percentage of explosions (out of 144) for which the "false scenario" could be rejected. Since the R score is the outcome of a numerical simulation of measurement and analysis (with expectation values derived from HYSPLIT/*Hysconc*-generated station concentrations), the score will be slightly different in each numerical experiment. The final result for each network was derived as an average of 400 numerical experiments on the 144 explosions.

6.2.3.3 Determination of Timing Power

The Timing Power score T is based on the average outcome of analyses of ^{135}Xe/^{133}Xe ratios in each data set. A timing estimate is done by an error-weighted least-squares fit of the "measured" ^{135}Xe/^{133}Xe ratios to the expected ^{135}Xe/^{133}Xe trajectory for the correct explosion scenario. The uncertainty in the estimate is given by the least-squares fit. If only one "measured" ^{135}Xe/^{133}Xe ratio is available, the timing uncertainty is derived from the error bars on that ratio.

To illustrate the timing analysis process, Fig. 6.6 shows example data sets and resulting timing estimates for one explosion, for the present SAUNA and the projected XI systems in a 39 station network operated with 12 h sample collection times. The sensitivity and precision of the XI-equipped network is considerably better, resulting in a higher-quality data set that can be used to obtain a better timing estimate.

Fig. 6.7 shows an example of timing outcomes for all 144 explosions. The timing errors are expressed as deviations from the true fission time. As the figure shows, many explosions can be timed with good precision (small uncertainties) and accuracy (close to zero error). Some explosions are timed with larger uncertainty, with statistical spreads in errors consistent with the larger uncertainty. A number of explosions have very large timing errors (and uncertainties). This is due to the effect of "spurious" detections (false positives) of ^{135}Xe and/or ^{133}Xe, which happen when the actual concentrations are zero or far below MDC, but an unusually large fluctuation in the stochastic "measurement" process results in a "detection" outcome. With the L_c at the conventional 5 % false-positive setting, this will happen on average once in 20 measurements. The effect of false positives is illustrated by Fig. 6.8, where another outcome of timing all 144 explosions is compared to a case where the ^{135}Xe concentrations have been set to zero – thus all ^{135}Xe/^{133}Xe data points result from false-positive ^{135}Xe (and possibly in a few cases also false-positive ^{133}Xe).

Fig. 6.9 shows average timing error and timing uncertainty (over 400 numerical experiments) for the six model systems operated at different sample collection times in a 39 and a 79 station network.

The Timing Power score T is incremented whenever the network data set from an explosion can be used to produce a fission time estimate to better precision than six hours. If no "measured" ^{135}Xe/^{133}Xe ratio is available, or if the uncertainty is greater than six hours, T is not incremented.

The choice of six hours as the limit of precision was guided by the consideration that the total uncertainty in timing determination from model uncertainties (differences between nuclear data evaluations as well as nuclear data uncertainties) and lack of knowledge of scenario details (primarily confinement time) would be of the order of 60 hours, see Fig. 6.10. We therefore define an adequately timed explosion as one where ^{135}Xe/^{133}Xe measured data quality does not add appreciably to this uncertainty – and define "not appreciably" to mean 10 % (or 6 hours).

The Timing Power (T) for a given network is the percentage of explosions (out of 144) for which precise enough timing could be obtained. As the Rejection Power, R, T is the outcome of a numerical simulation and will vary stochastically. The final result for each network was derived as an average of 400 numerical experiments on the 144 explosions.

6.3 Parametrization of Generic Xenon Detection Systems

In the network response analysis, we assume an analysis model for each isotope based on isotope net counts, N, determined by simple subtraction of isotope-specific background, n_0, from gross counts, n, in a region of interest relevant for the isotope: $N = n - n_0$. The two system parameters of the model (per isotope) are the expectation value of the background counts n_0 and the analysis power S, expressing the net counts per concentration unit.

$$C = \frac{N}{\varepsilon B} \frac{\lambda^2}{(1 - e^{-\lambda t_c}) e^{-\lambda t_p} (1 - e^{-\lambda t_a})} \frac{t_c}{V} = \frac{N}{S} = \frac{n - n_0}{S} \tag{6.3}$$

$$\sigma_C^2 = \frac{\sigma_n^2 + \sigma_0^2}{S^2} = \frac{n + n_0}{S^2} \tag{6.4}$$

$$L_c = \frac{k\sigma_0}{S} = \frac{k}{S}\sqrt{n_0} \tag{6.5}$$

$$\mathrm{MDC} = \frac{1}{S}(k^2 + 2k\sqrt{n_0}) \tag{6.6}$$

Note that:

> The parameter n_0 is affected by changing e.g. the detector shielding or the spectral resolution (changing the number of background counts in a spectral region used in the analysis).
>
> The parameter S is affected by changing e.g. the detection efficiency (changing the number of "signal" counts in the spectrum for a given concentration).
>
> If the background is all ambient background, i.e. unrelated to sample content, an increase in sample collection time but not in sample counting time should increase S but not affect n_0.
>
> An increase in sample counting time should increase both S and n_0.

It is important to recognize that although the parameters (S,n_0) can easily be calculated from sampling and measurement system parameters, they are designed to represent a generic process of radioactivity sampling, measurement and analysis. The (S,n_0) parametrization is introduced as an expedient to perform a large number of automated generic "measurements" and "analyses on radioxenon concentrations. In particular, the generic background parameter n_0 represents a sometimes drastic simplification compared to a real-world SAUNA

measurement analyzed using e.g. the net count algorithm in that it does not account for inter-isotope interference (i.e. the sensitivity and precision of a measurement of, say, ^{133m}Xe is not affected by the presence of, say, ^{133}Xe). A more complex parametrization could have been developed to account for such effects, but at considerable cost in clarity. More importantly, the more complex the model, the more general applicability would be sacrificed by necessary assumptions on detection system (SAUNA plastic scintillator – NaI beta-gamma detector) and analysis method (ROI-based net counts algorithm).

Examples of the variation of the generic parameters S and n_0 with some technical system parameters for an actual SAUNA system are given in Appendix B (e.g. Fig. B.29 and B.44). The latter figure illustrates the discussion in the previous paragraph: For a real (or at least fully realistic) system, measurement and analysis, n_0 for ^{131m}Xe is seen to increase with sample collection time t_c. This is because a SAUNA spectrum will contain more ^{133}Xe interference counts in the ^{131m}Xe region the more xenon was sampled. If a spectrum from a sample containing the radioxenon concentrations assumed in this particular case is analyzed using the net count algorithm, the result is the trend shown in the figure. In the generic (S,n_0) model, however, we do not wish to introduce the complexity of concentration-dependent background, so n_0 is independent of t_c.

The (S,n_0) model can be used to illustrate general behavior by calculating various network characteristics, including the Rejection Power, R, on an (S,n_0) grid. Fig. 6.11 shows the average results (over 400 numerical simulations) for selected network performance indicators. The calculation shown assumes a 39 station network of SAUNA systems operating with sample collection time 12 hours, the short-irradiation false scenario and the 1 h containment release scenario. The (S,n_0) scales are expressed as multipliers of the isotopic (S,n_0) parameters for present SAUNA (model system A). All isotopic (S,n_0) sets are assumed to vary by the same multiplier at each grid point. Fig. 6.12 shows the same results for a 79 station network of SAUNA systems.

6.4 Rejection Power Results

Results for the Rejection Power, R, of networks with the specific model systems A–F are shown in Fig. 6.13. Each curve represents a network equipped with a specific model system, operated with different sample collection times.

It is noticeable how releases of xenon confined for 24 h are more difficult than releases of xenon confined for 1 h to discriminate from the false scenario (in this case, release from a short irradiation of HEU – the *baxe_nrx93prc_30min* false scenario in Tab. 6.2), despite the considerably larger source term in the 24 h confinement scenario, see Tab. 3.1, and despite the fact that the 1 h confinement explosion ratios are generally closer to the false scenario trajectories, see Fig. 6.1. The reason is the infrequent detection of ^{131m}Xe for both explosion scenarios, due to the small source term in both scenarios. The absence of data for ^{131m}Xe most often restricts the discrimination algorithm to use of *Plot 4*, the only one of the five plots where the 24 h confinement scenario trajectory is closer to the false scenario than the 1 h confinement scenario trajectory, see Fig. 6.1.

In generating the R statistic, a particular false scenario must be chosen as the null hypothesis to be rejected if the data quality allows it. The results shown in Fig. 6.13 are therefore specific to a particular production and emission scenario, in this case a very short (30 minutes) irradiation of HEU with radioxenons separated from other fission products 15 minutes after the end of irradiation. This scenario (the *baxe_nrx93prc_30min* false scenario in Tab. 6.2)

is represented by the purple curves in Fig. 6.1 and discriminating it from the explosion scenarios (red and green curves) clearly represents something of a challenge. One may expect that a null scenario producing radioxenon less like that emitted from explosions should generate higher values of R, and this is indeed the case as can be seen by comparing Fig. 6.13 to Fig. 6.14. The R shown in the latter figure was generated using radioxenon ratios expected from a pressurized-water reactor (PWR) in equilibrium (the *baxe_pwr_300d* false scenario in Tab. 6.2), shown in blue in Fig. 6.1.

Also with the PWR false scenario, the Rejection Power tends to be lower for the 24 h confinement explosion scenario than for the 1 h confinement explosion scenario. In this case, the reason is more obvious: the 24 h confinement scenario trajectory is always closer to ratios from a reactor in equilibrium than is the 1 h confinement scenario. Using an emission from a reactor in equilibrium as the false scenario, the expected outcome is that longer confinement of the explosion xenon will lead to more difficult discrimination.

If an absolute interpretation of the R score is desired (i.e. in absolute terms, for a given network what fraction of explosions can be expected not to be consistent with a non-explosion source), careful consideration must be given to the selection of an appropriate design basis false scenario. In the present study, we are concerned not primarily with absolute performance, but with the relative gains to be made with different system design parameters, network configurations and mode of operation.

A final point to note is the rather weak, but positive, dependence of R on sample collection time. R is more dependent on network density (compare 39 station and 79 station results) and technology (compare different curves in each figure).

6.5 Timing Results

The Timing Power (T) for a 39 station and a 79 station network, respectively, are shown in Fig. 6.15.

Perhaps more surprisingly than for R, a weak dependence on sample collection time is also observed for T. However, while the Location Power (L) would be expected to (and does) benefit from higher time resolution (shorter sampling time and thus better-defined plume passage time), scoring T requires at least one reasonable-quality measurement of the ^{135}Xe/^{133}Xe activity ratio. Assuming no interference from other sources, such a ratio will always have a well-defined temporal behavior, so time resolution in the sense of well-defined plume passage time becomes less important. The ^{135}Xe measurement sensitivity and precision is the important factor. As long as the sample collection time is not so long that sensitivity is defeated by decay of ^{135}Xe, longer collection time improves sensitivity. The model systems included in this study (with collection times up to 24 hours) are in this regime, as is evident from e.g. Fig. B.22, showing the dependence of the power S (which determines both MDC and precision as shown in Eqn. 6.4 and 6.6) on sample collection time.

The potential gains in T from both increased network density and technology improvement, on the other hand, are even more pronounced than for R.

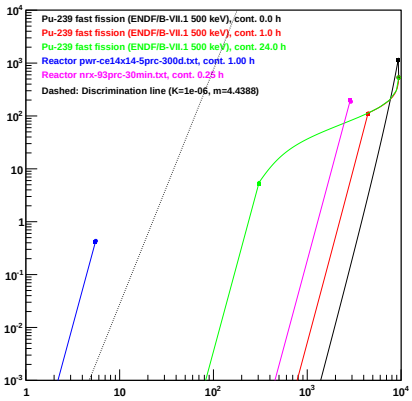

(a) *Plot 0*, using all isotopes: ^{135}Xe/^{133}Xe versus ^{133m}Xe/^{131m}Xe.

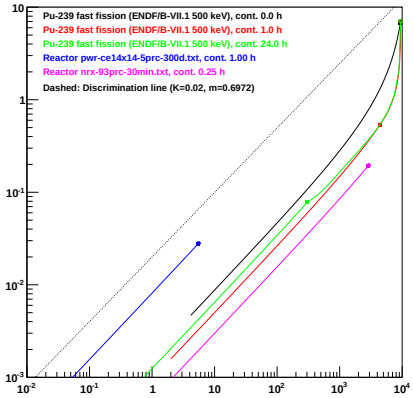

(b) *Plot 1*, using all isotopes except ^{135}Xe: ^{133m}Xe/^{133}Xe versus ^{133m}Xe/^{131m}Xe.

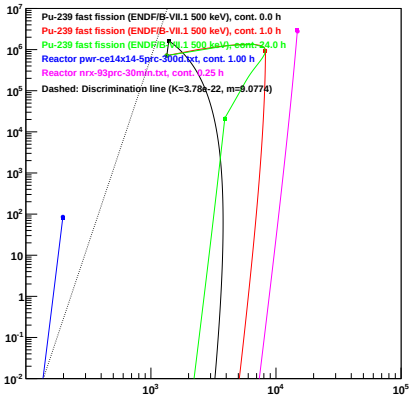

(c) *Plot 2*, using all isotopes except ^{133m}Xe: ^{135}Xe/^{131m}Xe versus ^{133}Xe/^{131m}Xe.

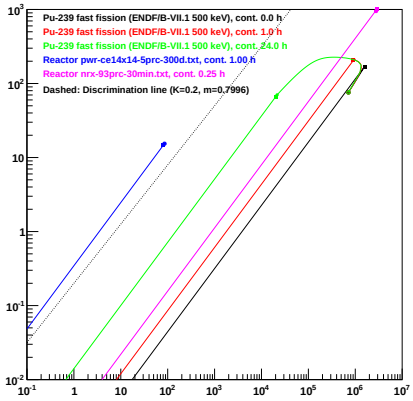

(d) *Plot 3*, using all isotopes except ^{133}Xe: ^{135}Xe/^{133m}Xe versus ^{135}Xe/^{131m}Xe.

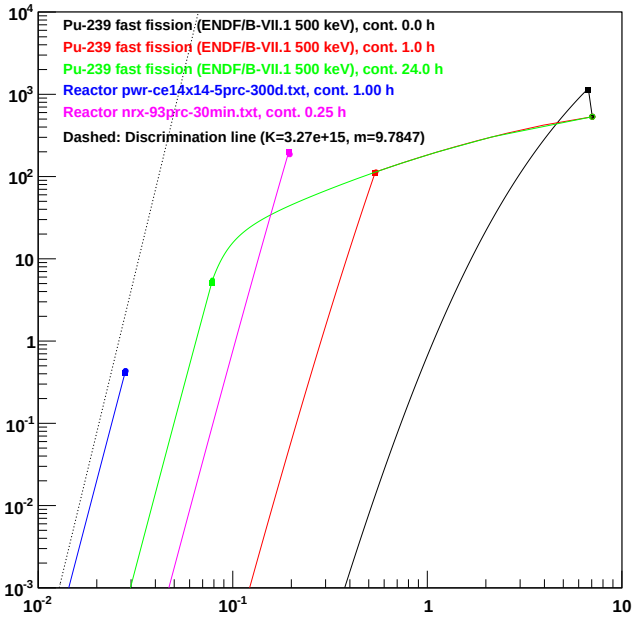

(e) *Plot 4*, using all isotopes except ^{131m}Xe: ^{135}Xe/^{133}Xe versus ^{133m}Xe/^{133}Xe.

Figure 6.1: Three- and four-isotope MIRC plots used by the automated analysis of network data, with trajectories produced by *Baxe* (using ENDF/B-VII.1 data) for various scenarios.

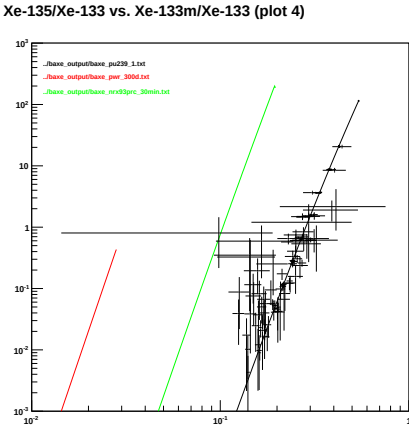

(a) Present SAUNA, 12 hours collection time. The rejection power for the green scenario curve is 41 %.

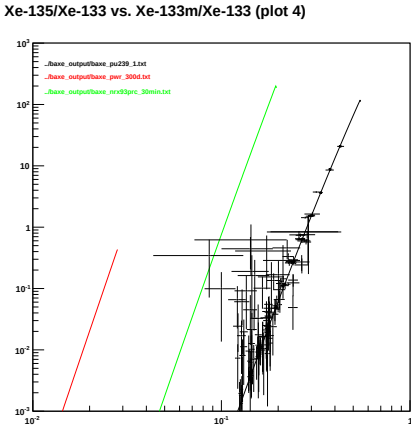

(b) Projected XI, 12 hours collection time. The rejection power for the green scenario curve is 54 %.

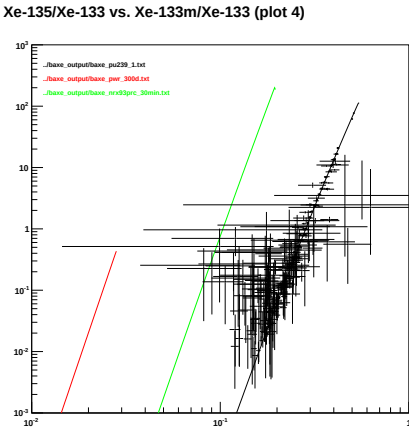

(c) Present SAUNA, 3 hours collection time. The rejection power for the green scenario curve is 35 %.

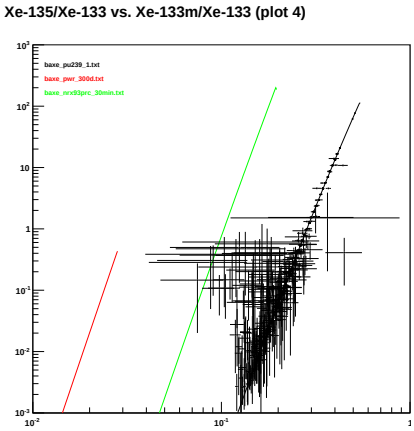

(d) Projected XI, 3 hours collection time. The rejection power for the green scenario curve is 51 %.

Figure 6.2: *Baxfit* output: Synthetic data sets from 144 explosions displayed in MIRC *Plot 4*, using all isotopes except ^{131m}Xe, for the present SAUNA system (model System A) and for the projected XI system (model System F) collecting for 3 hours and for 12 hours in a network of 39 stations with no down-time. No constraints are set on the actual concentration that is "measured". *Black curve*: Nuclear explosion scenario with 1 h containment time, *Green curve*: 93 % HEU irradiated during 30 minutes with 15 min containment time, *Red curve*: 5 % UO_2 PWR irradiated during 300 d with 1 h containment time.

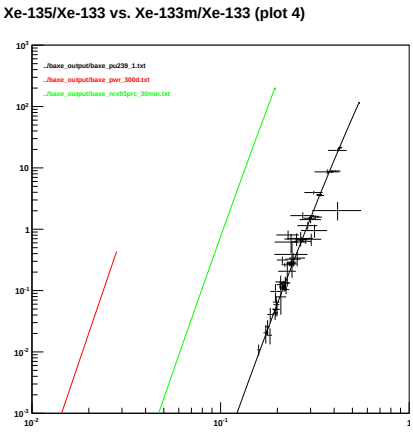

(a) Present SAUNA, 12 hours collection time. The rejection power for the green scenario curve is 40 %.

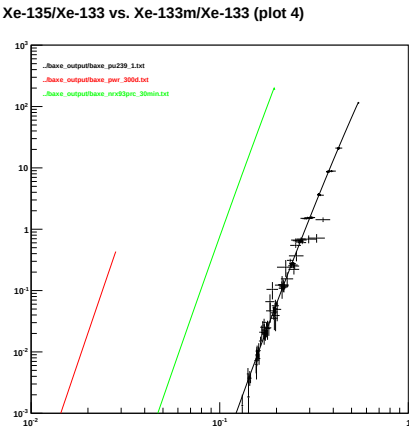

(b) Projected XI, 12 hours collection time. The rejection power for the green scenario curve is 52 %.

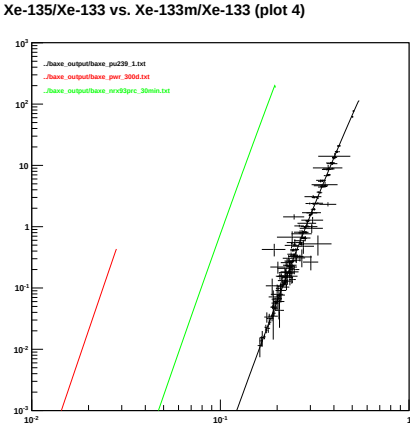

(c) Present SAUNA, 3 hours collection time. The rejection power for the green scenario curve is 33 %.

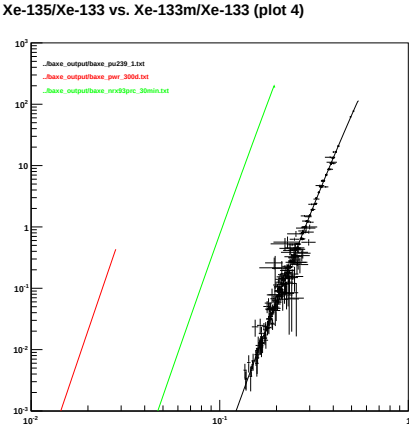

(d) Projected XI, 3 hours collection time. The rejection power for the green scenario curve is 52 %.

Figure 6.3: *Baxfit* output: Synthetic data sets from 144 explosions displayed in MIRC *Plot 4*, using all isotopes except ^{131m}Xe, for the present SAUNA system (model System A) and for the projected XI system (model System F) collecting for 3 hours and for 12 hours in a network of 39 stations with a no down-time. The actual concentration that is measured is required to be above the MDC for each system and sample collection time. *Black curve*: Nuclear explosion scenario with 1 h containment time, *Green curve*: 93 % HEU irradiated during 30 minutes with 15 min containment time, *Red curve*: 5 % UO_2 PWR irradiated during 300 d with 1 h containment time.

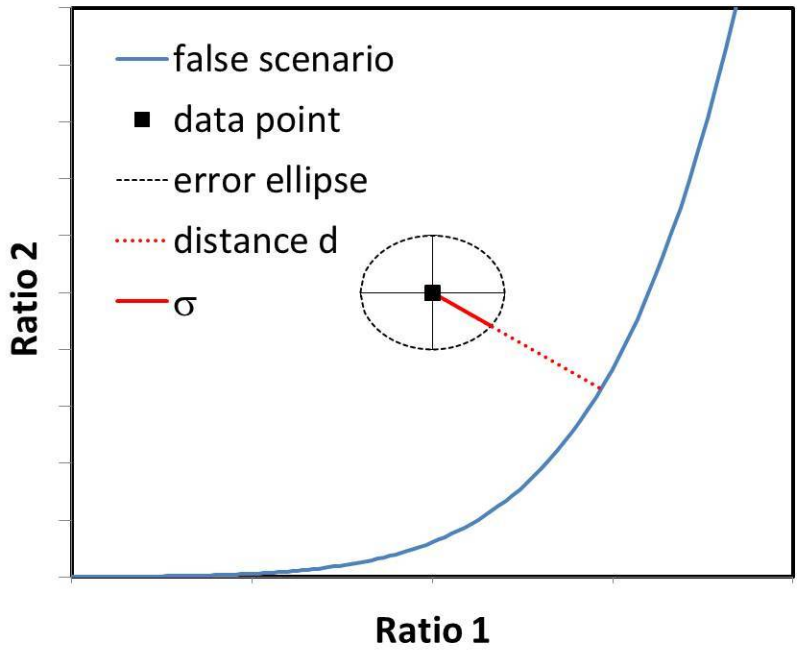

Figure 6.4: The definition of the distance of closest approach d and the uncertainty σ on the location of a data point relative to a scenario trajectory, as used in Eqn. 6.1.

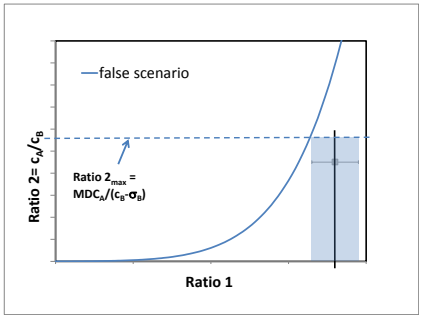

(a) Hypothesis scenario is outside the blue "consistency" area for all times: Data allow rejection of the scenario

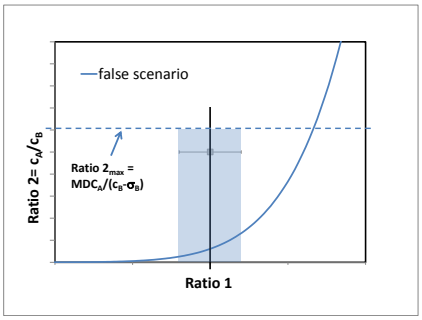

(b) Hypothesis scenario is inside the blue "consistency" area for some times: Data cannot be used to reject the scenario.

Figure 6.5: Graphic example of the application of conditions of the type specified in Eqn. 6.2 to reject (left) or fail to reject (right) a specific scenario. An example would be a measurement of ^{133}Xe and ^{133m}Xe (form Ratio 1) but not ^{135}Xe, where an upper limit for Ratio 2 (^{135}Xe/^{133}Xe) would be estimated based on the MDC for ^{135}Xe.

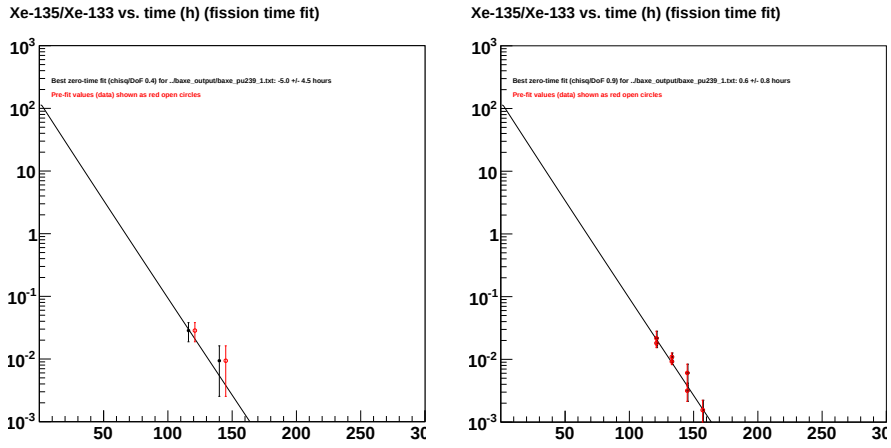

(a) Present SAUNA, 12 hours collection time.

(b) Projected XI, 12 hours collection time.

Figure 6.6: *Baxfit* output: Example of 39 station network timing estimates for Explosion 55. The red points are located at the correct point in time following fission. The black points have been shifted by a common displacement time to obtain the best fit of the measured ratios to the model decay curve (in black). The displacement of the black relative to the red points thus represent the timing error. In this case the timing error is -5.0 h for the SAUNA network and 0.6 h for the XI network. The timing precision is 4.5 h and 0.8 h, respectively. Note that the figures show only one example each of an outcome of "measuring" on the radioxenon concentrations produced by Explosion 55; the outcomes vary stochastically and to obtain final results the outcomes of many experiments must be averaged.

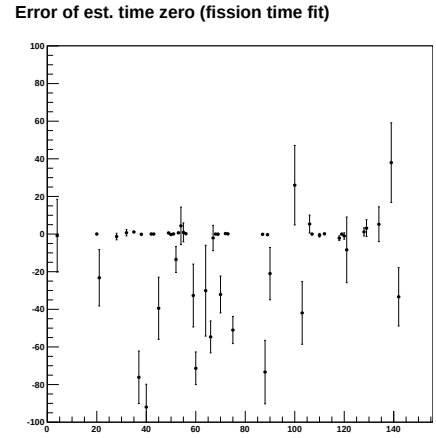

(a) Present SAUNA, 12 hours collection time. Average error 0.008 h, average uncertainty 6.7 h

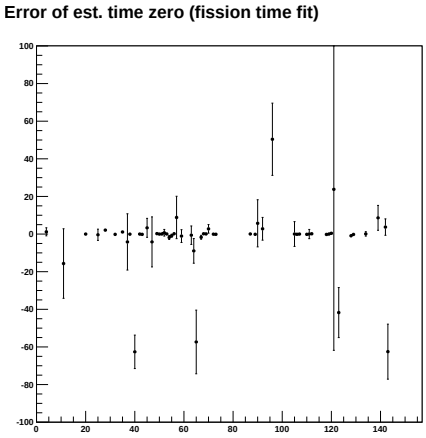

(b) Projected XI, 12 hours collection time. Average error 0.008 h, average uncertainty 5.5 h

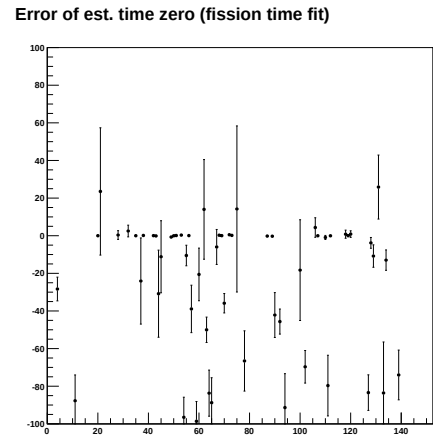

(c) Present SAUNA, 3 hours collection time. Average error 0.002 h, average uncertainty 8.7 h

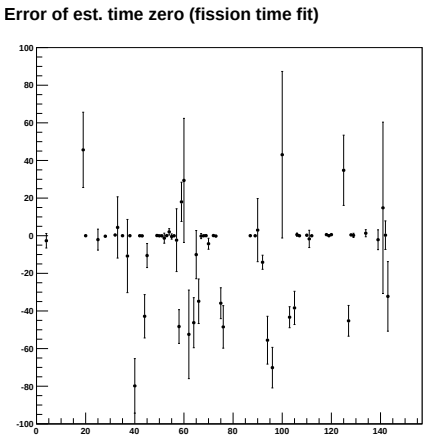

(d) Projected XI, 3 hours collection time. Average error -0.007 h, average uncertainty 7.5 h

Figure 6.7: *Baxfit* output: Example of 39 station network timing results per explosion (1 h containment scenario). The vertical axis shows deviation from true fission time in hours.

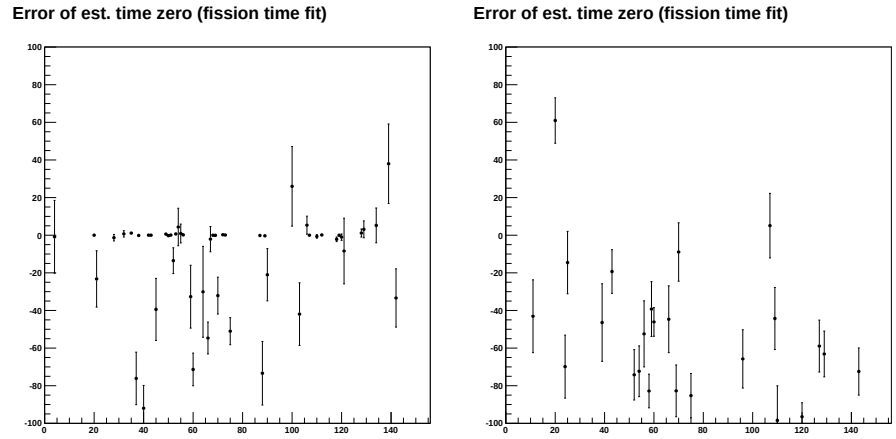

(a) Present SAUNA, 12 hours collection time. Network timing example.

(b) Present SAUNA, 12 hours collection time. All ^{135}Xe removed (i.e. *Hysconc*-provided station concentrations set to zero), so that only false positives remain.

Figure 6.8: *Baxfit* output: Examples of 39 station network timing estimates for all 144 explosions, to illustrate the effect of ^{135}Xe false positives.

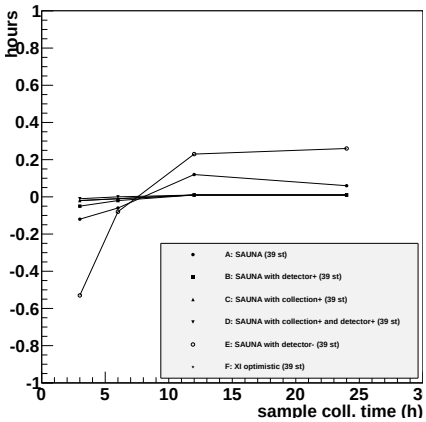

(a) Average network timing error for a 39 station network.

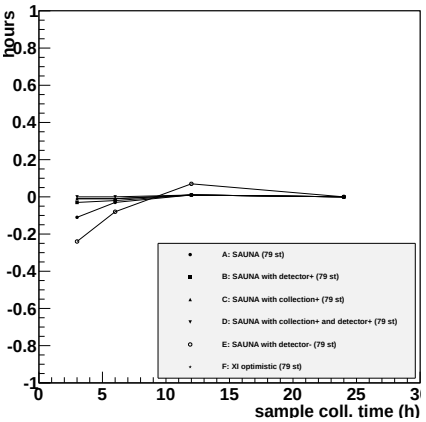

(b) Average network timing error for 79 station network.

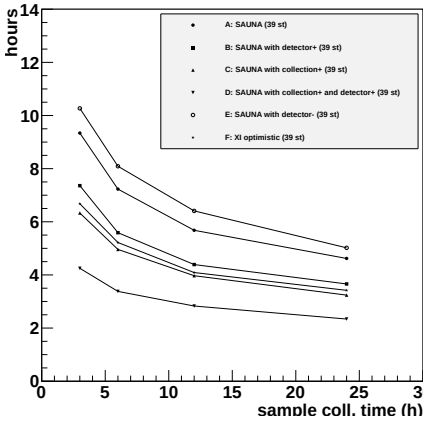

(c) Average network timing uncertainty for a 39 station network.

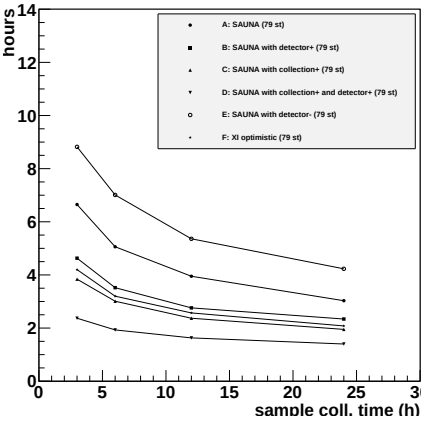

(d) Average network timing uncertainty for a 79 station network.

Figure 6.9: *Baxfit* output: Average network timing error and uncertainty for the 1 h containment explosion scenario as functions of sample collection time for each of the six model systems. Averages over 400 experiments.

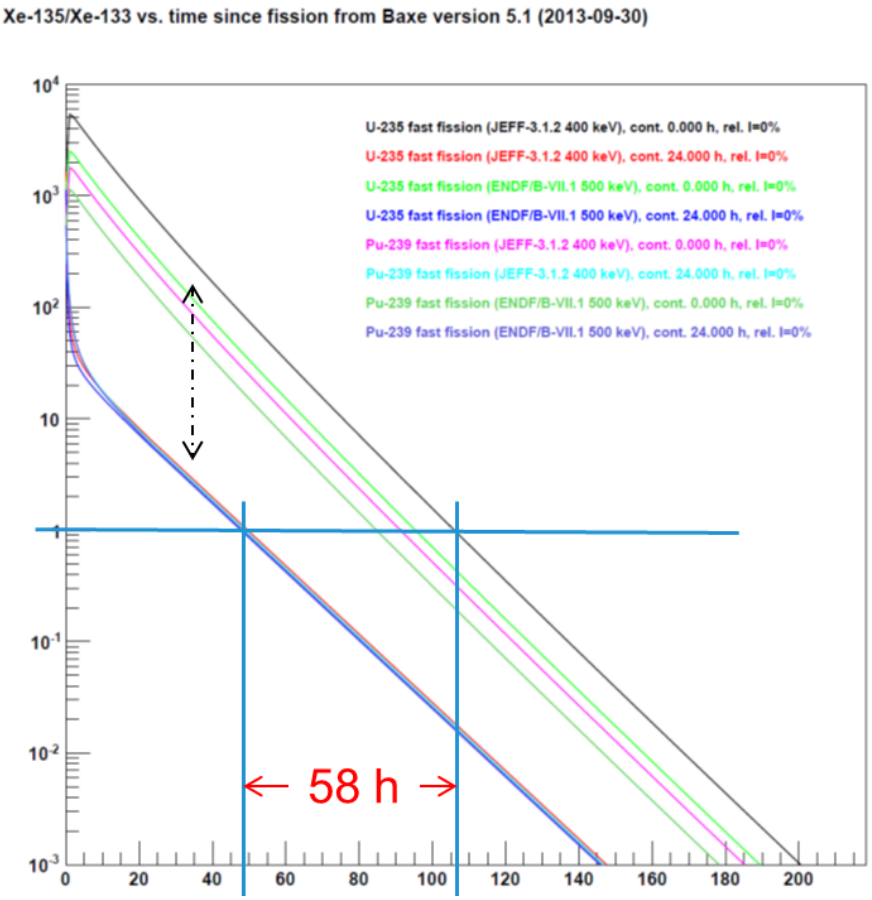

Figure 6.10: The ratio $^{135}Xe/^{133}Xe$ as a function of time after an explosion, modeled using different nuclear data evaluations and different assumptions on separation time for xenon from precursors. Releases of various amounts of iodine with xenon would yield ratios intermediate between the zero- and infinite (24 h) confinement scenarios (dashed arrow). As illustrated, due to nuclear data uncertainties and without knowledge of release details, the uncertainty in a zero-time estimate made on the basis of a perfectly measured ratio will be about 60 h.

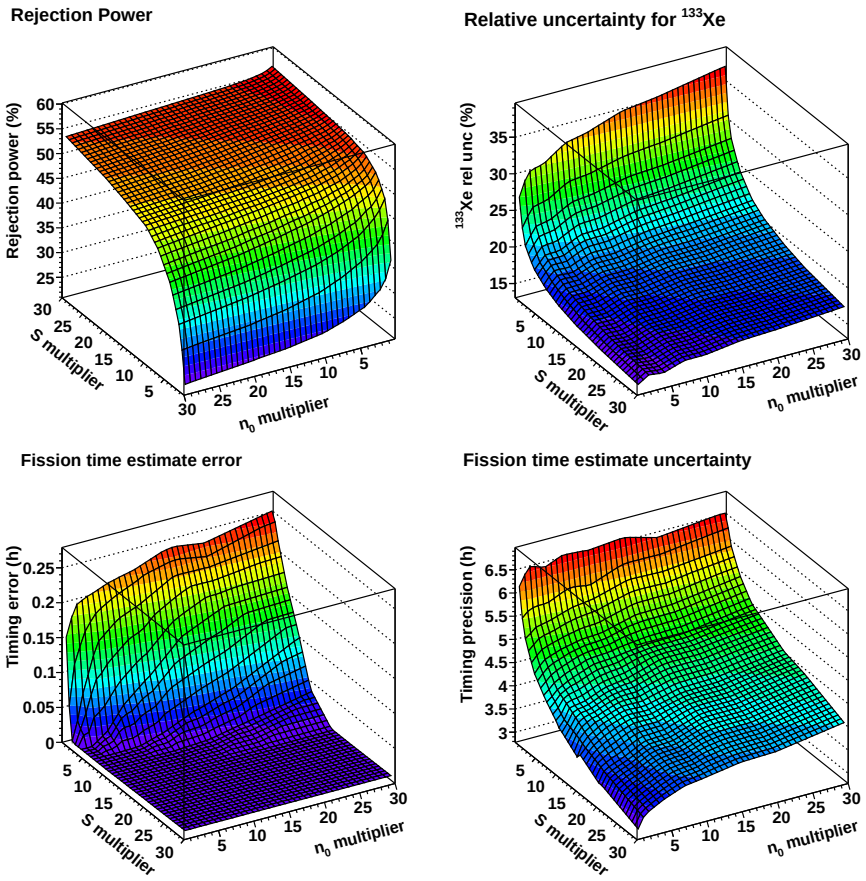

Figure 6.11: Examples of various network performance indicators as functions of the (S,n_0) parameters (expressed as multipliers of the parameters for present SAUNA (model system A). A network of 39 stations, with collection time t_c=12 h was assumed. The 1 h containment scenario was used for releases from the 144 explosions and the false scenario defining Rejection Power R was the short HEU irradiation.

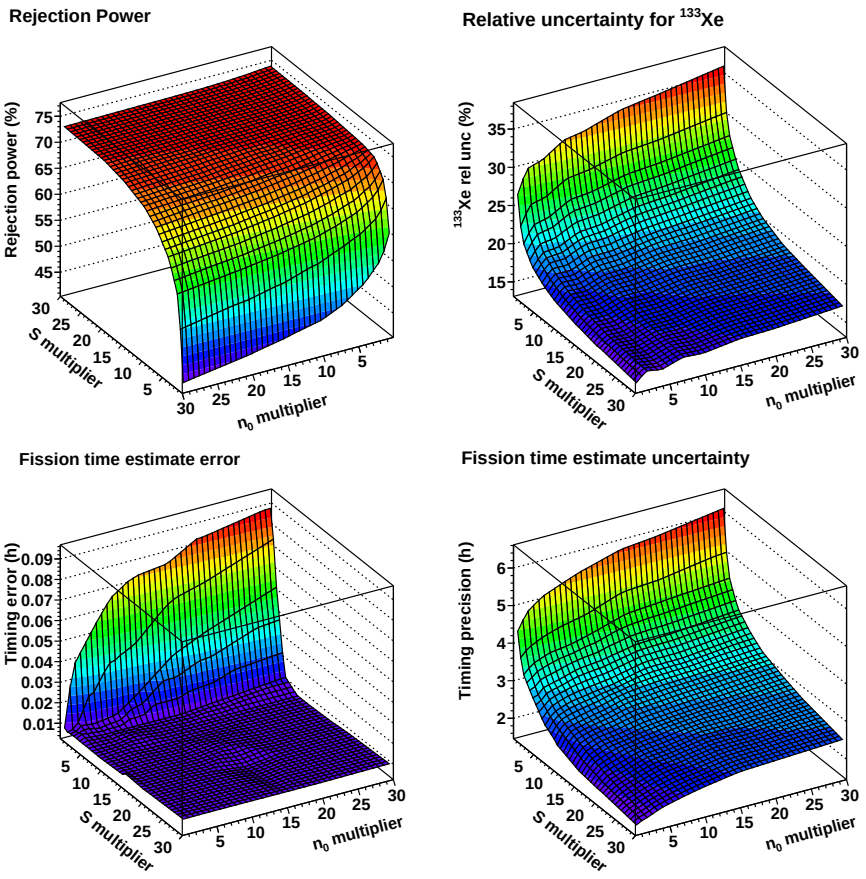

Figure 6.12: Examples of various network performance indicators as functions of the (S,n_0) parameters (expressed as multipliers of the parameters for present SAUNA (model system A). A network of 79 stations, with collection time t_c=12 h was assumed. The 1 h containment scenario was used for releases from the 144 explosions and the false scenario defining Rejection Power R was the short HEU irradiation.

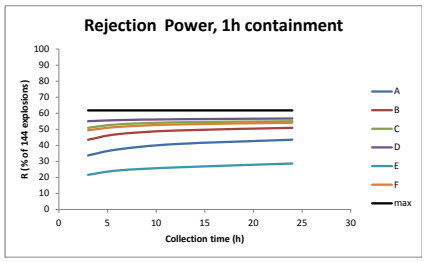

(a) 39 station network, 1 h containment scenario.

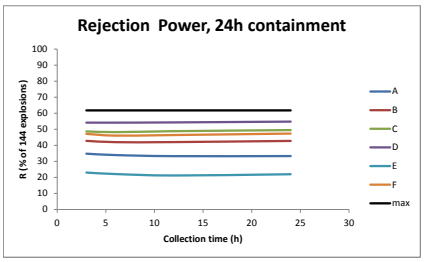

(b) 39 station network, 24 h containment scenario.

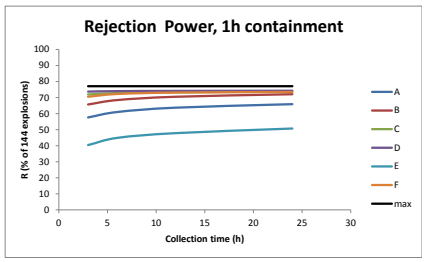

(c) 79 station network, 1 h containment scenario.

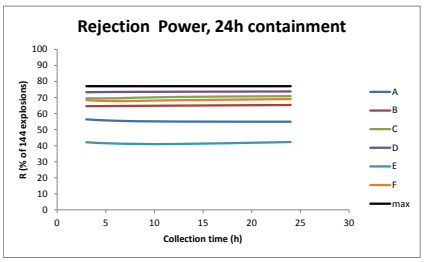

(d) 79 station network, 24 h containment scenario.

Figure 6.13: Rejection power as a function of sampling time using the six model systems in Tab. 6.1 and the short-HEU irradiation false scenario. The black line shows the maximum achievable rejection power according to the simulations.

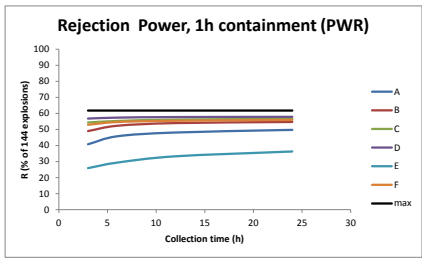

(a) 39 station network, 1 h containment scenario.

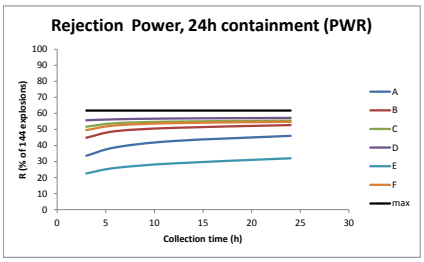

(b) 39 station network, 24 h containment scenario.

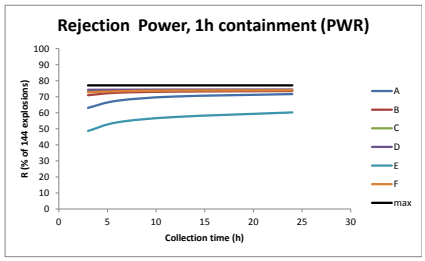

(c) 79 station network, 1 h containment scenario.

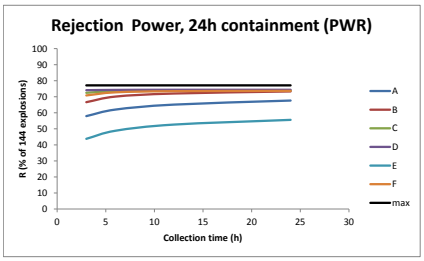

(d) 79 station network, 24 h containment scenario.

Figure 6.14: Rejection power as a function of sampling time using the six model systems in Tab. 6.1 and the PWR in equilibrium false scenario. The black line shows the maximum achievable rejection power according to the simulations.

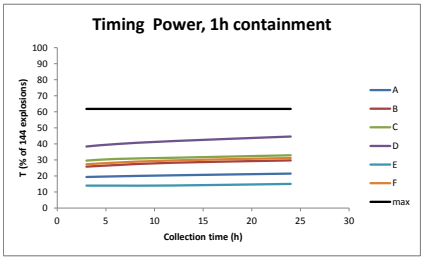

(a) 39 station network, 1 h containment scenario.

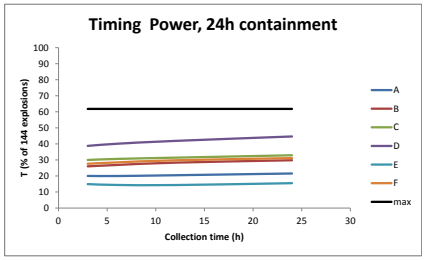

(b) 39 station network, 24 h containment scenario.

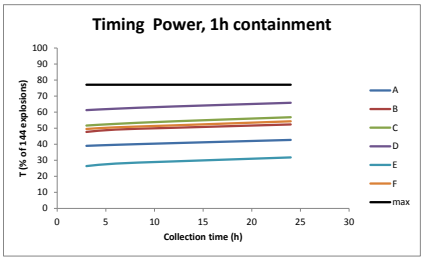

(c) 79 station network, 1 h containment scenario.

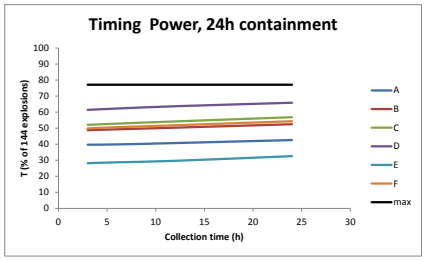

(d) 79 station network, 24 h containment scenario.

Figure 6.15: Timing power as a function of sampling time using the six model systems in Tab. 6.1. The black line shows the maximum achievable rejection power according to the simulations.

7 Network Verification Power

With the Detection-, Location-, Rejection-, and Timing Power calculated as described above, the Verification Power was calculated according to Eq. 2.1. The results for the different model systems, network configurations, and release scenarios are shown in Fig. 7.1. Since the distributions of D, L, R, and T all are very weak functions of system collection time, V obviously also display relatively flat distributions for the different model systems.

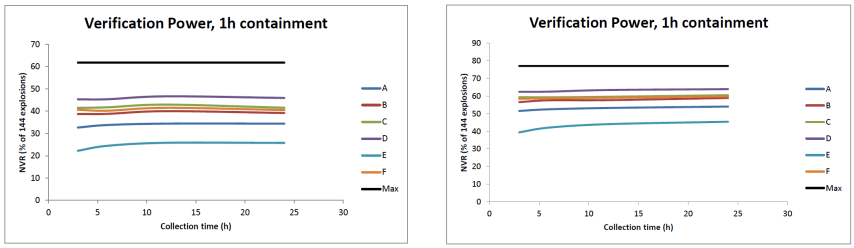

(a) The Network Verification Power as a function of sampling time for the 39 (left) and 79 (right) station network configurations and 1 h containment time.

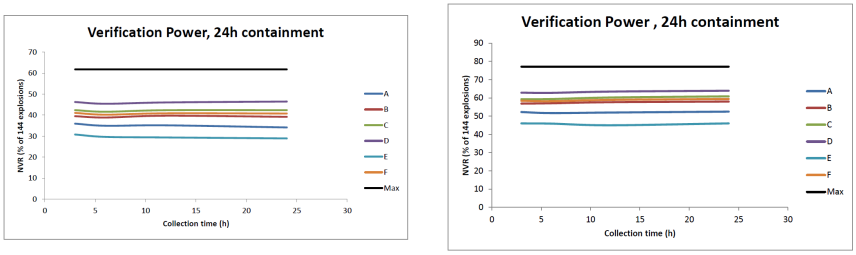

(b) The Network Verification Power as a function of sampling time for the 39 (left) and 79 (right) station network configurations and 24 h containment time.

Figure 7.1: The Network Verification Power as a function of model systems A-F sampling time for the 39 and 79 station network configurations and 1 h and 24 h containment time. The black line corresponds to maximum possible Network Verification Power according to the calculations.

8 System Measurement Sensitivity

In the study of Network Verification Power, the response of a network of "generic" detection systems characterized by a simplified set of detection and analysis parameters (n_0, S) was illustrated. A real xenon detection system is characterized by a larger number of actual technical parameters, such as the sample collection time t_c, sample processing time t_p, sample counting time t_a, ambient background rates B, sampling flow rate Φ, counting efficiencies $\varepsilon_{\beta\gamma}$, memory effect – the percentage of the activity from an immediately preceding sample that is not purged prior to measuring the next sample – and radon suppression factor. In this section, the effects on system-level performance indicators (MDC and the (n_0,S) parameters) of varying some actual technical parameters (t_c, t_p, t_a, B, Φ and $\varepsilon_{\beta\gamma}$) in a SAUNA system are studied. The intention is for the results to serve as a guide in system design, e.g. to identify how and which system technical parameters could or should be modified in order to best achieve a desired effect on high-level performance indicators.

A code *bgm* was written that reads IMS-format pulse-height data (*phd*) files (measured sample spectrum, measured gas background spectrum and detector background spectrum) and an input file specifying input concentrations, radon suppression and gas memory effect. The information in the *phd* files is used to generate the numbers of counts in each ROI that the concentrations specified in the input file would have resulted in had they been measured by the system that generated the *phd* files – i.e. the *phd* files are used as the source of system and measurement and analysis parameters such as sampling, processing and counting times, beta-gamma efficiencies, spectral Regions-of-Interest (ROI) definitions, interference factors etc. The code then passes the numbers of counts (rounded to nearest integer) to net-counts concentration analysis using the exact same method (and software library) as is used by the *Xecon* analysis code. The code varies selected system parameters in order to allow investigation of the impact of these parameters on system performance indicators (e.g. MDC).

Appendix B contains the results in the form 3D graphs of MDC, S and n_0 for each of the isotopes of interest ^{131m,133,133m,135}Xe versus pairs of the technical system parameters t_c, t_p, t_a, B, Φ and $\varepsilon_{\beta\gamma}$. The technical parameters are expressed as multiples of typical values for a present-day SAUNA system (see Tab. 8.1), so that the value of the indicator of interest (e.g. MDC) at grid point (1,1) corresponds to the value expected for a typical SAUNA system installed in the IMS.

Note that the technical parameter B is not the same as the generic background parameter n_0 used in the network study to characterize model systems. The former is simply the ambient background rate that for an IMS system is determined by a (preferably high-statistics) "detector background" measurement, and subsequently used to correct both the sample- and gas background measurements for the contribution of constant and non-sample related sources of background (such as cosmic or environmental radiation penetrating the lead shielding, or contributions from radioactive species in the shielding itself). The latter represents an attempt, for the sake of algorithmic simplicity in the context of automatic "analysis" in the network study, to amalgamate *all* forms of background affecting the analysis of each radioxenon isotope in one parameter. When a value for n_0 is computed from a full set of detailed system parameters and a full-scale net count analysis (as done in this chapter), the result will

reflect ambient background but also more complex sample-specific sources of background such as radon daughters, gas memory and inter-isotope interference.

Parameter	SAUNA	XI (system F) (indicative multipliers)
Φ	1.23 m^3/h	5
t_c	12.00 h	free parameter
t_p	6.97 h	1
t_a	11.17 h	1.1
$\varepsilon_{\beta\gamma}$ (^{131m}Xe)	0.60	1
$\varepsilon_{\beta\gamma}$ (^{133}Xe)	0.64	1
$\varepsilon_{\beta\gamma}$ (^{133}Xe, ROI 3)	0.60	1
$\varepsilon_{\beta\gamma}$ (^{135}Xe)	0.51	1
B (^{131m}Xe)	$1.4{\cdot}10^{-4}$ cps	0.5
B (^{133}Xe, ROI 3)	$7.6{\cdot}10^{-4}$ cps	0.5
B (^{133m}Xe)	$6.1{\cdot}10^{-5}$ cps	0.5
B (^{135}Xe)	$1.9{\cdot}10^{-3}$ cps	0.5

Table 8.1: Values of typical SAUNA system technical parameters corresponding to the "baseline" grid point (1,1) in studying the effect on MDC and (S,n_0) of varying the parameters (left column), and (as a guide when consulting the results in Appendix B) indicative multipliers for the XI system (right column).

A number of assumptions were made in generating the numbers shown in Appendix B:

Coincidence counting efficiencies $\varepsilon_{\beta\gamma}$ varied by the same multiplier for all ROI:s at each grid point; if application of a given multiplier to any counting efficiency value resulted in $\varepsilon_{\beta\gamma} > 1$, that value was set to 1;

Ambient background rates varied by same multiplier for all ROI:s at each grid point;

All four isotopes ^{131m,133,133m,135}Xe present at a concentration of 0.1 mBq/m^3 during sampling;

Beta-cell gas memory effect 2 %, applied to a previous sample assumed to have measured exactly the same radioxenon concentrations;

Radon present at a concentration of 100 Bq/m^3 during sampling;

Radon suppression factor 10^6.

As an example of how the *bgm* code and the results in Appendix B may be used, Fig. A.3 shows the estimated Detection Power (D) for three samples detected from a 1 kt explosion by an IMS network of 39 stations equipped with present-day SAUNA systems (taken to be represented by the technical parameters in Tab. 8.1 and operating with sample collection time t_c=12 h) to be around 35 %. Consulting Fig. A.3, we see that an improvement of ^{133}Xe MDC from the current SAUNA value of 0.24 mBq/m^3 (see Tab. 2.3) by about a factor of 7 would result in the three-sample D score reaching the plateau value of around 45 %. Suppose we decide that the parameters that may be changed include only the pair t_a (sample counting time) and Φ (sampling rate). Suppose further that the sampling rate can be increased by a factor of 5

relative to present SAUNA. Fig. B.13 then indicates that the sample counting time needs to be increased by about a factor 2.5 in order to reach the desired MDC of 0.24/7 mBq/m^3 = 0.034 mBq/m^3. This is of course subject to the underlying assumptions for the MDCs shown in the figure (radon, memory effect, interfering isotopes (^{135}Xe in this case), etc., as shown above).

9 Conclusions and Outlook

In this study, we have defined a small set of global network quality indicators or Figures of Merit (FoMs) that we believe capture the essential aspects of the verification mission of a radionuclide network for CTBT verification: Detection of effluents, location of the release and characterization of the source, which incorporates both event timing and the ability to discriminate between different types of sources. The FoMs are Detection Power (D), Location Power (L), Rejection Power (R) and Timing Power (T). We have aggregated them into a universal Figure of Merit: Network Verification Power (V) for a noble gas verification network.

The concept was studied with respect to different noble gas technology improvements (model systems) and technology applications (network densities). Network density was studied by comparing the currently planned International Monitoring System (IMS) noble gas component comprising 39 measuring stations to a network with noble gas capability installed at all 79 currently planned radionuclide stations of the IMS. Each network configuration (network density and equipment in terms of model system) was modeled for different assumptions on sample collection time (varying from 3 to 24 hours). The response was studied for two different release scenarios. Some high-level conclusions may be drawn:

Using current systems, the Network Detection Power (D) is already close to optimal for the two release scenarios, and it is not very sensitive to the sample collection time. Significant improvement of D is possible but would require a denser network.

The maximum achievable value of D, which is approached even with current measurement technology, is considerably less than 100 % due to global atmospheric conditions: Weather patterns can prevent detection within a given time span of some releases no matter how large (or equivalently, no matter the measurement sensitivity of network monitoring equipment). The time span of this study was one week; a longer time would have raised the maximum achievable D, but the additional detections would be increasingly unlikely to yield data useful for verification. The problem is particularly severe in the equatorial region. It can be mitigated but not solved by increasing the number of monitoring stations from 39 to 79.

The Network Location Power (L) is not very sensitive to system collection time, nor detection technology improvements. The improvement in L when using a denser network is also quite limited.

L is determined not only by network configuration, measurement sensitivity and data quality but also by Atmospheric Transport Modeling (ATM) capability.

Characterization (R and T) is relatively insensitive to changes in collection time but both R and T can be significantly improved by higher network density and detection technology improvements.

Network Verification Power (V) as a whole is almost insensitive to changes in collection time but can be improved both by higher network density and detection technology improvements.

The last point requires some careful consideration. While it is expected that it will sometimes be useful to summarize verification capability in one number, the FoMs D, L, R and T are each individually important to the verification mission. A V score that is achieved with any one of the components very low or zero is unlikely to represent a network of the same utility as one with the same V score achieved with all the components of similar magnitude.

This study has not explicitly addressed the issue of radioxenon background, except in the sense that the R score indicates the likelihood that a set of detections of pure explosion radioxenon could be discriminated from a selected background source. For successful use of verification data, the background problem must be handled by several methods, including characterization and identification of prominent individual sources of background and exclusion or subtraction of such sources by ATM combined with timing and discrimination based on measured data. We believe that the measurement system and network properties ultimately measured by each of the FoMs all contribute to the capability of analysts to accomplish this.

Since this is the first study to address the complete verification capability of a radionuclide network, it includes several new suggested concepts that needs to be further scrutinized. Furthermore, we believe that further studies are needed, using for instance a larger number of hypothetical explosions distributed over several years and seasons. Furthermore, a deeper analysis of the reasons behind some of the results obtained is necessary.

References

[1] James H. Ely, James C. Hayes, Derek A. Haas, Warren W. Harper, Jill C. Madison, Anders Ringbom, and Klas Elmgren. Next generation radio xenon systems: More reliability, better sensitivity, and more frequent measurements. Science and Technology 2013 Conference, Vienna, Austria (poster), (2013). Available from the CTBTO Preparatory Commission web site: http://www.ctbto.org.

[2] R.R. Draxler and G.D. Hess. An overview of the HYSPLIT 4 modeling system of trajectories, dispersion, and deposition. *Aust. Meteor. Mag.*, 47:295–308, 1998.

[3] Roland R. Draxler. Description of the HYSPLIT 4 modeling system. *NOAA Technical Memorandum ERL ARL-224*, (December 1997).

[4] Rene Brun and Fons Rademakers. ROOT - An Object Oriented Data Analysis Framework. *Nuclear Instruments and Methods in Physics Research Section A: Accelerators, Spectrometers, Detectors and Associated Equipment*, A389:81–86, September 1997. Proceedings AIHENP'96 Workshop, Lausanne, Sept. 1996. See also http://root.cern.ch/.

[5] Andreas Becker, Gerhard Wotawa, Lars-Erik De Geer, Petra Seibert, Roland R. Draxler, Craig Sloan, Real D'Amours, Matthew Hort, Hubert Glaab, Philippe Heinrich, Yves Grillon, Vyacheslav Shershakov, Keiichi Katayama, Yuetang Zhang, Paul Stewart, Marcus Hirtl, Michel Jean, and Peter Chen. Global backtracking of anthropogenic radionuclides by means of a receptor oriented ensemble dispersion modelling system in support of nuclear-test-ban treaty verification. *Atmospheric Environment*, 41(21):4520 – 4534, 2007.

[6] M.B. Chadwick, M. Herman, P. Obložinský, M.E. Dunn, Y. Danon, A.C. Kahle, D.L. Smith, B. Pritychenko, G. Arbanas, R. Arcilla, R. Brewer, D.A. Brown, R. Capote, A.D. Carlson, Y.S. Cho, H. Derrien, K. Guber, G.M. Hale, S. Hoblit, S. Holloway, T.D. Johnson, T. Kawano, B.C. Kiedrowski, H. Kim, S. Kunieda, N.M. Larson, L. Leal, J.P. Lestone, R.C. Little, E.A. McCutchan, R.E. MacFarlane, M. MacInnes, C.M. Mattoon, R.D. McKnight, S.F. Mughabghab, G.P.A. Nobre, G. Palmiotti, A. Palumbo, M.T. Pigni, V.G. Pronyaev, R.O. Sayer, A.A. Sonzogni, N.C. Summers, P. Talou, I.J. Thompson, A. Trkov, R.L. Vogt, S.C. van der Marck, A. Wallner, M.C. White, D. Wiarda, and P.G. Young. ENDF/B-VII.1 Nuclear Data for Science and Technology: Cross Sections, Covariances, Fission Product Yields and Decay Data. *Nuclear Data Sheets*, 112(12):2887 – 2996, 2011.
Data obtained from NEA Nuclear Data Services (http://www.oecd-nea.org).

[7] SCALE: A Comprehensive Modeling and Simulation Suite for Nuclear Safety Analysis and Design, ORNL/TM-2005/39, Version 6.1, Oak Ridge National Laboratory, Oak Ridge, Tennessee, June 2011. Available from Radiation Safety Information Computational Center at Oak Ridge National Laboratory as CCC-785.

[8] M. B. Kalinowski, A. Axelsson, M. Bean, X. Blanchard, T. W. Bowyer, G. Brachet, S. Hebel, J. I. McIntyre, J. Peters, C. Pistner, M. Raith,

A. Ringbom, P. R.J. Saey, C. Schlosser, T. J. Stocki, T. Taffary, and R. K. Ungar. Discrimination of Nuclear Explosions against Civilian Sources Based on Atmospheric Xenon Isotopic Activity Ratios. *Pure and Applied Geophysics*, 167:517 – 539, 2010.

[9] U. von Luxburg and V. H. Franz. A Geometric Approach to Confidence Sets for Ratios: Fieller's Theorem, Generalizations and Bootstrap. *Statistica Sinica*, 19:1095 – 1117, 2009.

A Detection Power

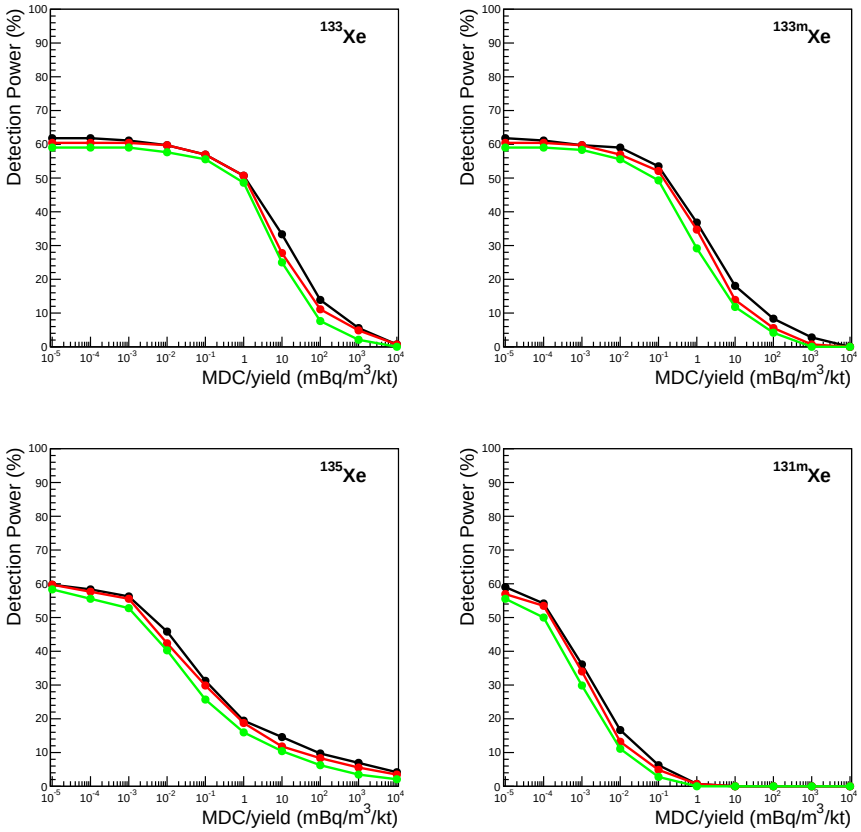

Figure A.1: Detection Power as a function of MDC/yield for the case 1 h containment, 3 h sampling time and 39 IMS stations. The three different curves correspond to at least one (black), two (red), and three (green) samples detected.

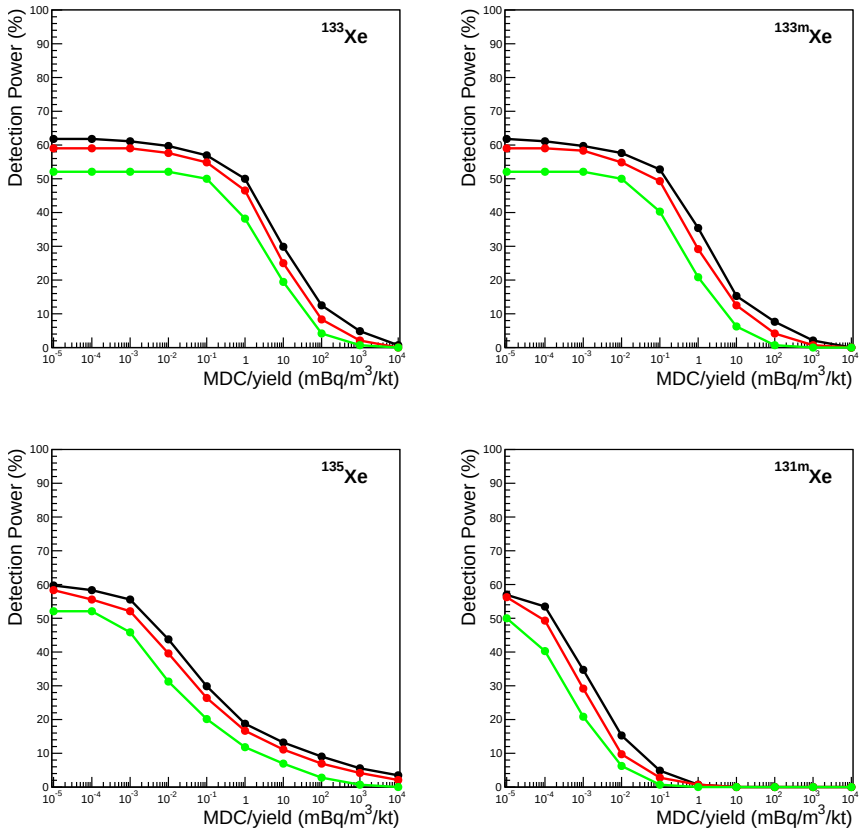

Figure A.2: Detection Power as a function of MDC/yield for the case 1 h containment, 6 h sampling time and 39 IMS stations. The three different curves correspond to at least one (black), two (red), and three (green) samples detected.

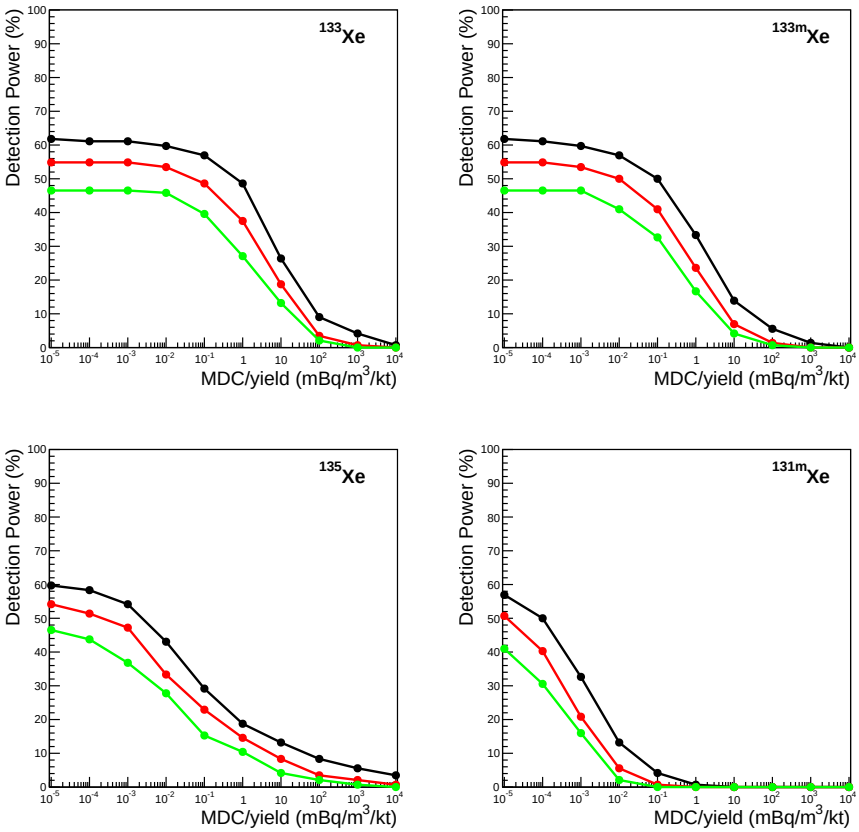

Figure A.3: Detection Power as a function of MDC/yield for the case 1 h containment, 12 h sampling time and 39 IMS stations. The three different curves correspond to at least one (black), two (red), and three (green) samples detected.

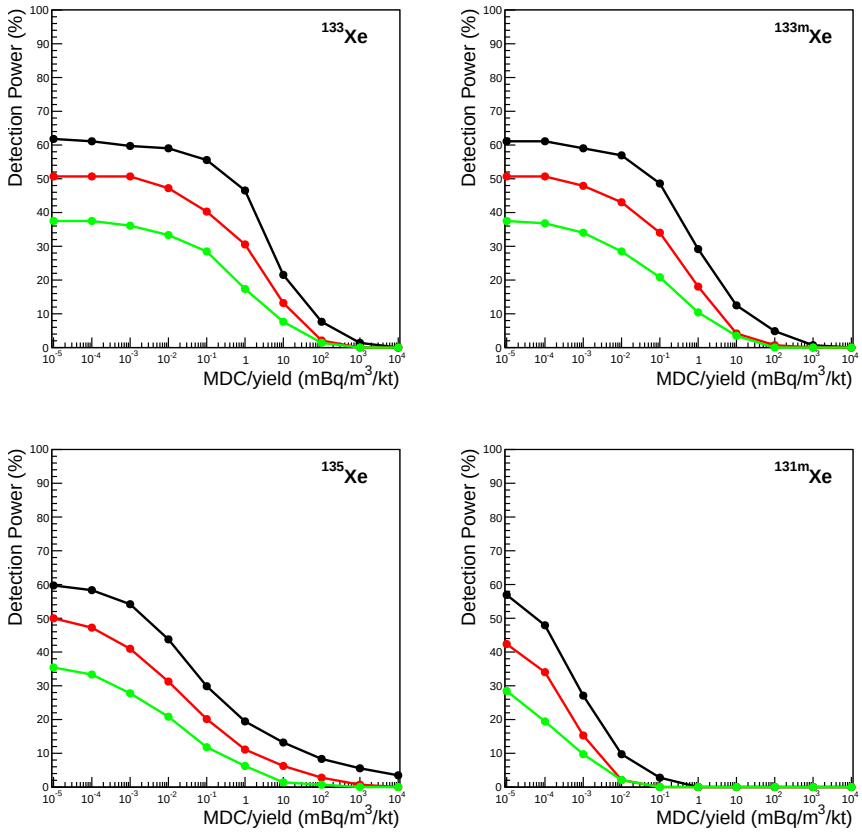

Figure A.4: Detection Power as a function of MDC/yield for the case 1 h containment, 24 h sampling time and 39 IMS stations. The three different curves correspond to at least one (black), two (red), and three (green) samples detected.

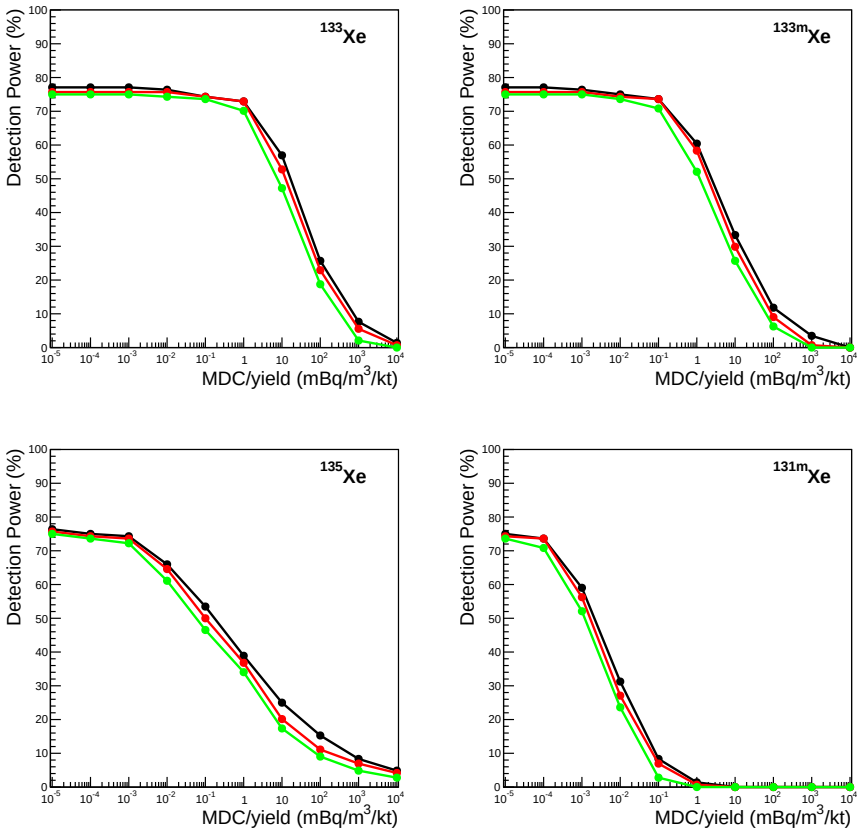

Figure A.5: Detection Power as a function of MDC/yield for the case 1 h containment, 3 h sampling time and 79 IMS stations. The three different curves correspond to at least one (black), two (red), and three (green) samples detected.

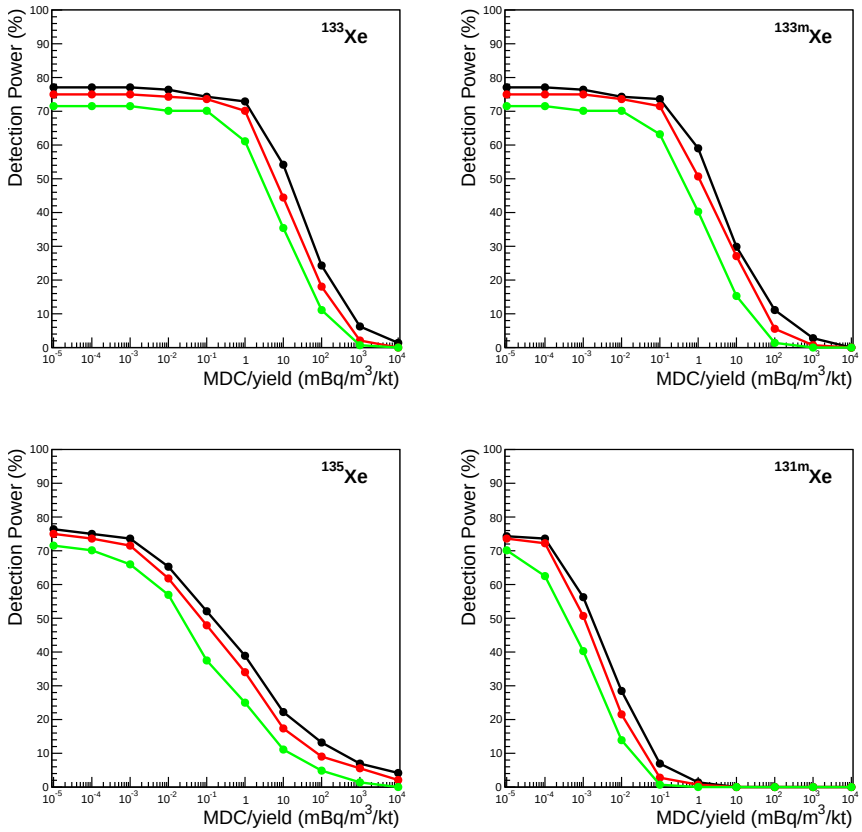

Figure A.6: Detection Power as a function of MDC/yield for the case 1 h containment, 6 h sampling time and 79 IMS stations. The three different curves correspond to at least one (black), two (red), and three (green) samples detected.

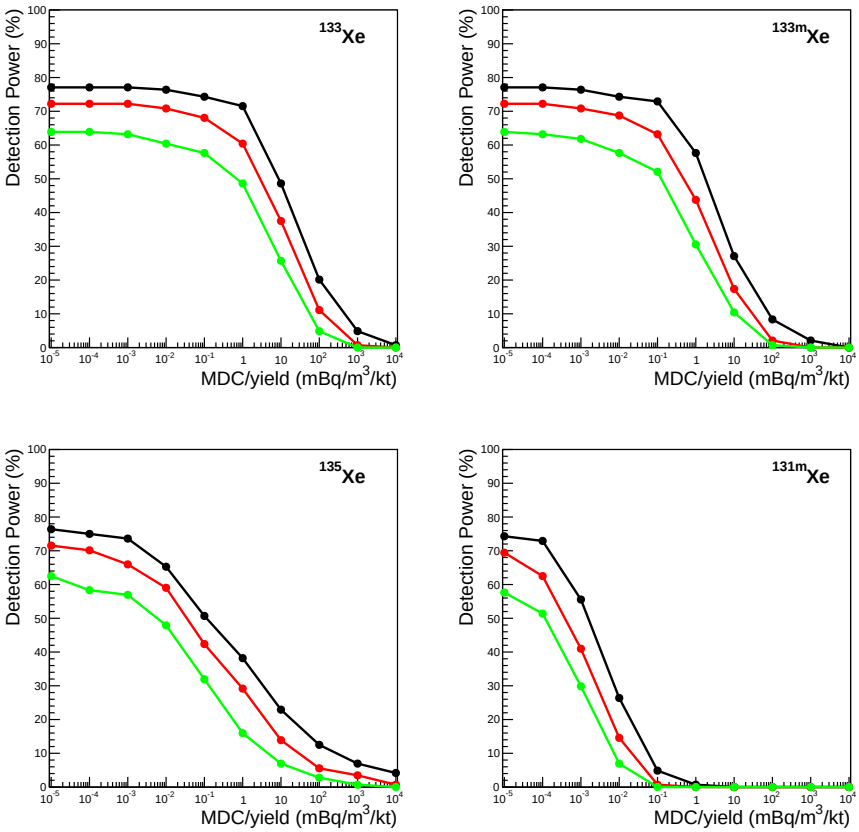

Figure A.7: Detection Power as a function of MDC/yield for the case 1 h containment, 12 h sampling time and 79 IMS stations. The three different curves correspond to at least one (black), two (red), and three (green) samples detected.

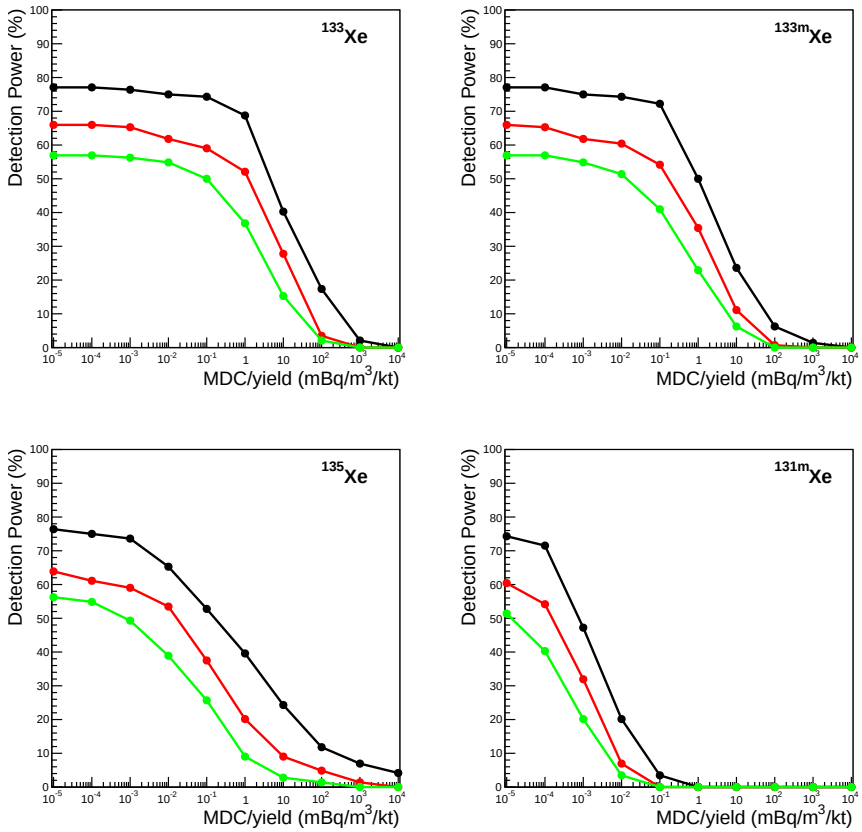

Figure A.8: Detection Power as a function of MDC/yield for the case 1 h containment, 24 h sampling time and 79 IMS stations. The three different curves correspond to at least one (black), two (red), and three (green) samples detected.

B Variation of System Performance Indicators with Technical System Parameters

The results on MDC and the (S,n_0) generic measurement and analysis parameters of varying six system parameters (ambient background rate B, sampling rate Φ, beta-gamma coincidence counting efficiency $\varepsilon_{\beta\gamma}$, sample collection time t_c, sample processing time t_p and sample collection time t_c) relative to the present SAUNA IMS system are shown in the following pages.

The MDC dependence on variation of the technical parameters is presented first, then S and finally n_0.

The details of the method are given in Chapter 8.

B.1 Variation of Minimum Detectable Concentration (MDC) with Technical System Parameters

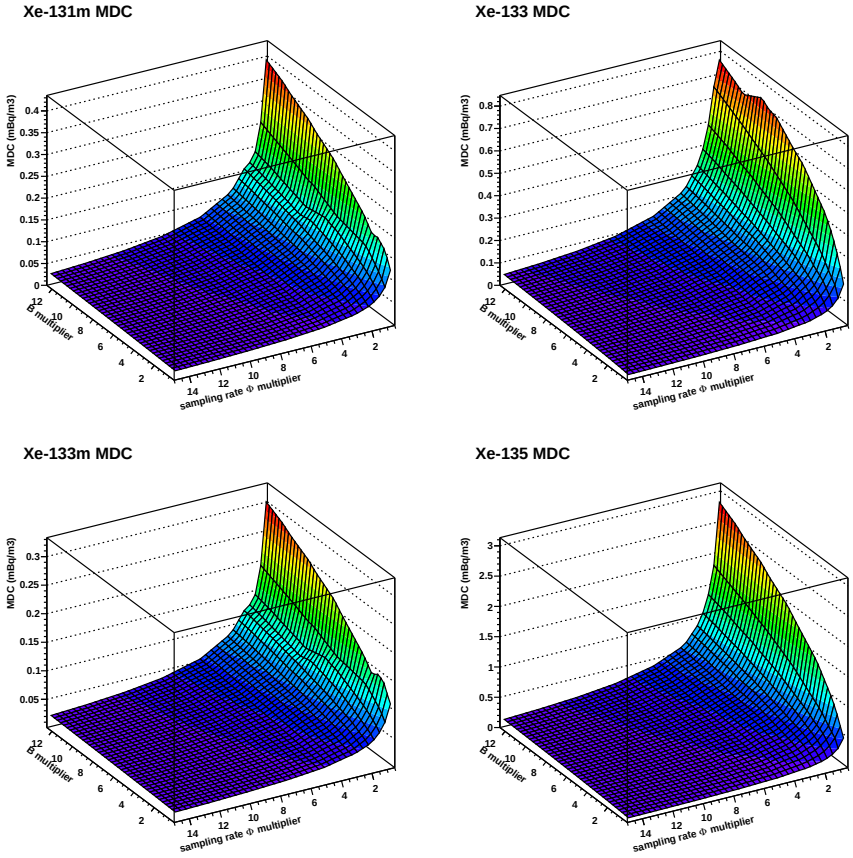

Figure B.1: The MDC as a function of ambient background rate (B) and sampling rate (Φ). The parameters are expressed as multiples of their values for a present SAUNA system operated as in the IMS, so that values of (1,1) yields an MDC expected from an IMS SAUNA system. The calculation assumes all four isotopes ^{131m,133,133m,135}Xe to be present with a concentration of 0.1 mBq/m^3 during sampling, a memory effect of 2 % (applied to a previous sample assumed to have measured exactly the same concentrations), radon at a concentration of 100 Bq/m^3 and a radon suppression factor of 10^6.

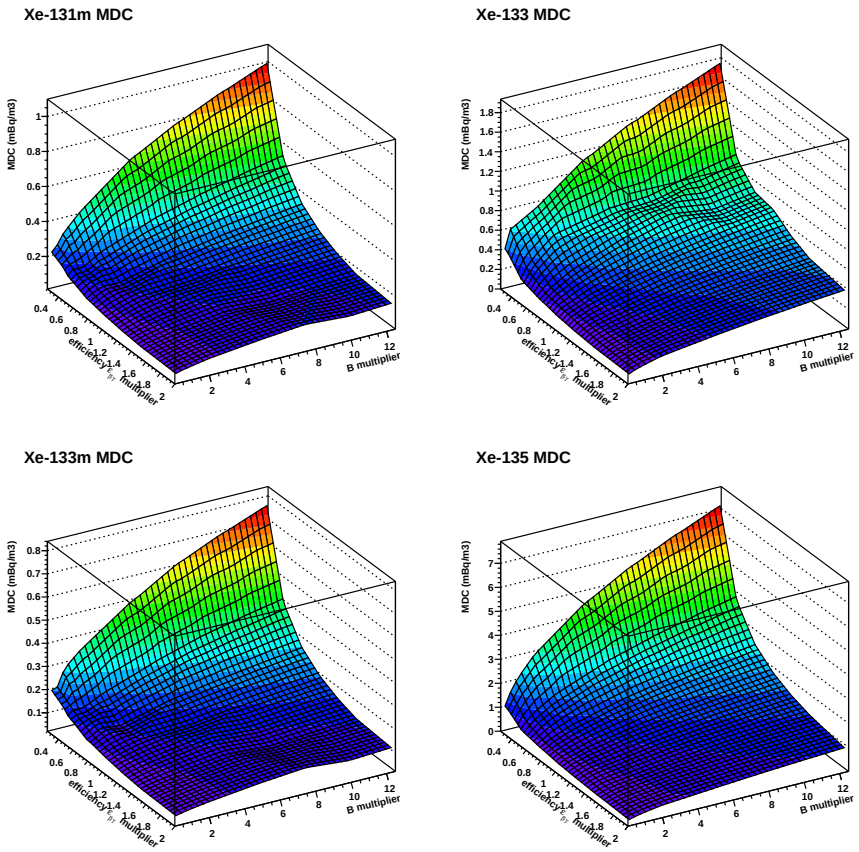

Figure B.2: The MDC as a function of beta-gamma coincidence counting efficiency ($\varepsilon_{\beta\gamma}$) and ambient background rate (B). The parameters are expressed as multiples of their values for a present SAUNA system operated as in the IMS, so that values of (1,1) yields an MDC expected from an IMS SAUNA system. The calculation assumes all four isotopes ^{131m,133,133m,135}Xe to be present with a concentration of 0.1 mBq/m^3 during sampling, a memory effect of 2 % (applied to a previous sample assumed to have measured exactly the same concentrations), radon at a concentration of 100 Bq/m^3 and a radon suppression factor of 10^6.

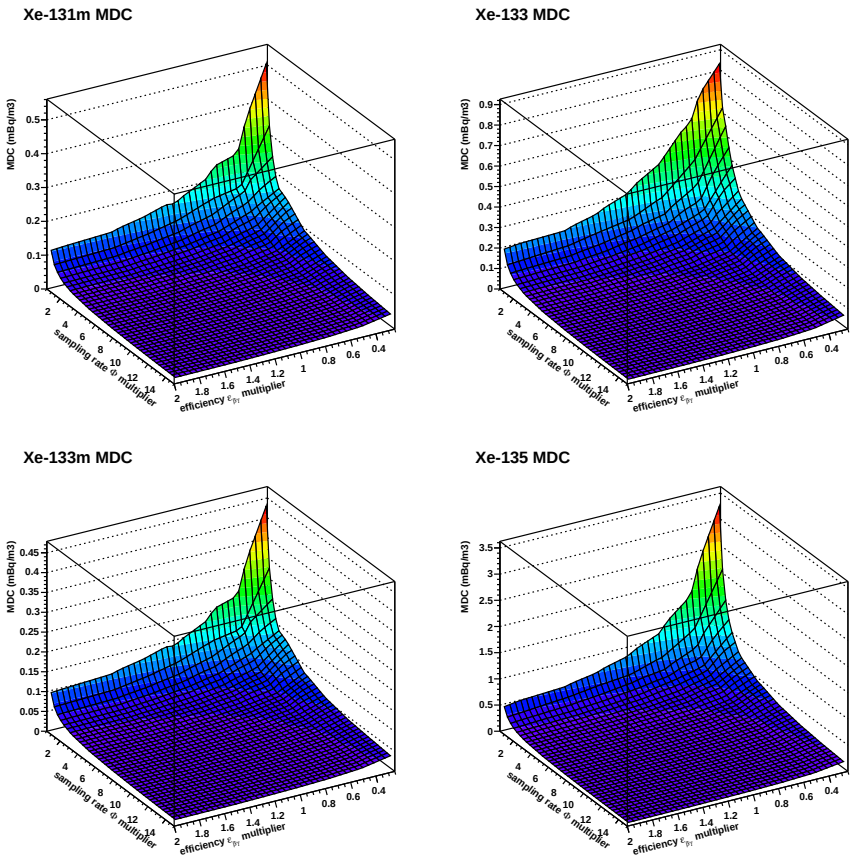

Figure B.3: The MDC as a function of beta-gamma coincidence counting efficiency ($\varepsilon_{\beta\gamma}$) and sampling rate ($\Phi$). The parameters are expressed as multiples of their values for a present SAUNA system operated as in the IMS, so that values of (1,1) yields an MDC expected from an IMS SAUNA system. The calculation assumes all four isotopes ^{131m,133,133m,135}Xe to be present with a concentration of 0.1 mBq/m^3 during sampling, a memory effect of 2 % (applied to a previous sample assumed to have measured exactly the same concentrations), radon at a concentration of 100 Bq/m^3 and a radon suppression factor of 10^6.

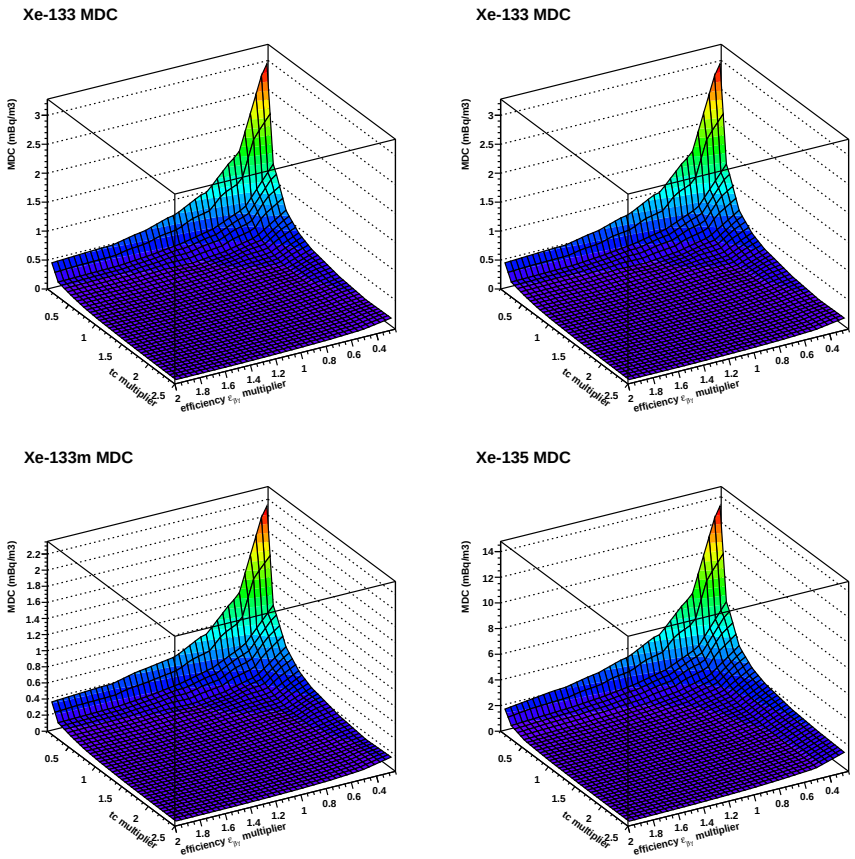

Figure B.4: The MDC as a function of beta-gamma coincidence counting efficiency ($\varepsilon_{\beta\gamma}$) and sample collection time (t_c). The parameters are expressed as multiples of their values for a present SAUNA system operated as in the IMS, so that values of (1,1) yields an MDC expected from an IMS SAUNA system. The calculation assumes all four isotopes ^{131m,133,133m,135}Xe to be present with a concentration of 0.1 mBq/m^3 during sampling, a memory effect of 2 % (applied to a previous sample assumed to have measured exactly the same concentrations), radon at a concentration of 100 Bq/m^3 and a radon suppression factor of 10^6.

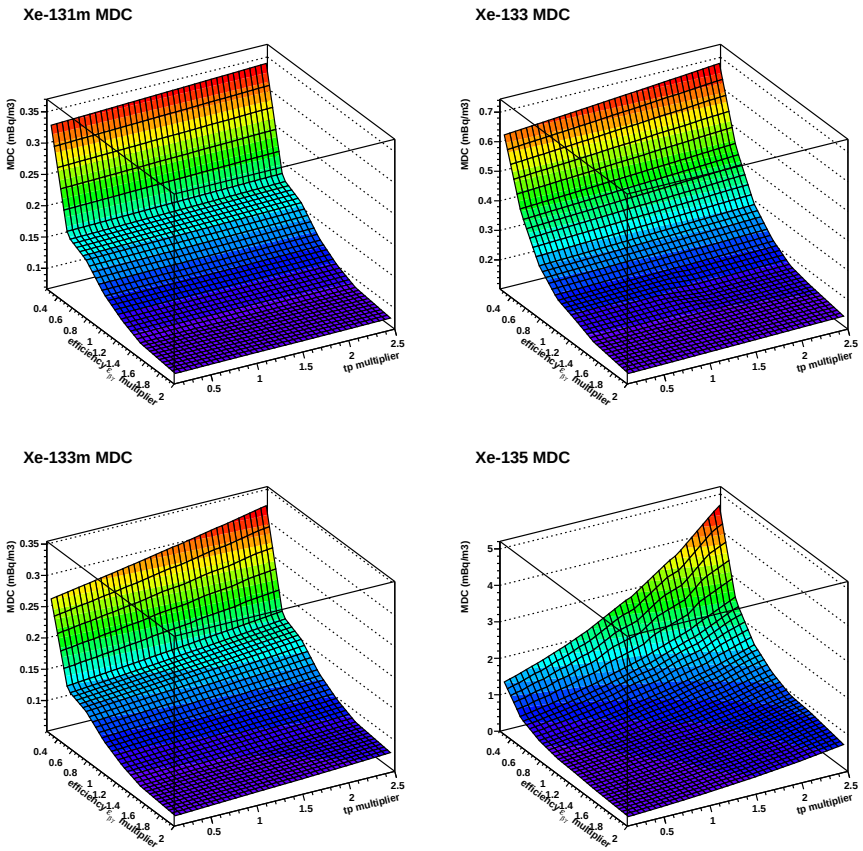

Figure B.5: The MDC as a function of beta-gamma coincidence counting efficiency ($\varepsilon_{\beta\gamma}$) and sample processing time (t_p). The parameters are expressed as multiples of their values for a present SAUNA system operated as in the IMS, so that values of (1,1) yields an MDC expected from an IMS SAUNA system. The calculation assumes all four isotopes ^{131m,133,133m,135}Xe to be present with a concentration of 0.1 mBq/m^3 during sampling, a memory effect of 2 % (applied to a previous sample assumed to have measured exactly the same concentrations), radon at a concentration of 100 Bq/m^3 and a radon suppression factor of 10^6.

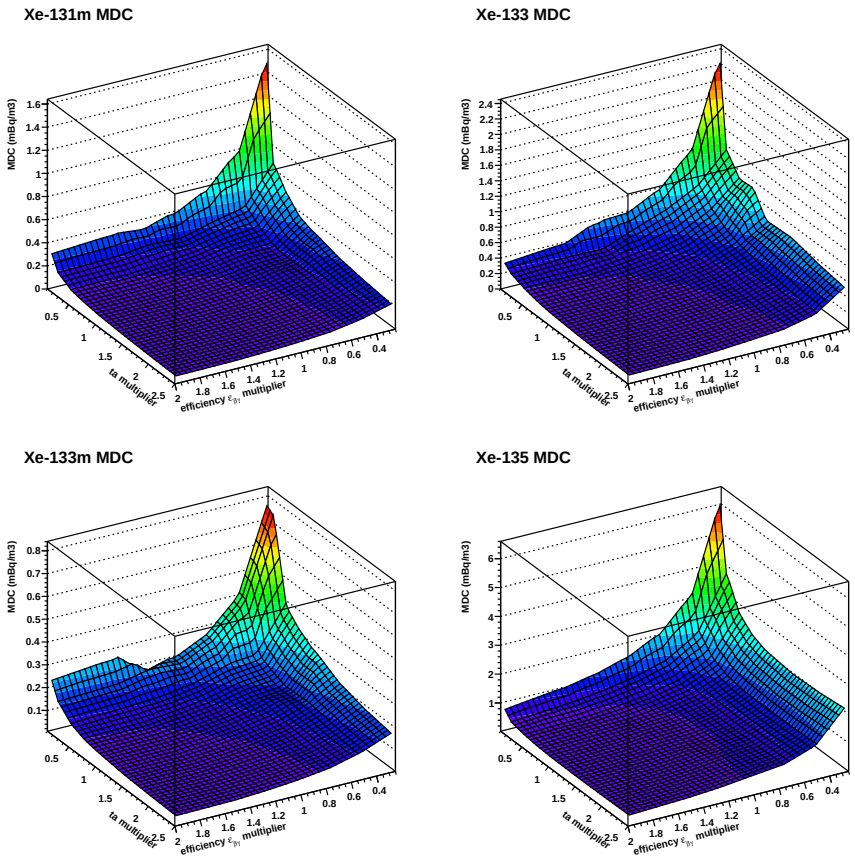

Figure B.6: The MDC as a function of beta-gamma coincidence counting efficiency ($\varepsilon_{\beta\gamma}$) and sample counting time (t_a). The parameters are expressed as multiples of their values for a present SAUNA system operated as in the IMS, so that values of (1,1) yields an MDC expected from an IMS SAUNA system. The calculation assumes all four isotopes ^{131m,133,133m,135}Xe to be present with a concentration of 0.1 mBq/m^3 during sampling, a memory effect of 2 % (applied to a previous sample assumed to have measured exactly the same concentrations), radon at a concentration of 100 Bq/m^3 and a radon suppression factor of 10^6.

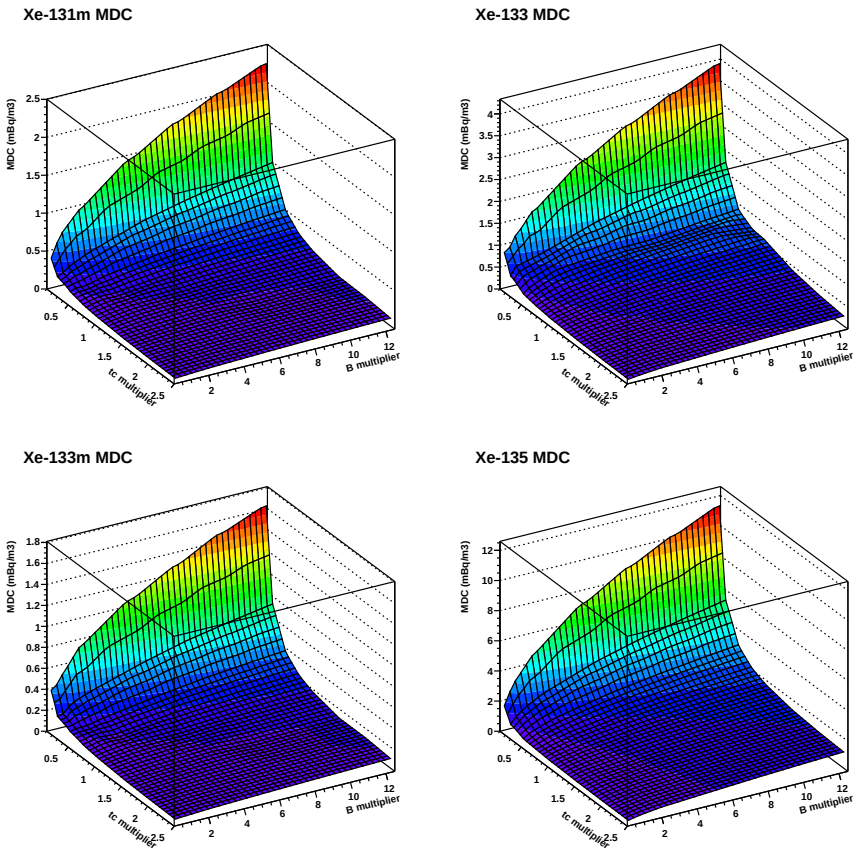

Figure B.7: The MDC as a function of sample collection time (t_c) and ambient background rate (B). The parameters are expressed as multiples of their values for a present SAUNA system operated as in the IMS, so that values of (1,1) yields an MDC expected from an IMS SAUNA system. The calculation assumes all four isotopes ^{131m,133,133m,135}Xe to be present with a concentration of 0.1 mBq/m^3 during sampling, a memory effect of 2 % (applied to a previous sample assumed to have measured exactly the same concentrations), radon at a concentration of 100 Bq/m^3 and a radon suppression factor of 10^6.

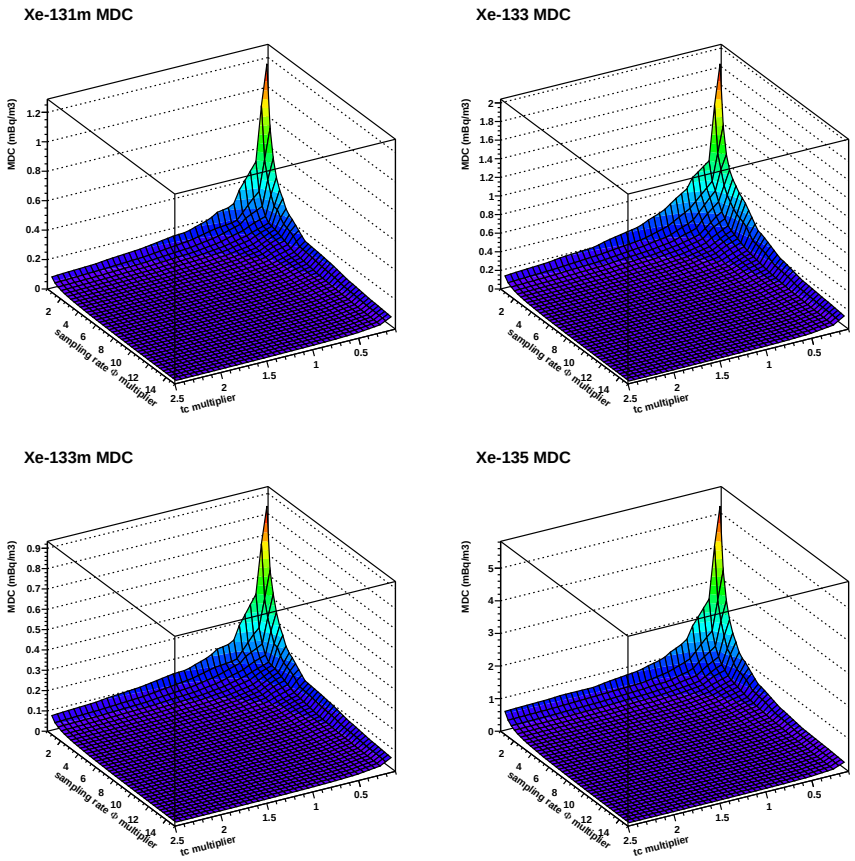

Figure B.8: The MDC as a function of sample collection time (t_c) and sample collection rate (Φ). The parameters are expressed as multiples of their values for a present SAUNA system operated as in the IMS, so that values of (1,1) yields an MDC expected from an IMS SAUNA system. The calculation assumes all four isotopes ^{131m,133,133m,135}Xe to be present with a concentration of 0.1 mBq/m^3 during sampling, a memory effect of 2 % (applied to a previous sample assumed to have measured exactly the same concentrations), radon at a concentration of 100 Bq/m^3 and a radon suppression factor of 10^6.

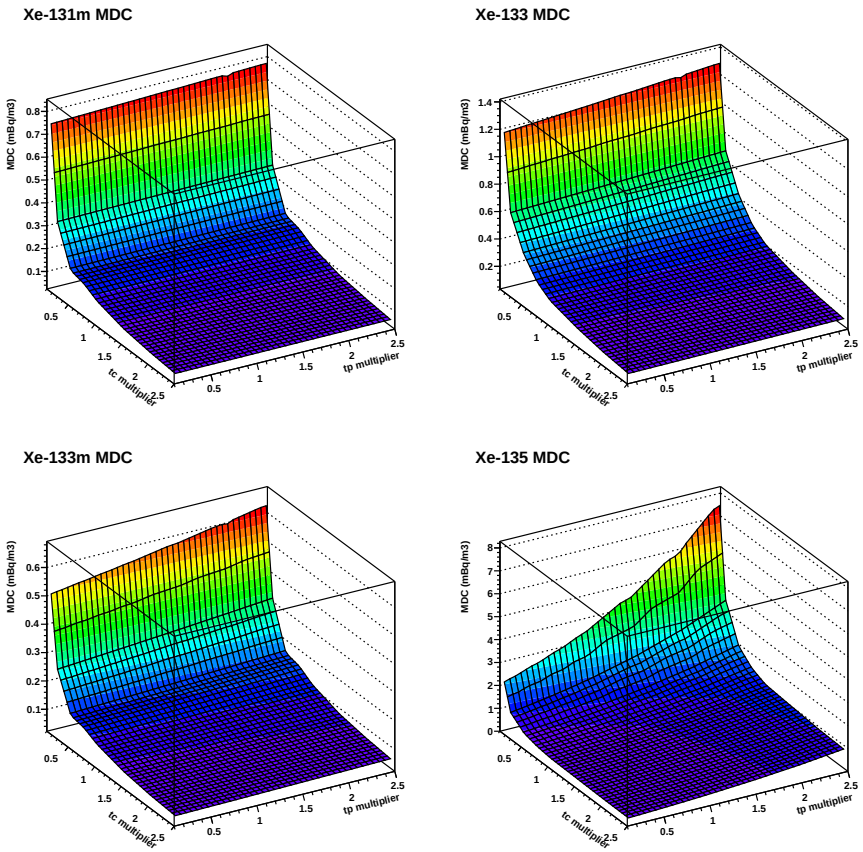

Figure B.9: The MDC as a function of sample collection time (t_c) and sample processing time (t_p). The parameters are expressed as multiples of their values for a present SAUNA system operated as in the IMS, so that values of (1,1) yields an MDC expected from an IMS SAUNA system. The calculation assumes all four isotopes ^{131m,133,133m,135}Xe to be present with a concentration of 0.1 mBq/m^3 during sampling, a memory effect of 2 % (applied to a previous sample assumed to have measured exactly the same concentrations), radon at a concentration of 100 Bq/m^3 and a radon suppression factor of 10^6.

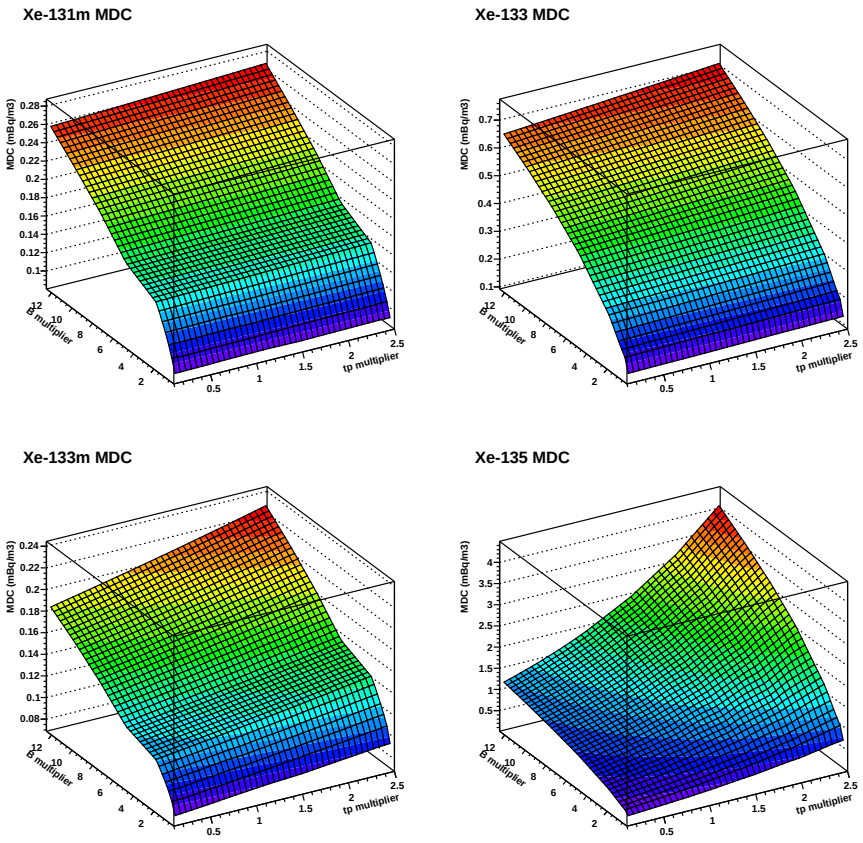

Figure B.10: The MDC as a function of sample processing time (t_p) and ambient background rate (B). The parameters are expressed as multiples of their values for a present SAUNA system operated as in the IMS, so that values of (1,1) yields an MDC expected from an IMS SAUNA system. The calculation assumes all four isotopes ^{131m,133,133m,135}Xe to be present with a concentration of 0.1 mBq/m^3 during sampling, a memory effect of 2 % (applied to a previous sample assumed to have measured exactly the same concentrations), radon at a concentration of 100 Bq/m^3 and a radon suppression factor of 10^6.

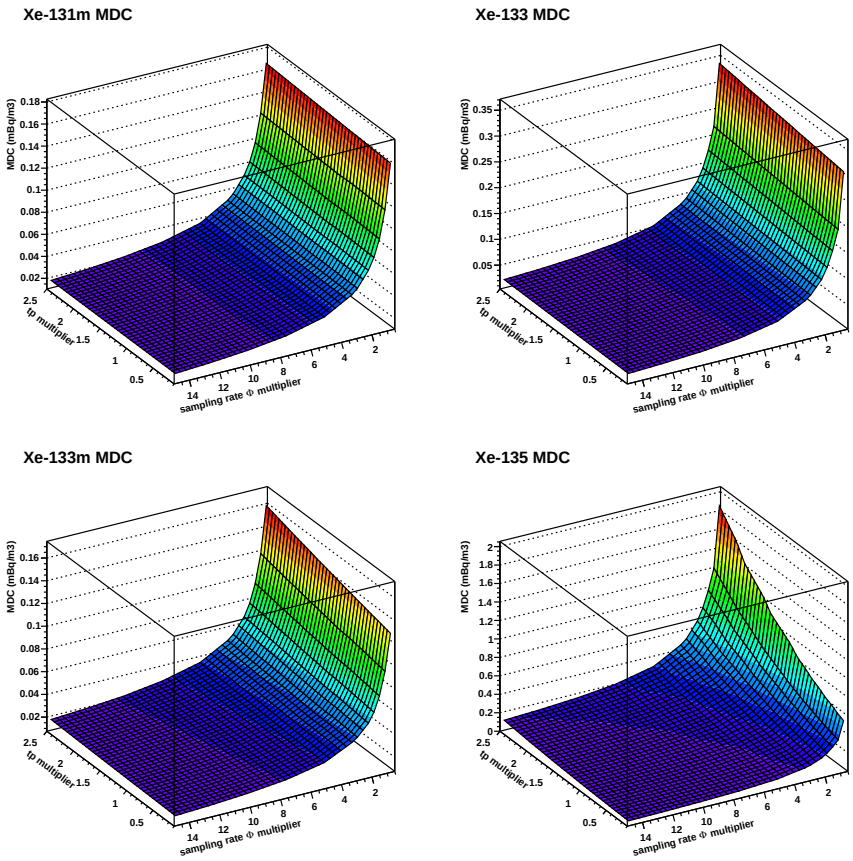

Figure B.11: The MDC as a function of sample processing time (t_p) and sample collection rate (Φ). The parameters are expressed as multiples of their values for a present SAUNA system operated as in the IMS, so that values of (1,1) yields an MDC expected from an IMS SAUNA system. The calculation assumes all four isotopes ^{131m,133,133m,135}Xe to be present with a concentration of 0.1 mBq/m^3 during sampling, a memory effect of 2 % (applied to a previous sample assumed to have measured exactly the same concentrations), radon at a concentration of 100 Bq/m^3 and a radon suppression factor of 10^6.

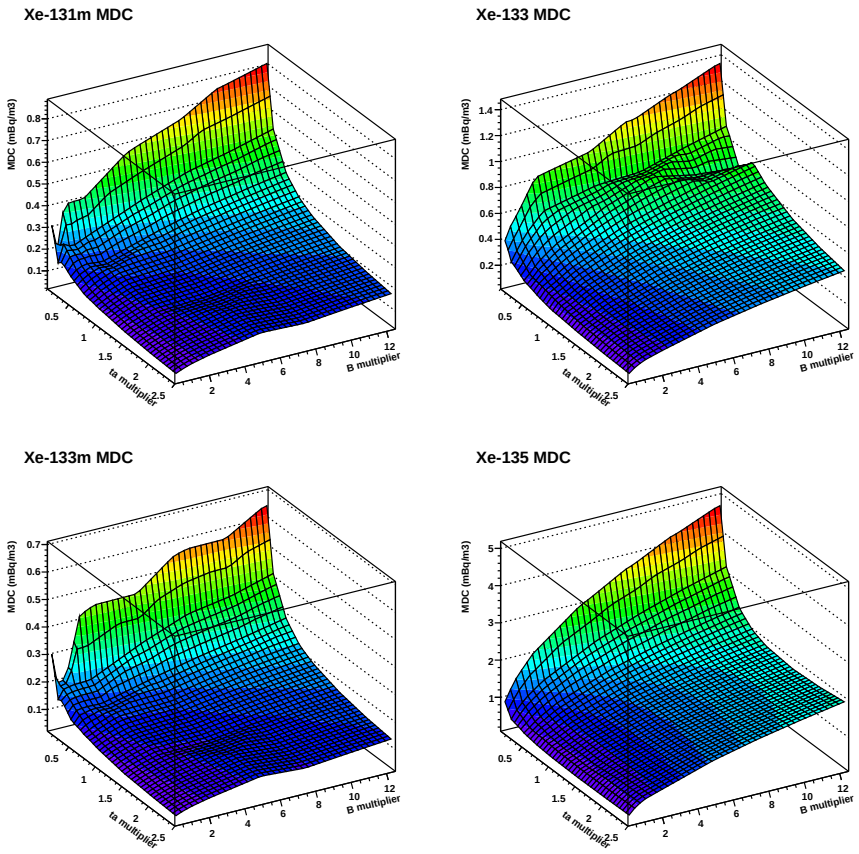

Figure B.12: The MDC as a function of sample counting time (t_a) and ambient background rate (B). The parameters are expressed as multiples of their values for a present SAUNA system operated as in the IMS, so that values of (1,1) yields an MDC expected from an IMS SAUNA system. The calculation assumes all four isotopes ^{131m,133,133m,135}Xe to be present with a concentration of 0.1 mBq/m^3 during sampling, a memory effect of 2 % (applied to a previous sample assumed to have measured exactly the same concentrations), radon at a concentration of 100 Bq/m^3 and a radon suppression factor of 10^6.

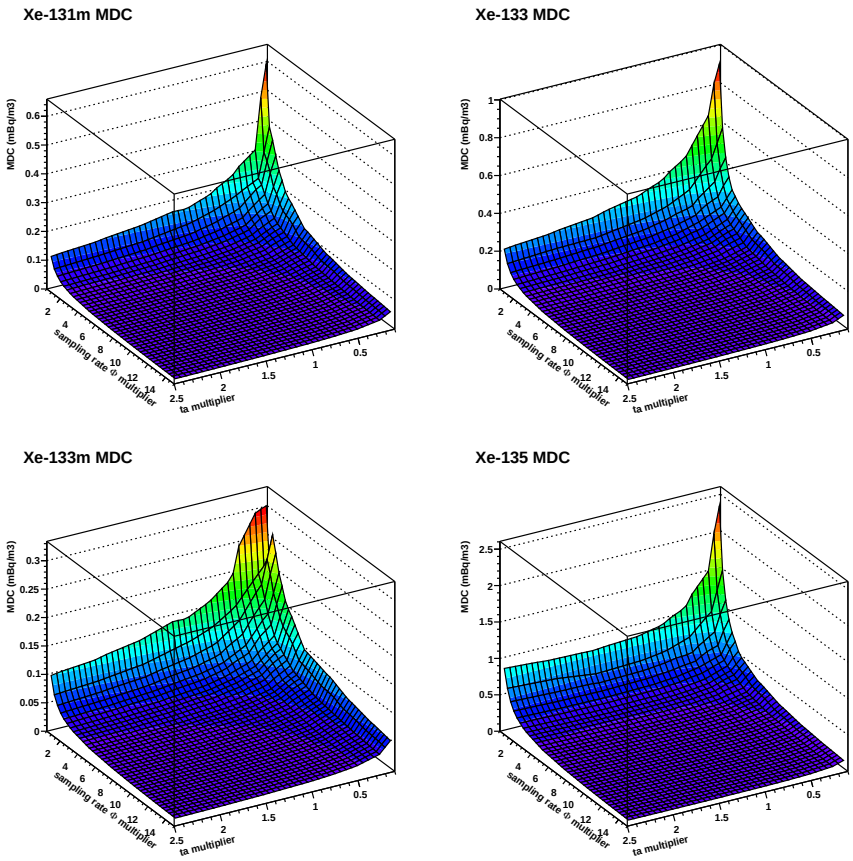

Figure B.13: The MDC as a function of sample counting time (t_a) and sample collection rate (Φ). The parameters are expressed as multiples of their values for a present SAUNA system operated as in the IMS, so that values of (1,1) yields an MDC expected from an IMS SAUNA system. The calculation assumes all four isotopes ^{131m,133,133m,135}Xe to be present with a concentration of 0.1 mBq/m^3 during sampling, a memory effect of 2 % (applied to a previous sample assumed to have measured exactly the same concentrations), radon at a concentration of 100 Bq/m^3 and a radon suppression factor of 10^6.

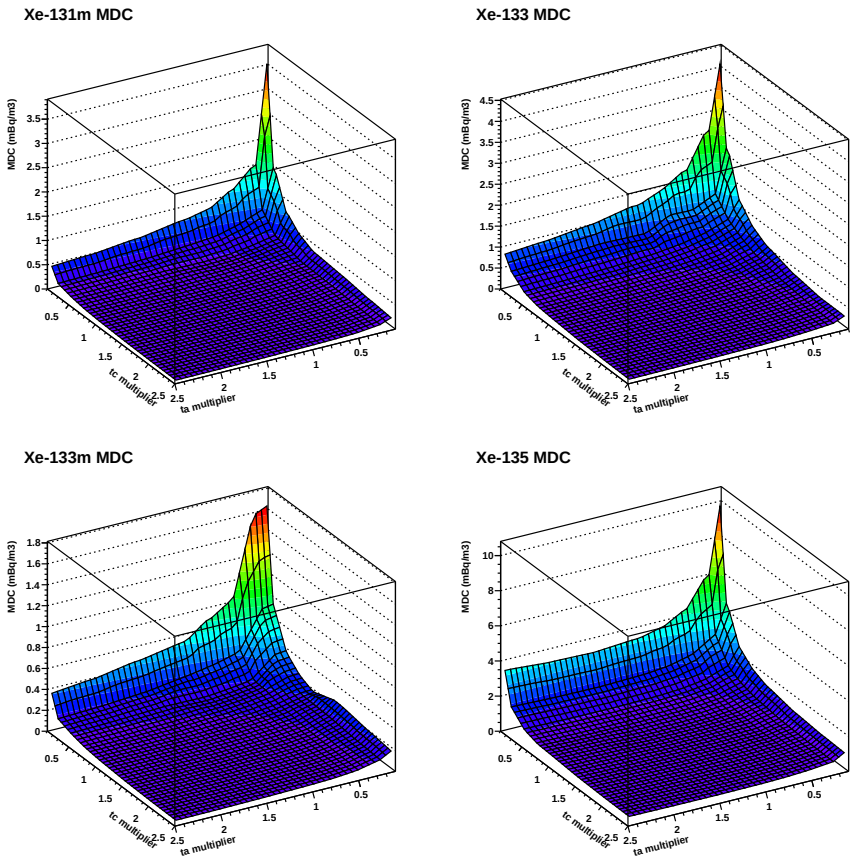

Figure B.14: The MDC as a function of sample counting time (t_a) and sample collection time (t_c). The parameters are expressed as multiples of their values for a present SAUNA system operated as in the IMS, so that values of (1,1) yields an MDC expected from an IMS SAUNA system. The calculation assumes all four isotopes ^{131m,133,133m,135}Xe to be present with a concentration of 0.1 mBq/m^3 during sampling, a memory effect of 2 % (applied to a previous sample assumed to have measured exactly the same concentrations), radon at a concentration of 100 Bq/m^3 and a radon suppression factor of 10^6.

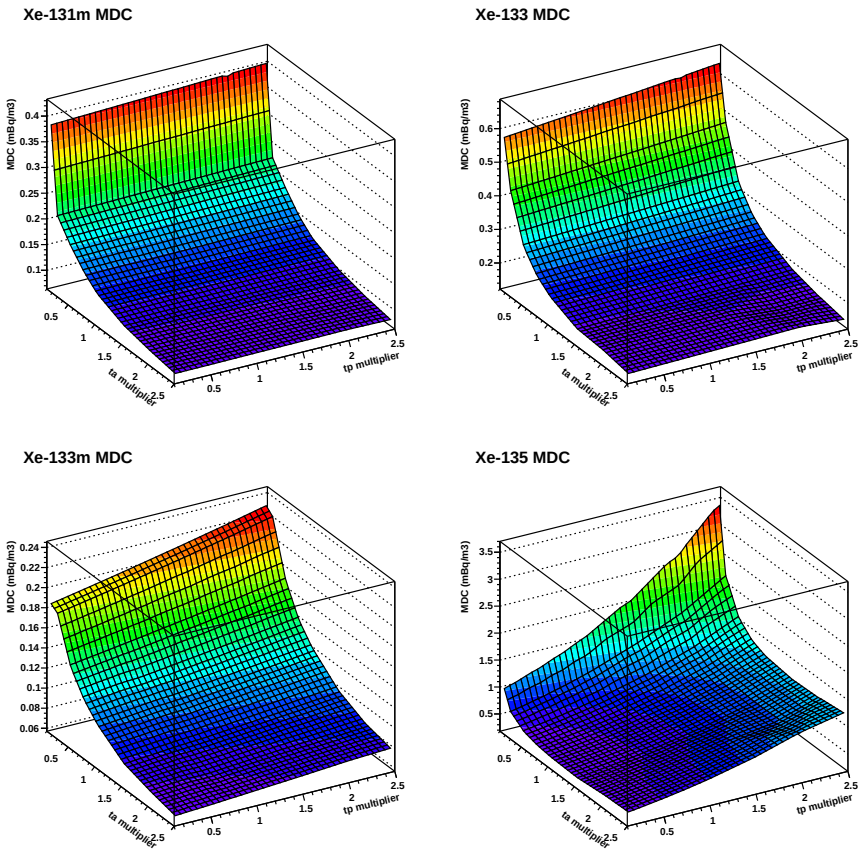

Figure B.15: The MDC as a function of sample counting time (t_a) and sample processing time (t_p). The parameters are expressed as multiples of their values for a present SAUNA system operated as in the IMS, so that values of (1,1) yields an MDC expected from an IMS SAUNA system. The calculation assumes all four isotopes ^{131m,133,133m,135}Xe to be present with a concentration of 0.1 mBq/m^3 during sampling, a memory effect of 2 % (applied to a previous sample assumed to have measured exactly the same concentrations), radon at a concentration of 100 Bq/m^3 and a radon suppression factor of 10^6.

B.2 Variation of Power S with Technical System Parameters

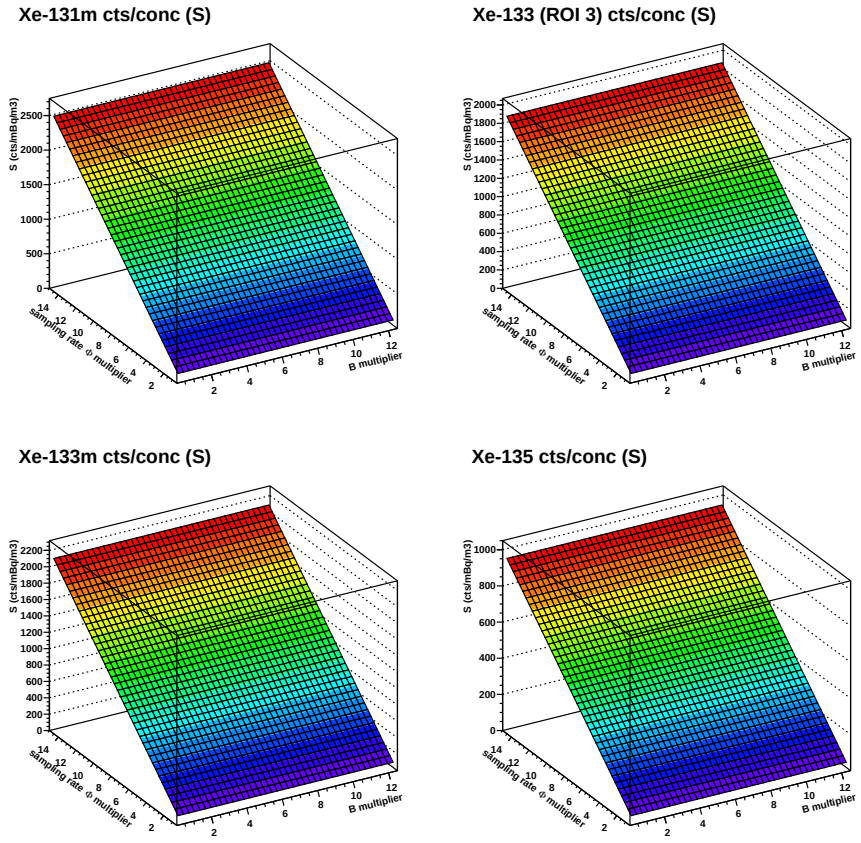

Figure B.16: Power S as a function of ambient background rate (B) and sampling rate (Φ). The parameters are expressed as multiples of their values for a present SAUNA system operated as in the IMS, so that values of (1,1) yields a value of S expected from an IMS SAUNA system. The calculation assumes all four isotopes ^{131m,133,133m,135}Xe to be present with a concentration of 0.1 mBq/m^3 during sampling, a memory effect of 2 % (applied to a previous sample assumed to have measured exactly the same concentrations), radon at a concentration of 100 Bq/m^3 and a radon suppression factor of 10^6.

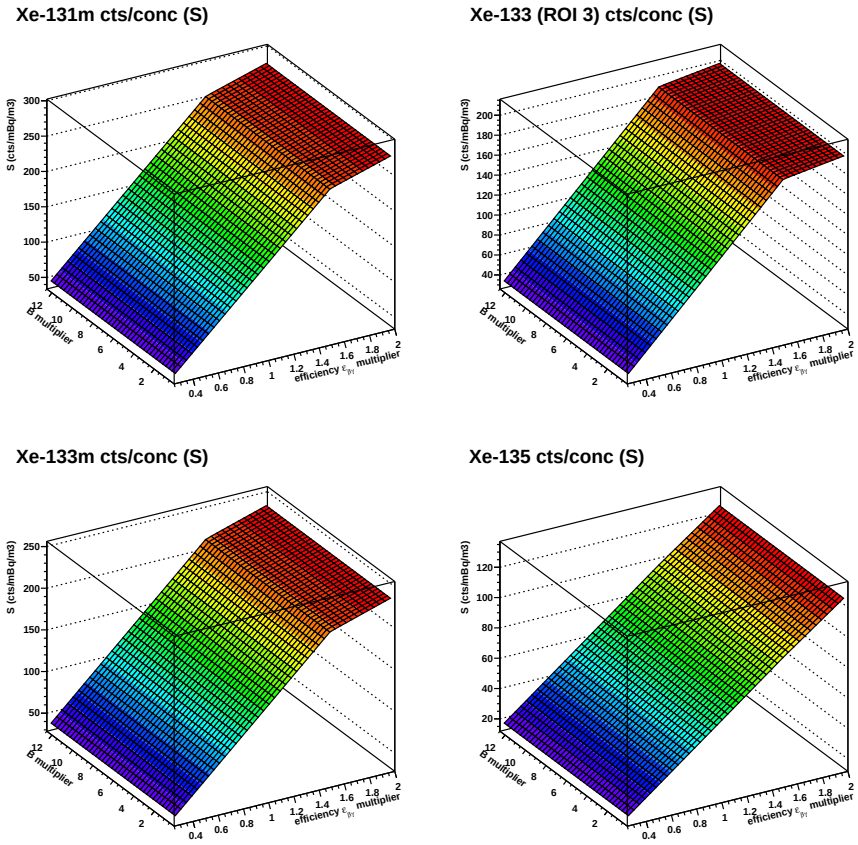

Figure B.17: Power S as a function of beta-gamma coincidence counting efficiency ($\varepsilon_{\beta\gamma}$) and ambient background rate (B). The parameters are expressed as multiples of their values for a present SAUNA system operated as in the IMS, so that values of (1,1) yields a value of S expected from an IMS SAUNA system. The calculation assumes all four isotopes ^{131m,133,133m,135}Xe to be present with a concentration of 0.1 mBq/m^3 during sampling, a memory effect of 2 % (applied to a previous sample assumed to have measured exactly the same concentrations), radon at a concentration of 100 Bq/m^3 and a radon suppression factor of 10^6.

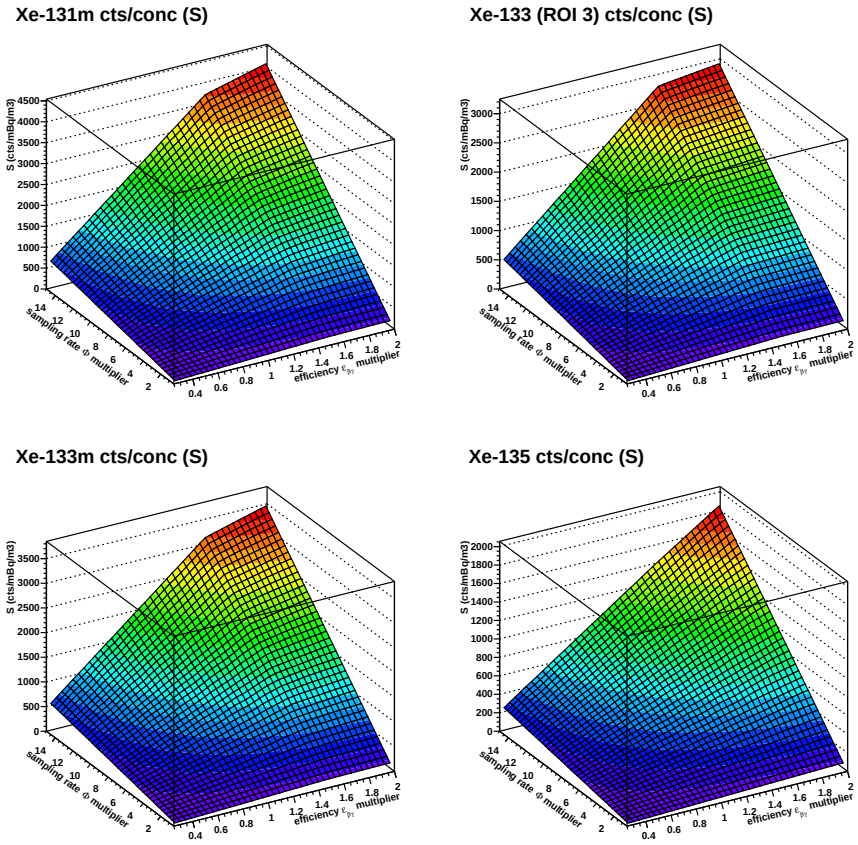

Figure B.18: Power S as a function of beta-gamma coincidence counting efficiency ($\varepsilon_{\beta\gamma}$) and sampling rate ($\Phi$). The parameters are expressed as multiples of their values for a present SAUNA system operated as in the IMS, so that values of (1,1) yields a value of S expected from an IMS SAUNA system. The calculation assumes all four isotopes ^{131m,133,133m,135}Xe to be present with a concentration of 0.1 mBq/m^3 during sampling, a memory effect of 2 % (applied to a previous sample assumed to have measured exactly the same concentrations), radon at a concentration of 100 Bq/m^3 and a radon suppression factor of 10^6.

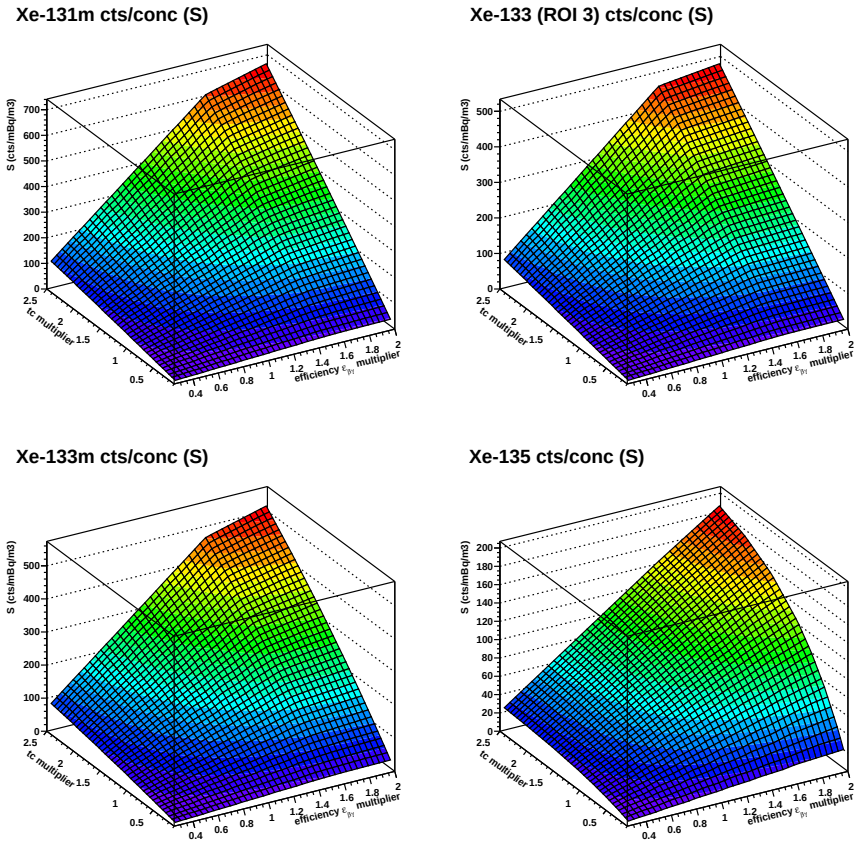

Figure B.19: Power S as a function of beta-gamma coincidence counting efficiency ($\varepsilon_{\beta\gamma}$) and sample collection time (t_c). The parameters are expressed as multiples of their values for a present SAUNA system operated as in the IMS, so that values of (1,1) yields a value of S expected from an IMS SAUNA system. The calculation assumes all four isotopes ^{131m,133,133m,135}Xe to be present with a concentration of 0.1 mBq/m^3 during sampling, a memory effect of 2 % (applied to a previous sample assumed to have measured exactly the same concentrations), radon at a concentration of 100 Bq/m^3 and a radon suppression factor of 10^6.

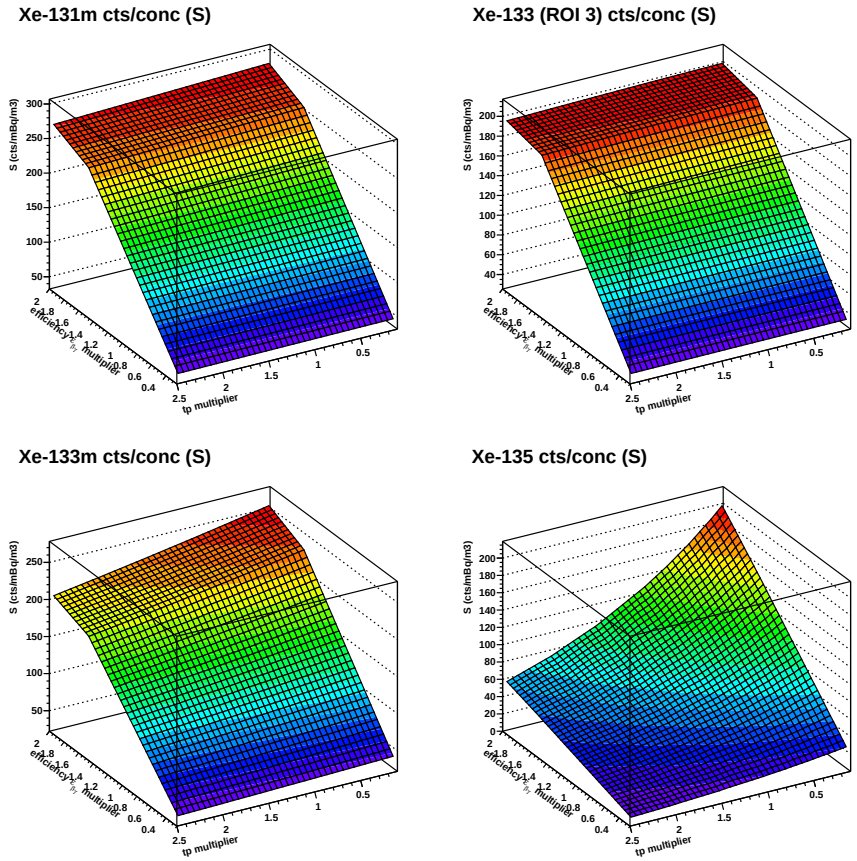

Figure B.20: Power S as a function of beta-gamma coincidence counting efficiency ($\varepsilon_{\beta\gamma}$) and sample processing time (t_p). The parameters are expressed as multiples of their values for a present SAUNA system operated as in the IMS, so that values of (1,1) yields a value of S expected from an IMS SAUNA system. The calculation assumes all four isotopes ^{131m,133,133m,135}Xe to be present with a concentration of 0.1 mBq/m^3 during sampling, a memory effect of 2 % (applied to a previous sample assumed to have measured exactly the same concentrations), radon at a concentration of 100 Bq/m^3 and a radon suppression factor of 10^6.

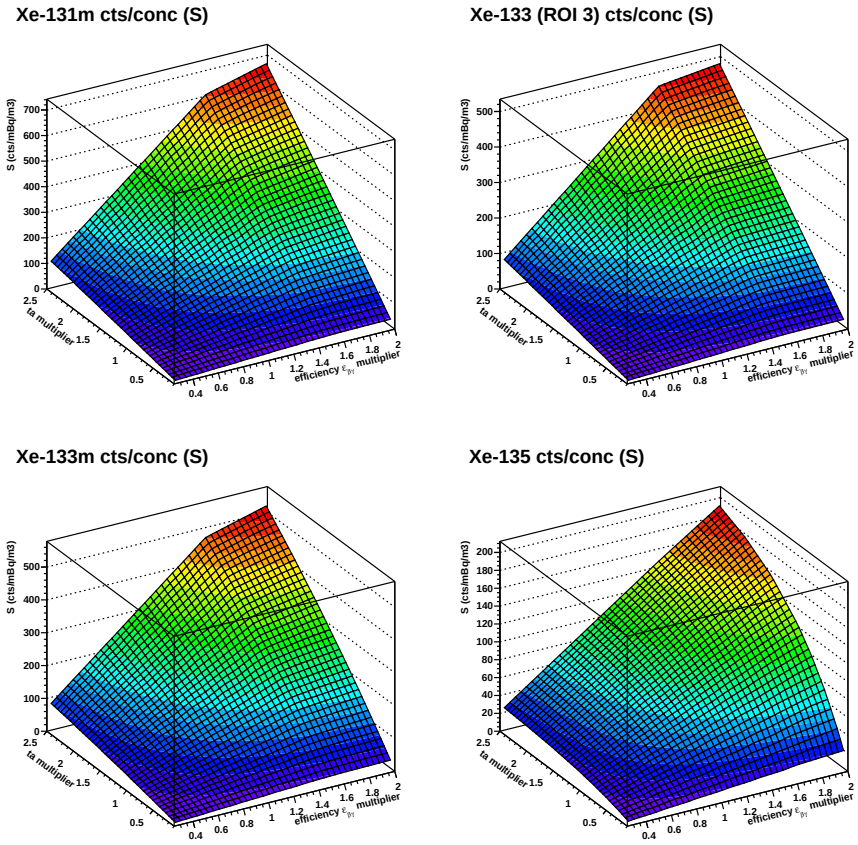

Figure B.21: Power S as a function of beta-gamma coincidence counting efficiency ($\varepsilon_{\beta\gamma}$) and sample counting time (t_a). The parameters are expressed as multiples of their values for a present SAUNA system operated as in the IMS, so that values of (1,1) yields a value of S expected from an IMS SAUNA system. The calculation assumes all four isotopes ^{131m,133,133m,135}Xe to be present with a concentration of 0.1 mBq/m^3 during sampling, a memory effect of 2 % (applied to a previous sample assumed to have measured exactly the same concentrations), radon at a concentration of 100 Bq/m^3 and a radon suppression factor of 10^6.

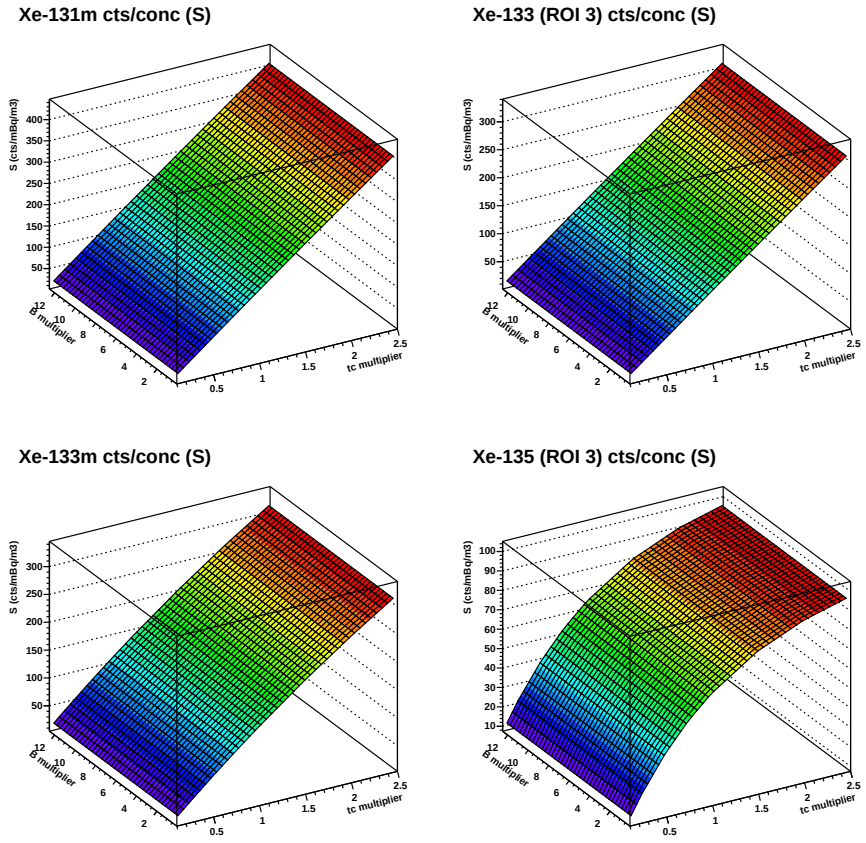

Figure B.22: Power S as a function of sample collection time (t_c) and ambient background rate (B). The parameters are expressed as multiples of their values for a present SAUNA system operated as in the IMS, so that values of (1,1) yields a value of S expected from an IMS SAUNA system. The calculation assumes all four isotopes ^{131m,133,133m,135}Xe to be present with a concentration of 0.1 mBq/m^3 during sampling, a memory effect of 2 % (applied to a previous sample assumed to have measured exactly the same concentrations), radon at a concentration of 100 Bq/m^3 and a radon suppression factor of 10^6.

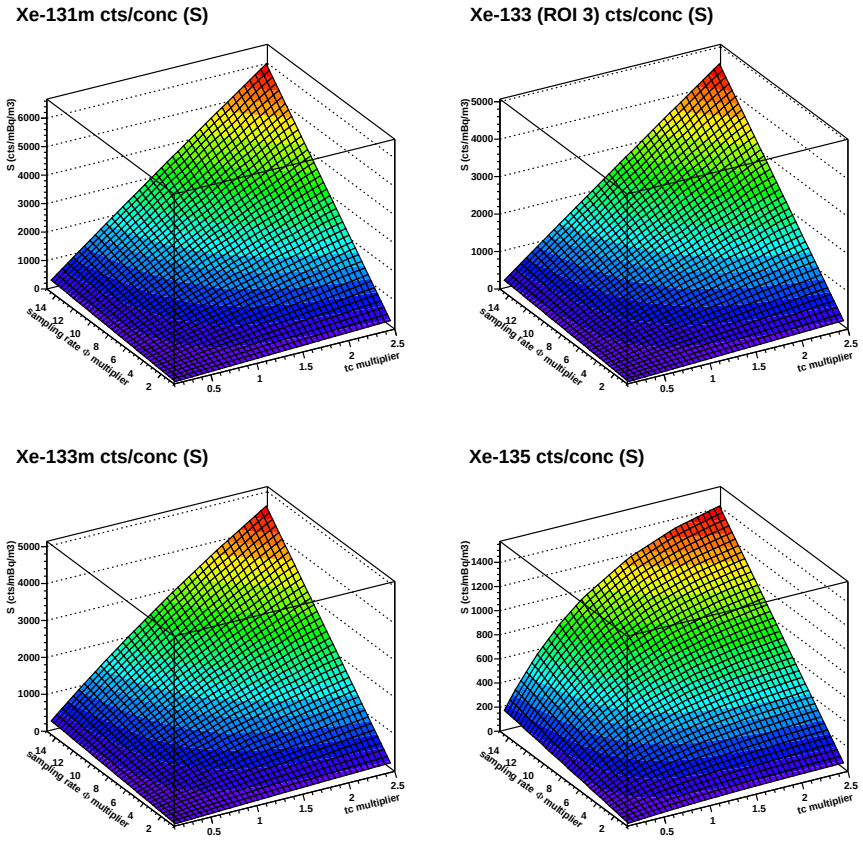

Figure B.23: Power S as a function of sample collection time (t_c) and sample collection rate (Φ). The parameters are expressed as multiples of their values for a present SAUNA system operated as in the IMS, so that values of (1,1) yields a value of S expected from an IMS SAUNA system. The calculation assumes all four isotopes ^{131m,133,133m,135}Xe to be present with a concentration of 0.1 mBq/m^3 during sampling, a memory effect of 2 % (applied to a previous sample assumed to have measured exactly the same concentrations), radon at a concentration of 100 Bq/m^3 and a radon suppression factor of 10^6.

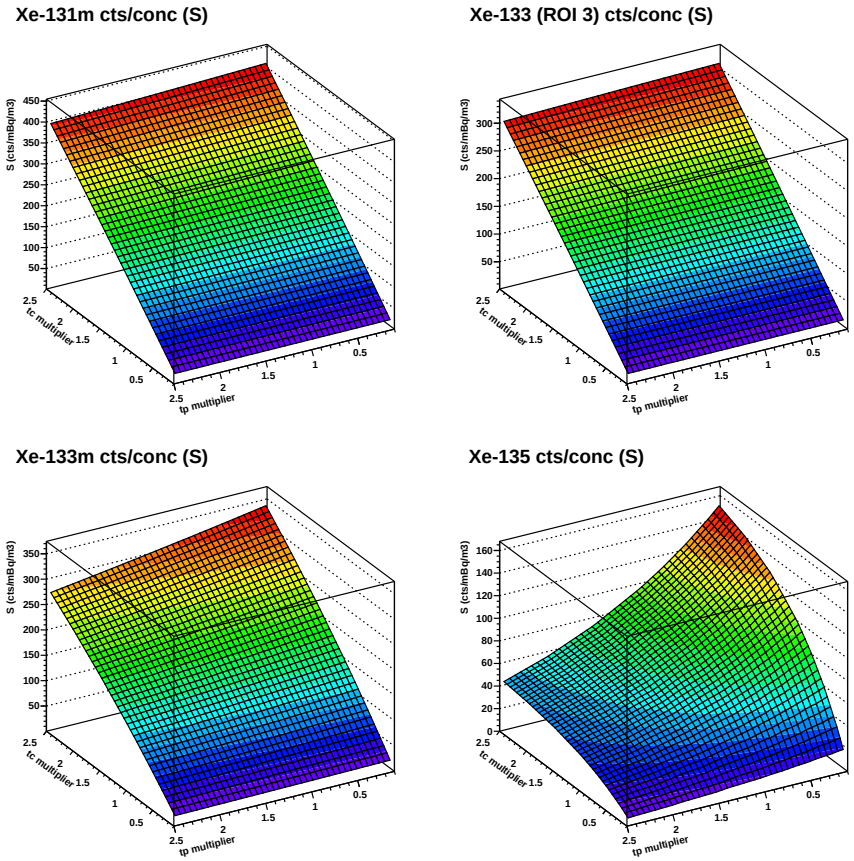

Figure B.24: Power S as a function of sample collection time (t_c) and sample processing time (t_p). The parameters are expressed as multiples of their values for a present SAUNA system operated as in the IMS, so that values of (1,1) yields a value of S expected from an IMS SAUNA system. The calculation assumes all four isotopes ^{131m,133,133m,135}Xe to be present with a concentration of 0.1 mBq/m^3 during sampling, a memory effect of 2 % (applied to a previous sample assumed to have measured exactly the same concentrations), radon at a concentration of 100 Bq/m^3 and a radon suppression factor of 10^6.

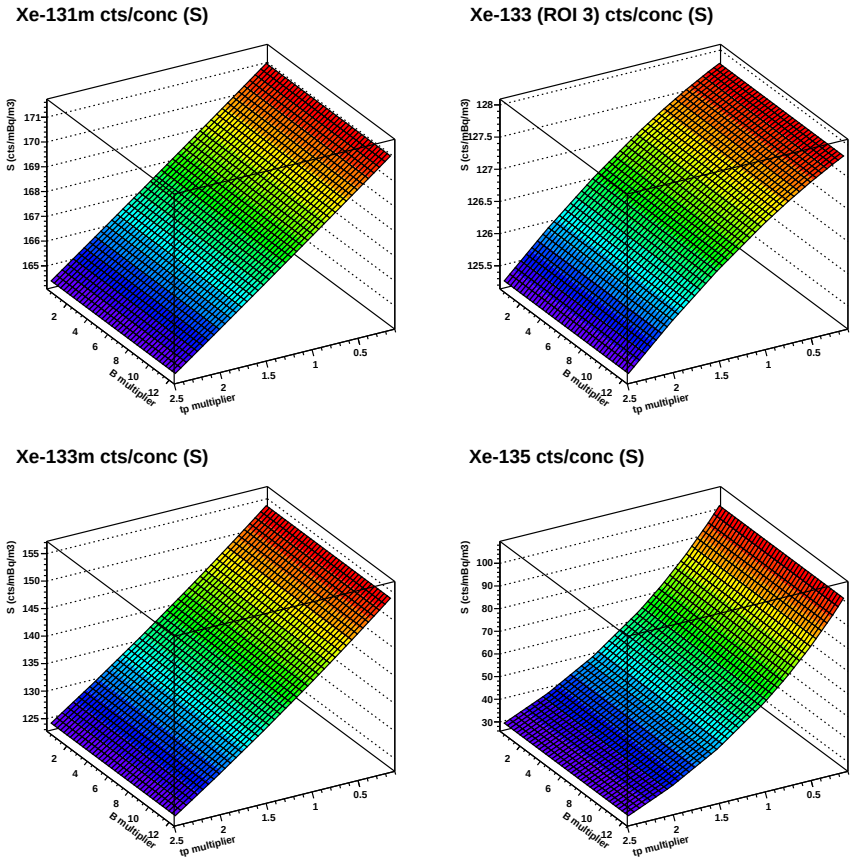

Figure B.25: Power S as a function of sample processing time (t_p) and ambient background rate (B). The parameters are expressed as multiples of their values for a present SAUNA system operated as in the IMS, so that values of (1,1) yields a value of S expected from an IMS SAUNA system. The calculation assumes all four isotopes ^{131m,133,133m,135}Xe to be present with a concentration of 0.1 mBq/m^3 during sampling, a memory effect of 2 % (applied to a previous sample assumed to have measured exactly the same concentrations), radon at a concentration of 100 Bq/m^3 and a radon suppression factor of 10^6.

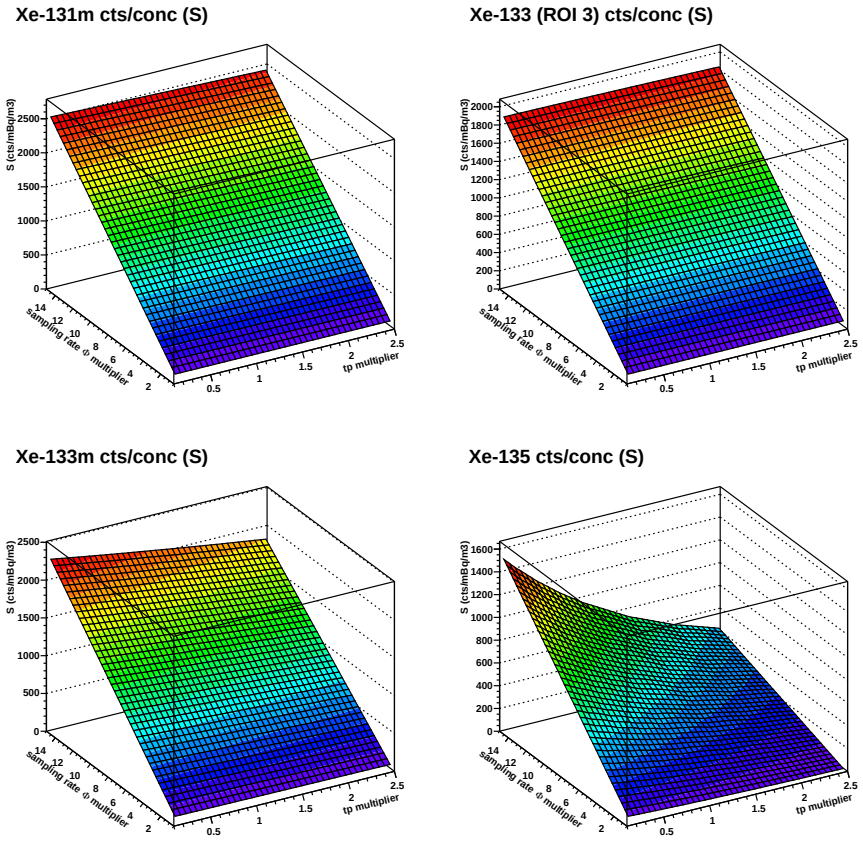

Figure B.26: Power S as a function of sample processing time (t_p) and sample collection rate (Φ). The parameters are expressed as multiples of their values for a present SAUNA system operated as in the IMS, so that values of (1,1) yields a value of S expected from an IMS SAUNA system. The calculation assumes all four isotopes ^{131m,133,133m,135}Xe to be present with a concentration of 0.1 mBq/m^3 during sampling, a memory effect of 2 % (applied to a previous sample assumed to have measured exactly the same concentrations), radon at a concentration of 100 Bq/m^3 and a radon suppression factor of 10^6.

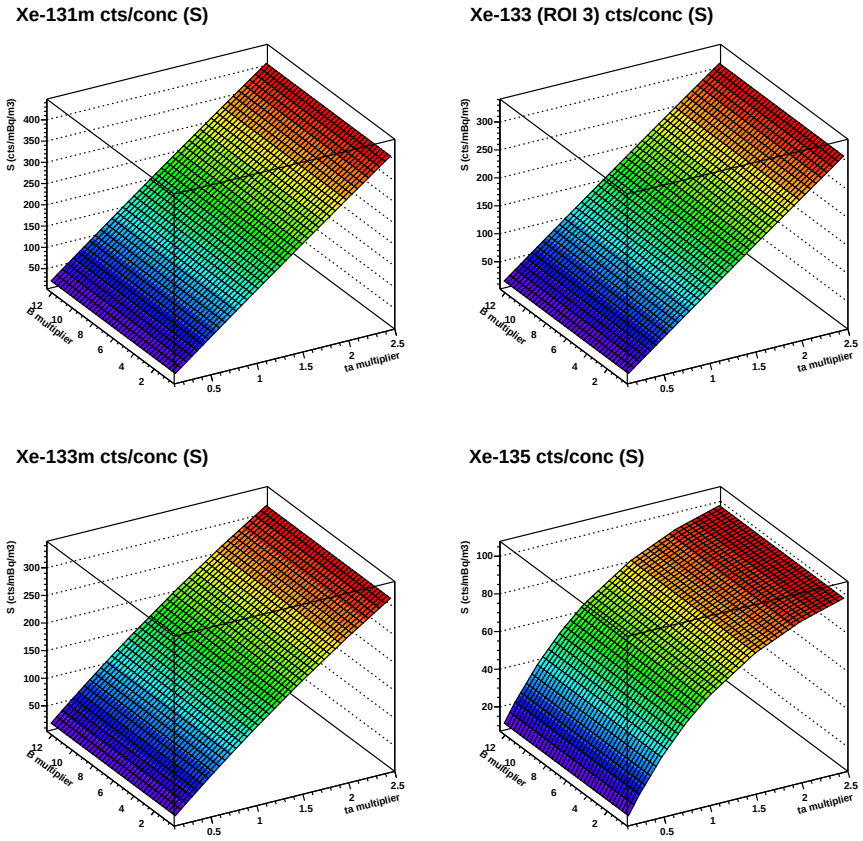

Figure B.27: Power S as a function of sample counting time (t_a) and ambient background rate (B). The parameters are expressed as multiples of their values for a present SAUNA system operated as in the IMS, so that values of (1,1) yields a value of S expected from an IMS SAUNA system. The calculation assumes all four isotopes ^{131m,133,133m,135}Xe to be present with a concentration of 0.1 mBq/m^3 during sampling, a memory effect of 2 % (applied to a previous sample assumed to have measured exactly the same concentrations), radon at a concentration of 100 Bq/m^3 and a radon suppression factor of 10^6.

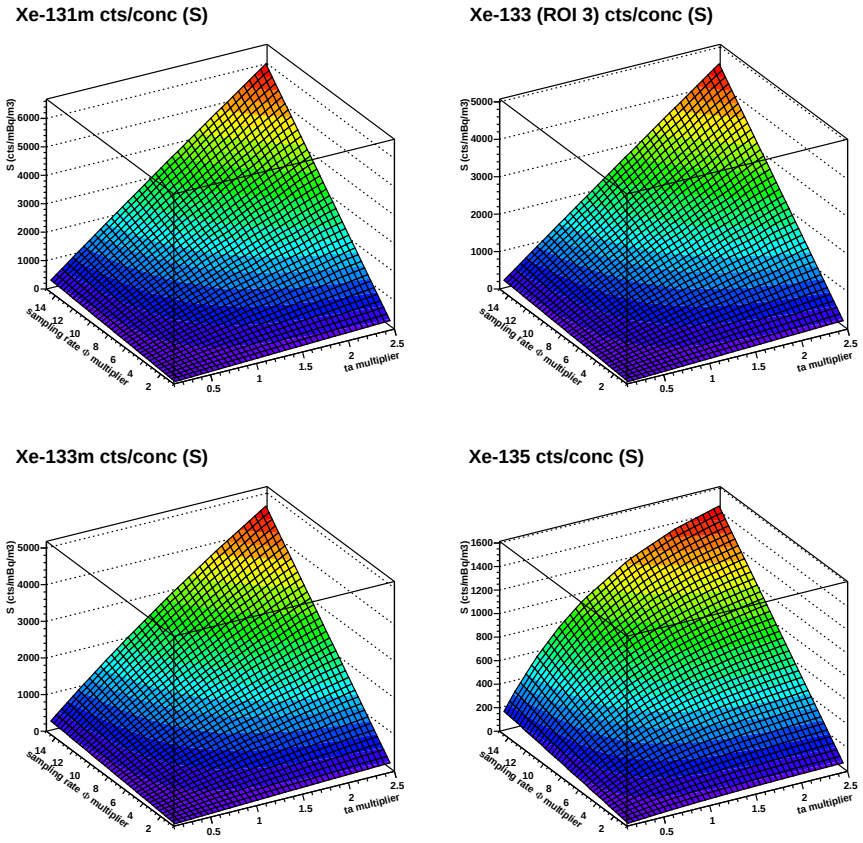

Figure B.28: Power S as a function of sample counting time (t_a) and sample collection rate (Φ). The parameters are expressed as multiples of their values for a present SAUNA system operated as in the IMS, so that values of (1,1) yields a value of S expected from an IMS SAUNA system. The calculation assumes all four isotopes ^{131m,133,133m,135}Xe to be present with a concentration of 0.1 mBq/m^3 during sampling, a memory effect of 2 % (applied to a previous sample assumed to have measured exactly the same concentrations), radon at a concentration of 100 Bq/m^3 and a radon suppression factor of 10^6.

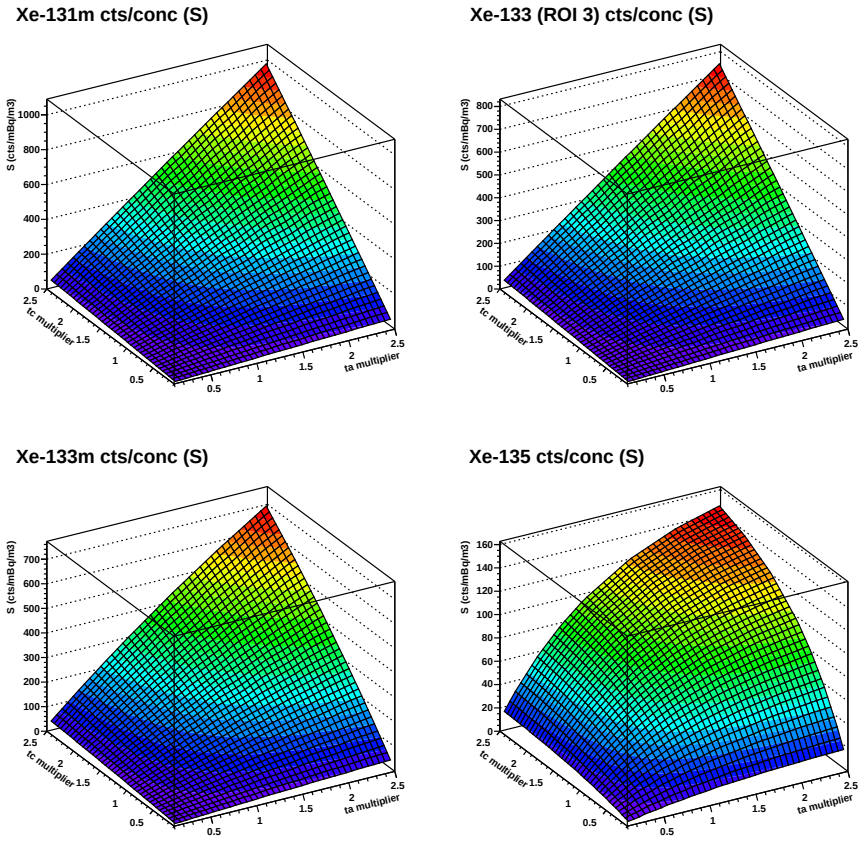

Figure B.29: Power S as a function of sample counting time (t_a) and sample collection time (t_c). The parameters are expressed as multiples of their values for a present SAUNA system operated as in the IMS, so that values of (1,1) yields a value of S expected from an IMS SAUNA system. The calculation assumes all four isotopes ^{131m,133,133m,135}Xe to be present with a concentration of 0.1 mBq/m^3 during sampling, a memory effect of 2 % (applied to a previous sample assumed to have measured exactly the same concentrations), radon at a concentration of 100 Bq/m^3 and a radon suppression factor of 10^6.

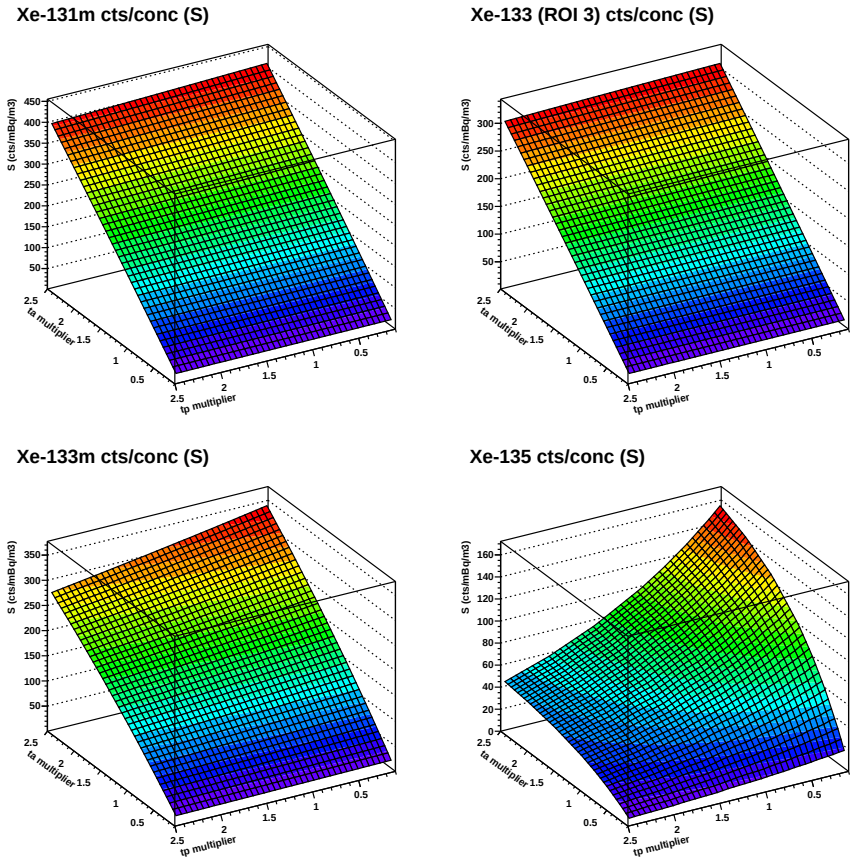

Figure B.30: Power S as a function of sample counting time (t_a) and sample processing time (t_p). The parameters are expressed as multiples of their values for a present SAUNA system operated as in the IMS, so that values of (1,1) yields a value of S expected from an IMS SAUNA system. The calculation assumes all four isotopes ^{131m,133,133m,135}Xe to be present with a concentration of 0.1 mBq/m^3 during sampling, a memory effect of 2 % (applied to a previous sample assumed to have measured exactly the same concentrations), radon at a concentration of 100 Bq/m^3 and a radon suppression factor of 10^6.

B.3 Variation of Background n_0 with Technical System Parameters

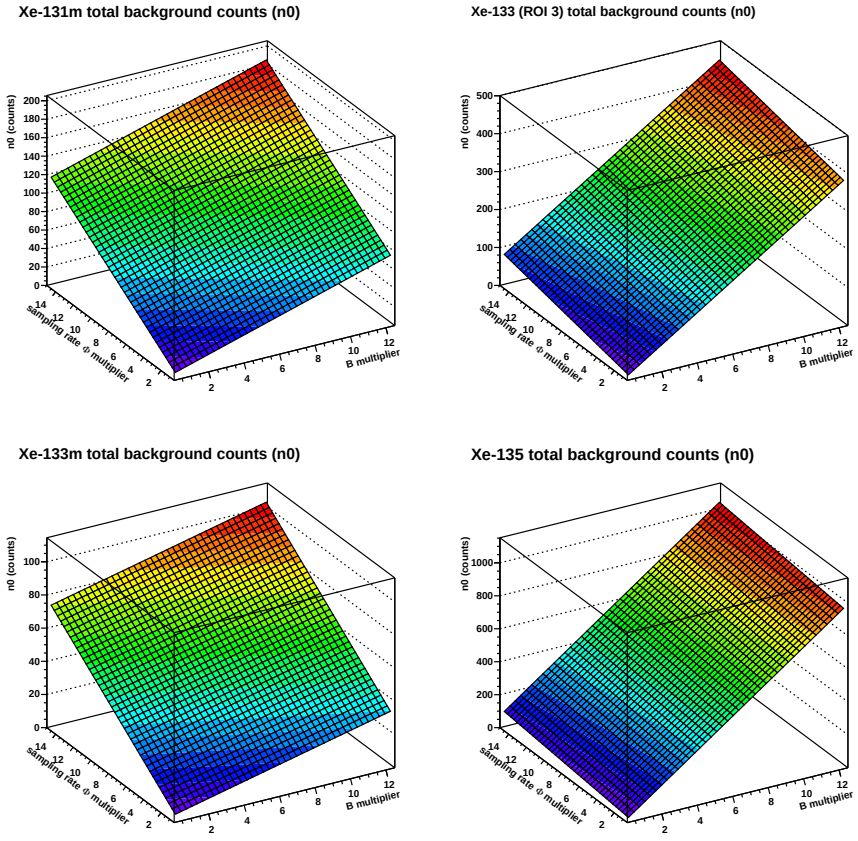

Figure B.31: Background counts n_0 as a function of ambient background rate (B) and sampling rate (Φ). The parameters are expressed as multiples of their values for a present SAUNA system operated as in the IMS, so that values of (1,1) yields a value of n_0 expected from an IMS SAUNA system. The calculation assumes all four isotopes ^{131m,133,133m,135}Xe to be present with a concentration of 0.1 mBq/m^3 during sampling, a memory effect of 2 % (applied to a previous sample assumed to have measured exactly the same concentrations), radon at a concentration of 100 Bq/m^3 and a radon suppression factor of 10^6.

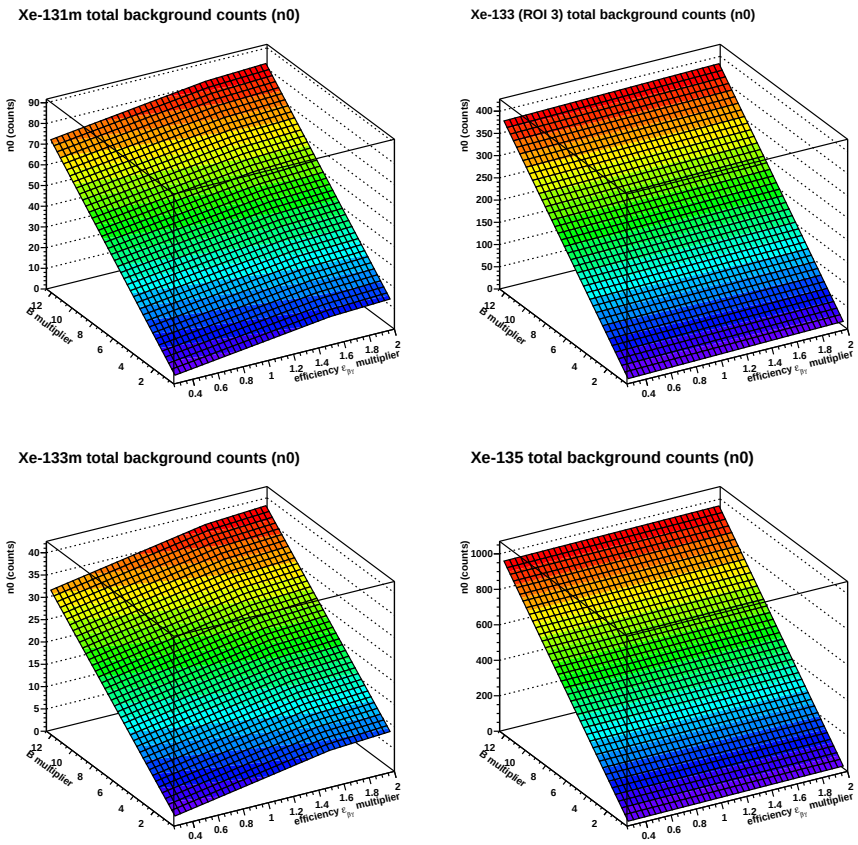

Figure B.32: Background counts n_0 as a function of beta-gamma coincidence counting efficiency ($\varepsilon_{\beta\gamma}$) and ambient background rate (B). The parameters are expressed as multiples of their values for a present SAUNA system operated as in the IMS, so that values of (1,1) yields a value of n_0 expected from an IMS SAUNA system. The calculation assumes all four isotopes ^{131m,133,133m,135}Xe to be present with a concentration of 0.1 mBq/m^3 during sampling, a memory effect of 2 % (applied to a previous sample assumed to have measured exactly the same concentrations), radon at a concentration of 100 Bq/m^3 and a radon suppression factor of 10^6.

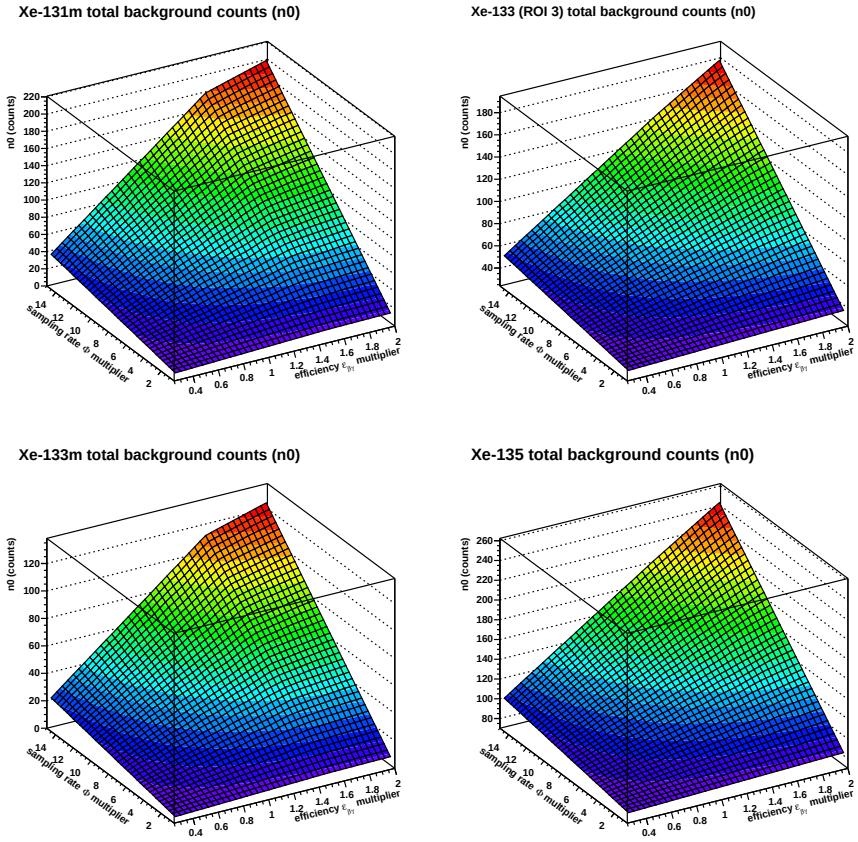

Figure B.33: Background counts n_0 as a function of beta-gamma coincidence counting efficiency ($\varepsilon_{\beta\gamma}$) and sampling rate ($\Phi$). The parameters are expressed as multiples of their values for a present SAUNA system operated as in the IMS, so that values of (1,1) yields a value of n_0 expected from an IMS SAUNA system. The calculation assumes all four isotopes ^{131m,133,133m,135}Xe to be present with a concentration of 0.1 mBq/m^3 during sampling, a memory effect of 2 % (applied to a previous sample assumed to have measured exactly the same concentrations), radon at a concentration of 100 Bq/m^3 and a radon suppression factor of 10^6.

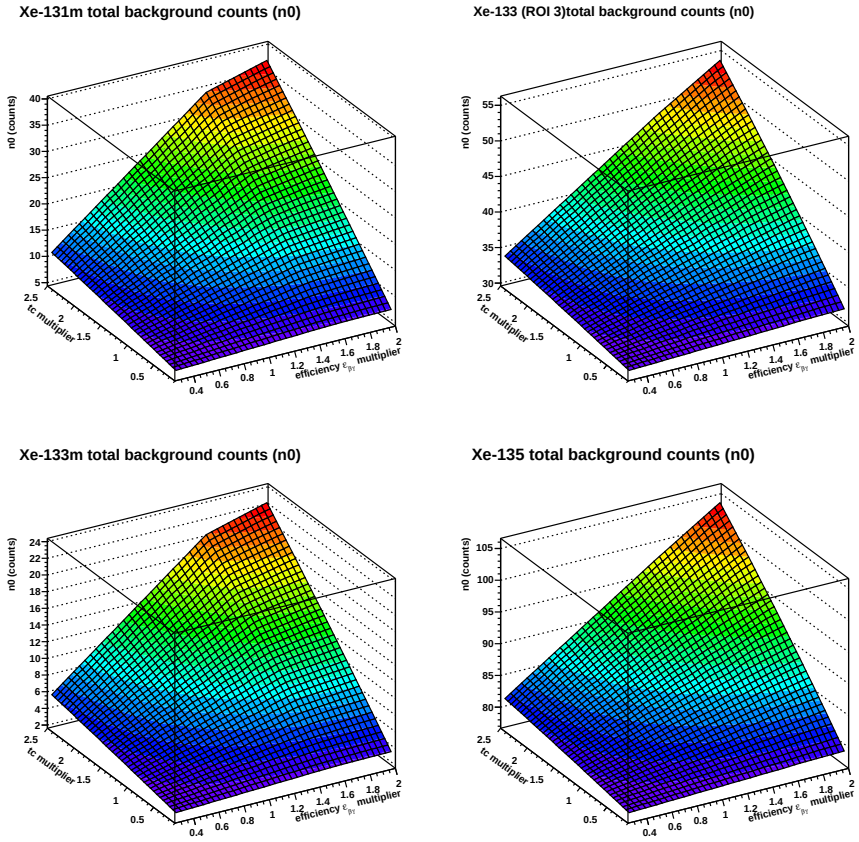

Figure B.34: Background counts n_0 as a function of beta-gamma coincidence counting efficiency ($\varepsilon_{\beta\gamma}$) and sample collection time (t_c). The parameters are expressed as multiples of their values for a present SAUNA system operated as in the IMS, so that values of (1,1) yields a value of n_0 expected from an IMS SAUNA system. The calculation assumes all four isotopes ^{131m,133,133m,135}Xe to be present with a concentration of 0.1 mBq/m^3 during sampling, a memory effect of 2 % (applied to a previous sample assumed to have measured exactly the same concentrations), radon at a concentration of 100 Bq/m^3 and a radon suppression factor of 10^6.

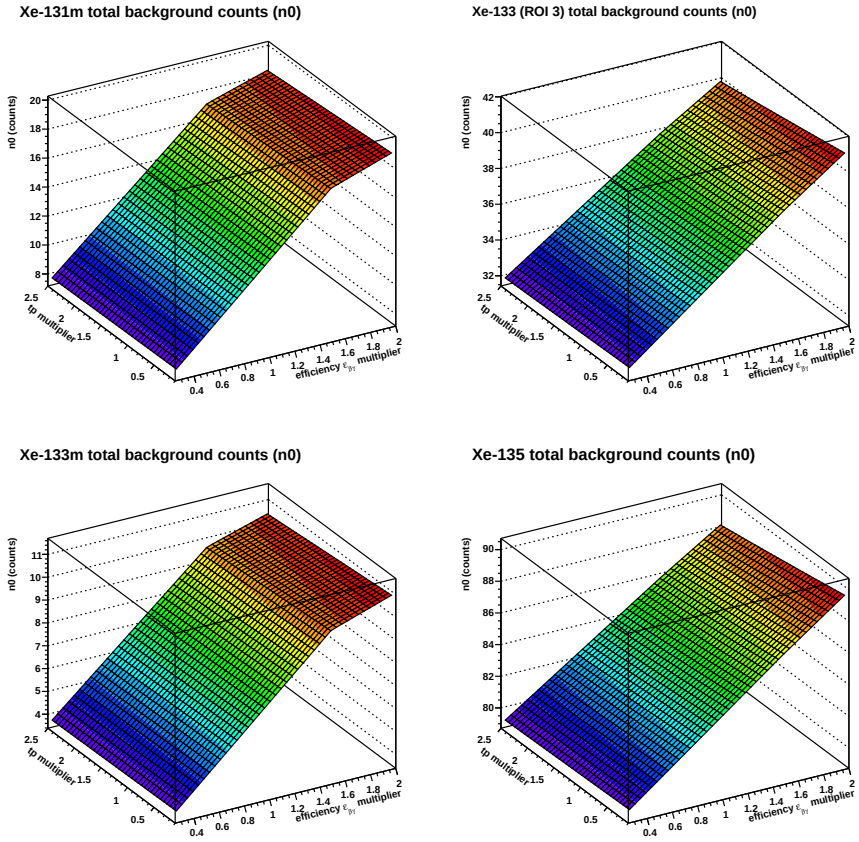

Figure B.35: Background counts n_0 as a function of beta-gamma coincidence counting efficiency ($\varepsilon_{\beta\gamma}$) and sample processing time (t_p). The parameters are expressed as multiples of their values for a present SAUNA system operated as in the IMS, so that values of (1,1) yields a value of n_0 expected from an IMS SAUNA system. The calculation assumes all four isotopes ^{131m,133,133m,135}Xe to be present with a concentration of 0.1 mBq/m^3 during sampling, a memory effect of 2 % (applied to a previous sample assumed to have measured exactly the same concentrations), radon at a concentration of 100 Bq/m^3 and a radon suppression factor of 10^6.

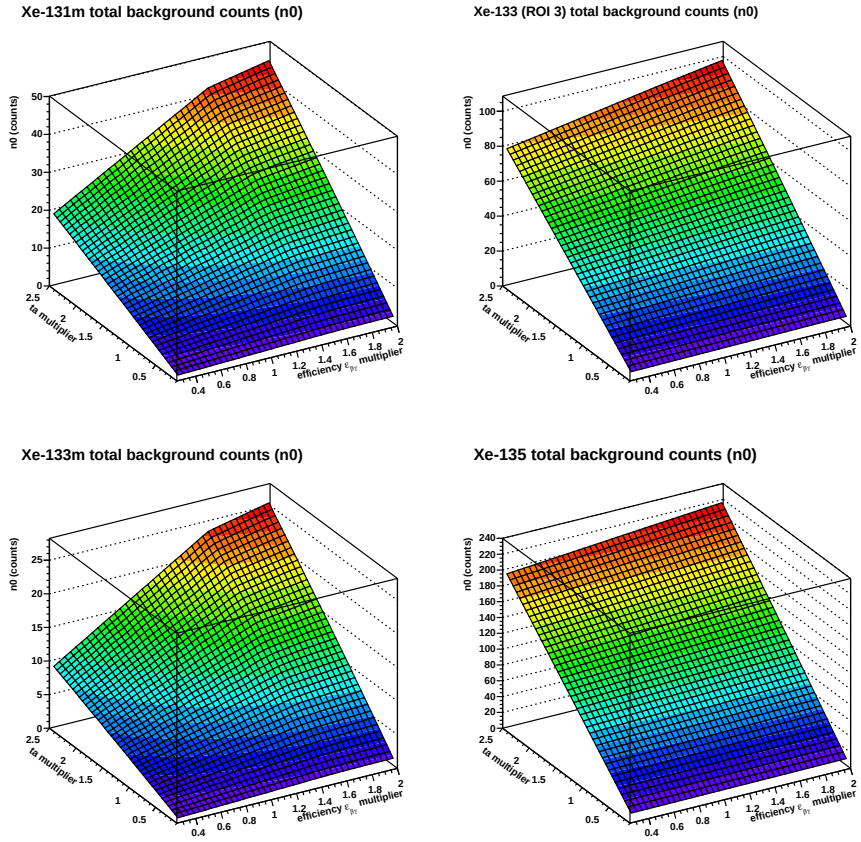

Figure B.36: Background counts n_0 as a function of beta-gamma coincidence counting efficiency ($\varepsilon_{\beta\gamma}$) and sample counting time (t_a). The parameters are expressed as multiples of their values for a present SAUNA system operated as in the IMS, so that values of (1,1) yields a value of n_0 expected from an IMS SAUNA system. The calculation assumes all four isotopes ^{131m,133,133m,135}Xe to be present with a concentration of 0.1 mBq/m^3 during sampling, a memory effect of 2 % (applied to a previous sample assumed to have measured exactly the same concentrations), radon at a concentration of 100 Bq/m^3 and a radon suppression factor of 10^6.

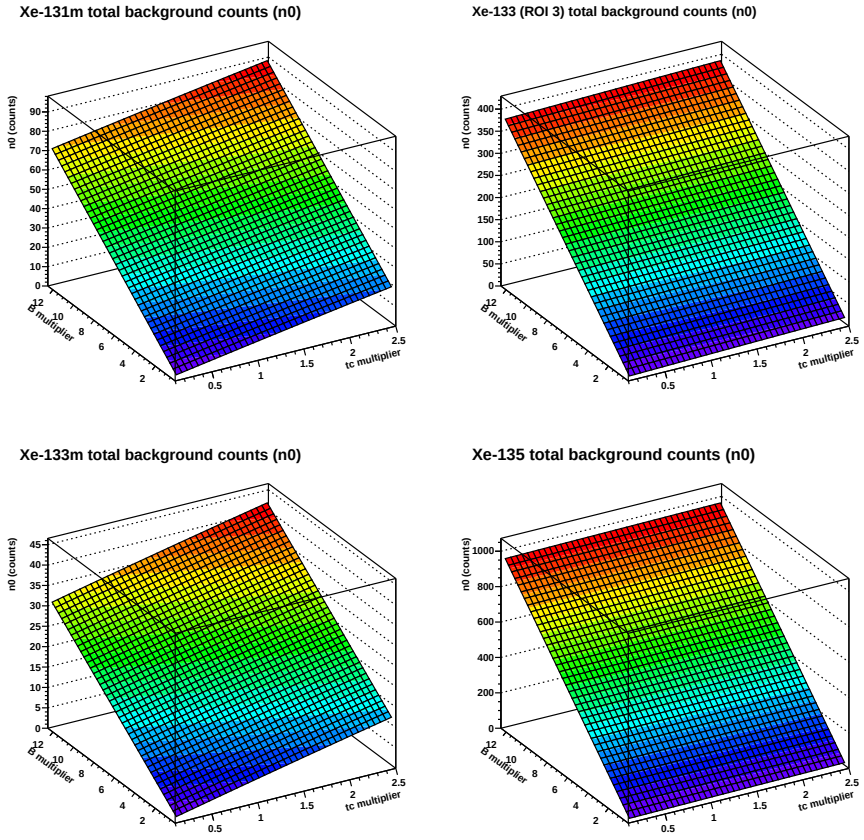

Figure B.37: Background counts n_0 as a function of sample collection time (t_c) and ambient background rate (B). The parameters are expressed as multiples of their values for a present SAUNA system operated as in the IMS, so that values of (1,1) yields a value of n_0 expected from an IMS SAUNA system. The calculation assumes all four isotopes ^{131m,133,133m,135}Xe to be present with a concentration of 0.1 mBq/m^3 during sampling, a memory effect of 2 % (applied to a previous sample assumed to have measured exactly the same concentrations), radon at a concentration of 100 Bq/m^3 and a radon suppression factor of 10^6.

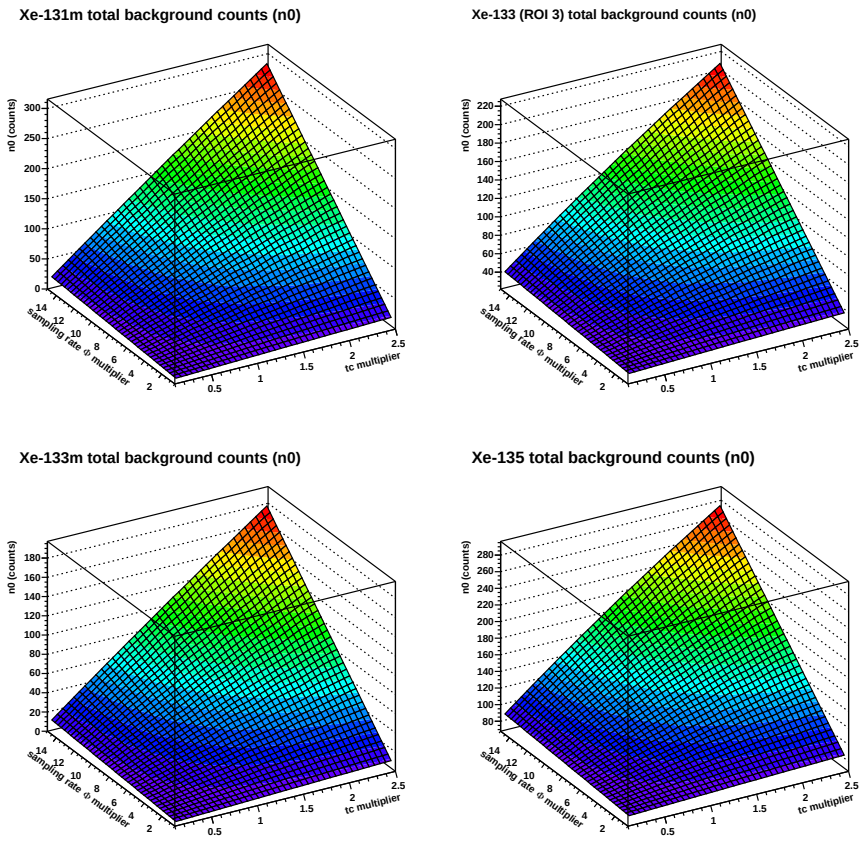

Figure B.38: Background counts n_0 as a function of sample collection time (t_c) and sample collection rate (Φ). The parameters are expressed as multiples of their values for a present SAUNA system operated as in the IMS, so that values of (1,1) yields a value of n_0 expected from an IMS SAUNA system. The calculation assumes all four isotopes ^{131m,133,133m,135}Xe to be present with a concentration of 0.1 mBq/m^3 during sampling, a memory effect of 2 % (applied to a previous sample assumed to have measured exactly the same concentrations), radon at a concentration of 100 Bq/m^3 and a radon suppression factor of 10^6.

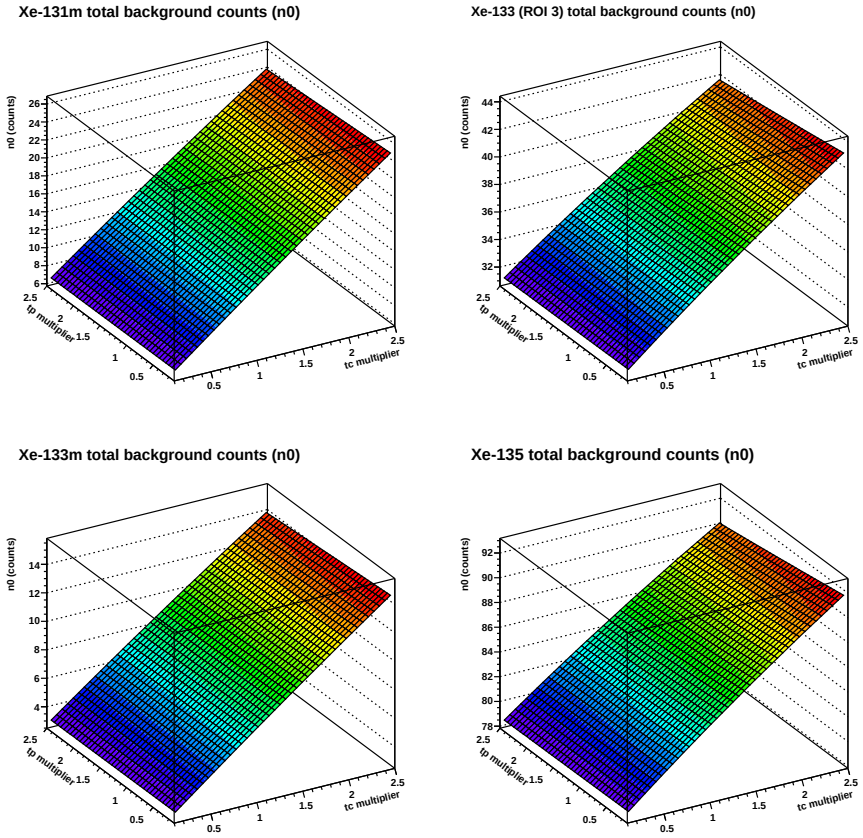

Figure B.39: Background counts n_0 as a function of sample collection time (t_c) and sample processing time (t_p). The parameters are expressed as multiples of their values for a present SAUNA system operated as in the IMS, so that values of (1,1) yields a value of n_0 expected from an IMS SAUNA system. The calculation assumes all four isotopes ^{131m,133,133m,135}Xe to be present with a concentration of 0.1 mBq/m^3 during sampling, a memory effect of 2 % (applied to a previous sample assumed to have measured exactly the same concentrations), radon at a concentration of 100 Bq/m^3 and a radon suppression factor of 10^6.

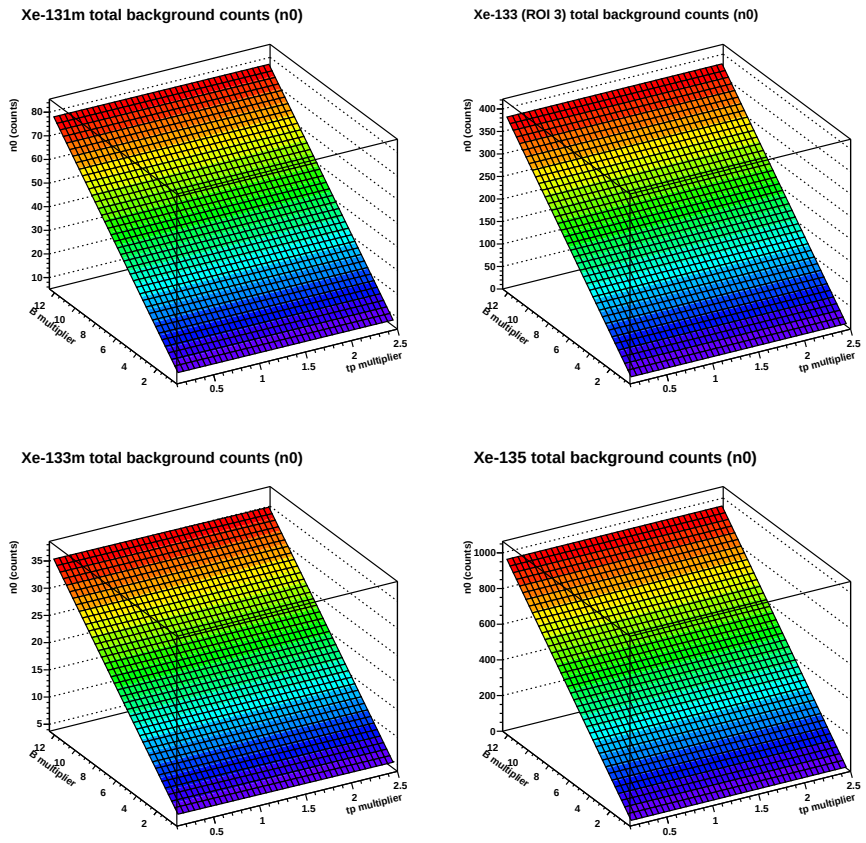

Figure B.40: Background counts n_0 as a function of sample processing time (t_p) and ambient background rate (B). The parameters are expressed as multiples of their values for a present SAUNA system operated as in the IMS, so that values of (1,1) yields a value of n_0 expected from an IMS SAUNA system. The calculation assumes all four isotopes ^{131m,133,133m,135}Xe to be present with a concentration of 0.1 mBq/m^3 during sampling, a memory effect of 2 % (applied to a previous sample assumed to have measured exactly the same concentrations), radon at a concentration of 100 Bq/m^3 and a radon suppression factor of 10^6.

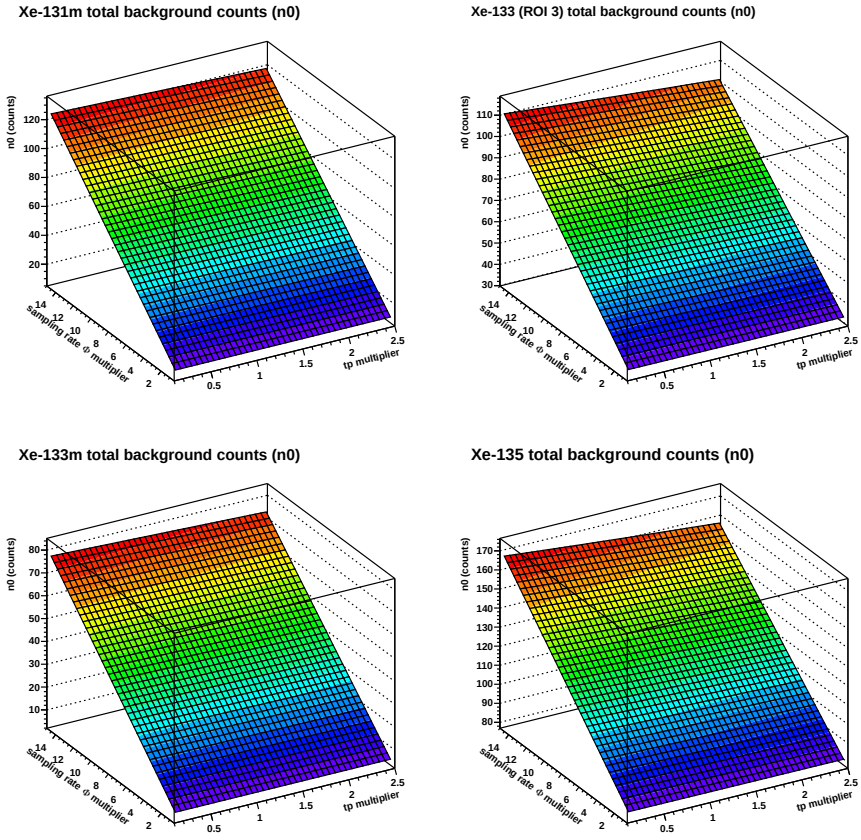

Figure B.41: Background counts n_0 as a function of sample processing time (t_p) and sample collection rate (Φ). The parameters are expressed as multiples of their values for a present SAUNA system operated as in the IMS, so that values of (1,1) yields a value of n_0 expected from an IMS SAUNA system. The calculation assumes all four isotopes ^{131m,133,133m,135}Xe to be present with a concentration of 0.1 mBq/m^3 during sampling, a memory effect of 2 % (applied to a previous sample assumed to have measured exactly the same concentrations), radon at a concentration of 100 Bq/m^3 and a radon suppression factor of 10^6.

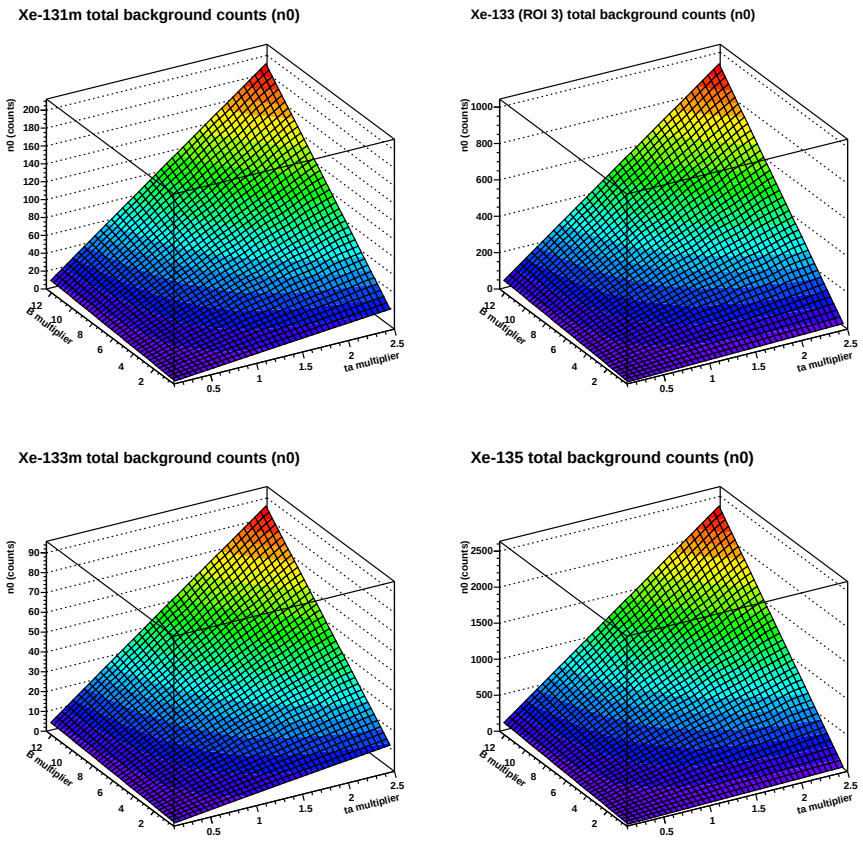

Figure B.42: Background counts n_0 as a function of sample counting time (t_a) and ambient background rate (B). The parameters are expressed as multiples of their values for a present SAUNA system operated as in the IMS, so that values of (1,1) yields a value of n_0 expected from an IMS SAUNA system. The calculation assumes all four isotopes ^{131m,133,133m,135}Xe to be present with a concentration of 0.1 mBq/m^3 during sampling, a memory effect of 2 % (applied to a previous sample assumed to have measured exactly the same concentrations), radon at a concentration of 100 Bq/m^3 and a radon suppression factor of 10^6.

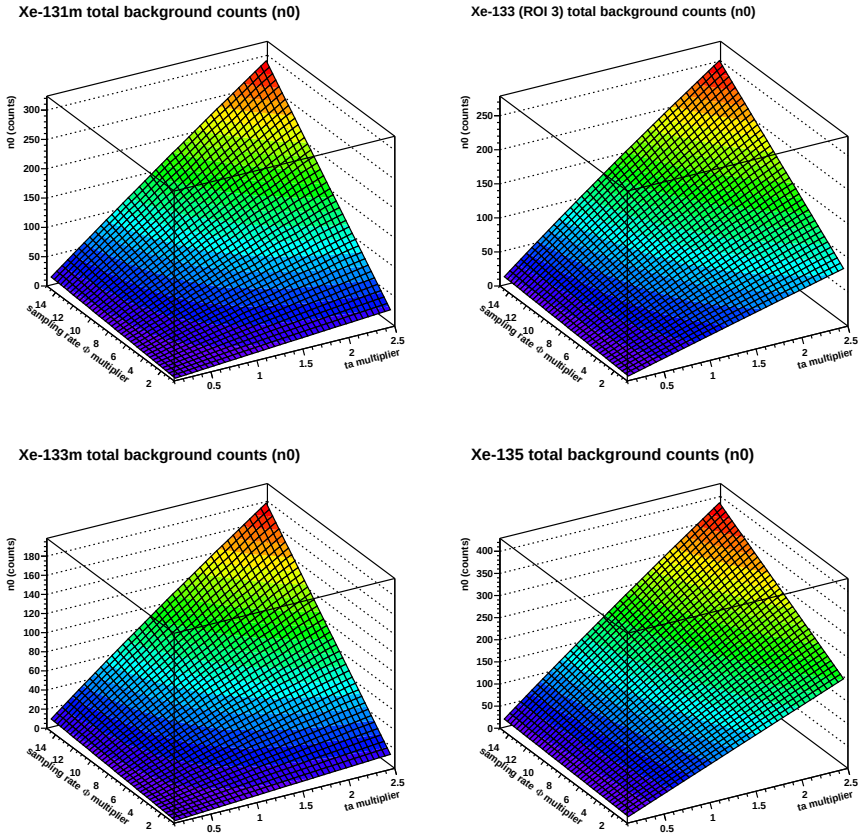

Figure B.43: Background counts n_0 as a function of sample counting time (t_a) and sample collection rate (Φ). The parameters are expressed as multiples of their values for a present SAUNA system operated as in the IMS, so that values of (1,1) yields a value of n_0 expected from an IMS SAUNA system. The calculation assumes all four isotopes ^{131m,133,133m,135}Xe to be present with a concentration of 0.1 mBq/m^3 during sampling, a memory effect of 2 % (applied to a previous sample assumed to have measured exactly the same concentrations), radon at a concentration of 100 Bq/m^3 and a radon suppression factor of 10^6.

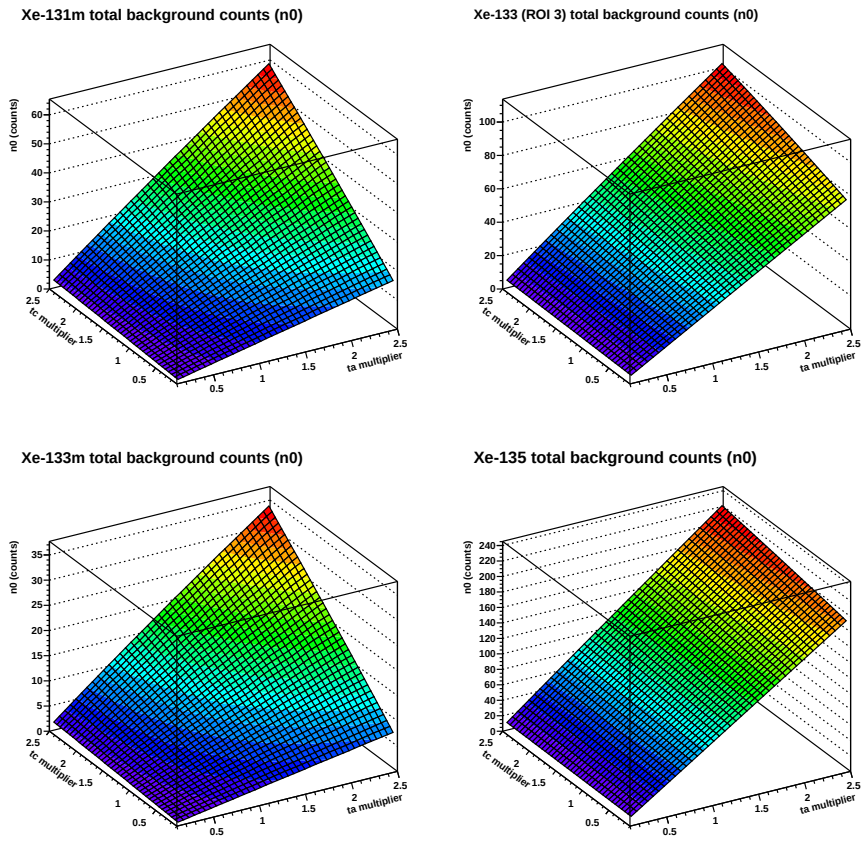

Figure B.44: Background counts n_0 as a function of sample counting time (t_a) and sample collection time (t_c). The parameters are expressed as multiples of their values for a present SAUNA system operated as in the IMS, so that values of (1,1) yields a value of n_0 expected from an IMS SAUNA system. The calculation assumes all four isotopes ^{131m,133,133m,135}Xe to be present with a concentration of 0.1 mBq/m^3 during sampling, a memory effect of 2 % (applied to a previous sample assumed to have measured exactly the same concentrations), radon at a concentration of 100 Bq/m^3 and a radon suppression factor of 10^6.

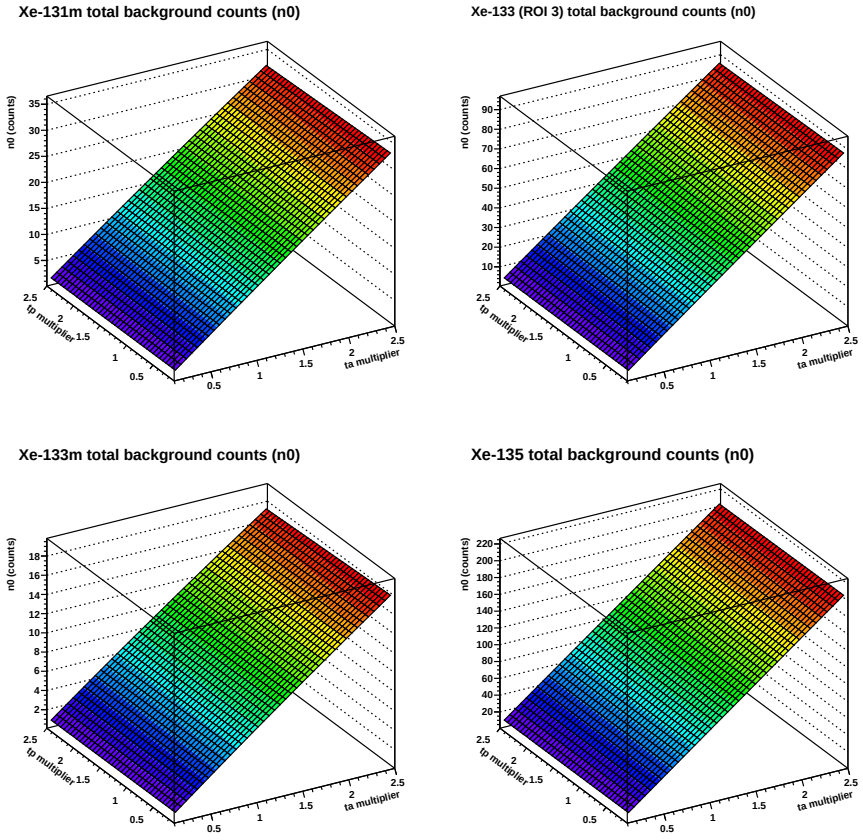

Figure B.45: Background counts n_0 as a function of sample counting time (t_a) and sample processing time (t_p). The parameters are expressed as multiples of their values for a present SAUNA system operated as in the IMS, so that values of (1,1) yields a value of n_0 expected from an IMS SAUNA system. The calculation assumes all four isotopes ^{131m,133,133m,135}Xe to be present with a concentration of 0.1 mBq/m^3 during sampling, a memory effect of 2 % (applied to a previous sample assumed to have measured exactly the same concentrations), radon at a concentration of 100 Bq/m^3 and a radon suppression factor of 10^6.

FOI, Swedish Defence Research Agency, is a mainly assignment-funded agency under the Ministry of Defence. The core activities are research, method and technology development, as well as studies conducted in the interests of Swedish defence and the safety and security of society. The organisation employs approximately 1000 personnel of whom about 800 are scientists. This makes FOI Sweden's largest research institute. FOI gives its customers access to leading-edge expertise in a large number of fields such as security policy studies, defence and security related analyses, the assessment of various types of threat, systems for control and management of crises, protection against and management of hazardous substances, IT security and the potential offered by new sensors.

FOI
Defence Research Agency
SE-164 90 Stockholm

Phone: +46 8 555 030 00
Fax: +46 8 555 031 00

www.foi.se